4-2016

Crop modeling for assessing and mitigating the impacts of extreme climatic events on the US agriculture system

Zhenong Jin
Purdue University

Graduate School Form
30 Updated 12/26/2015

PURDUE UNIVERSITY
GRADUATE SCHOOL
Thesis/Dissertation Acceptance

This is to certify that the thesis/dissertation prepared

By Zhenong Jin

Entitled
CROP MODELING FOR ASSESSING AND MITIGATING THE IMPACTS OF EXTREME CLIMATIC EVENTS ON THE US AGRICULTURE SYSTEM

For the degree of Doctor of Philosophy

Is approved by the final examining committee:

Qianlai Zhuang
Chair

Jeffrey S. Dukes

Melba M. Crawford

Hao Zhang

To the best of my knowledge and as understood by the student in the Thesis/Dissertation Agreement, Publication Delay, and Certification Disclaimer (Graduate School Form 32), this thesis/dissertation adheres to the provisions of Purdue University's "Policy of Integrity in Research" and the use of copyright material.

Approved by Major Professor(s): Qianlai Zhuang

Approved by: Indrajeet Chaubey 04/27/2016

Head of the Departmental Graduate Program Date

CROP MODELING FOR ASSESSING AND MITIGATING THE IMPACTS OF EXTREME CLIMATIC EVENTS ON THE US AGRICULTURE SYSTEM

A Dissertation

Submitted to the Faculty

of

Purdue University

by

Zhenong Jin

In Partial Fulfillment of the

Requirements for the Degree

of

Doctor of Philosophy

May 2016

Purdue University

West Lafayette, Indiana

ACKNOWLEDGEMENTS

A little more than two years ago, my research passion shifted from modeling the vegetation phenology and carbon cycles to agriculture modeling. This was trigged by my attending the class of *A life of Faculty Entrepreneur* where I learned how faculty at Purdue was translating their laboratory work into commercial product, and how people used system models to build a billion-dollar company for forecasting and risk management. I re-evaluated my background, identified agriculture modeling as my career direction, worked with increasing passion and confidence on my own choice, and eventually reached where I am now. But undoubtedly, I won't come through without the support of a large number of people, to whom I would like to express my deep gratitude.

I am grateful and deeply appreciated to my advisor, Professor Qianlai Zhuang, who has given me the full autonomy to pursue my research interests. He has not hesitated his support for my attempts to try different ideas before I finally find my passion. Meanwhile, his advice is always inspirational, encouraging and reassuring. I am also very thankful that he has been offering me Research Assistantship, which ensures me a plenty of time to focus on research. I am so lucky and so proud to be a student of Professor Zhuang.

I would like to thank my advisory committee members: Drs. Melba Crawford, Jeffrey Dukes and Hao Zhang. Their helps are indispensable to the achievement of my

PhD program. I have taken three statistics courses from Professor Zhang, which helped me build a solid foundation of quantitative analysis. Dr. Crawford is very knowledgeable, and always reminds me to reflect on the big picture of science instead of focusing too much on trial technical issues. I should particularly thank Jeff, who is my superstar even before I come to Purdue, for his efforts on helping me become a scientist. The many hours he has spent discussing ideas and editing manuscripts with me are invaluable. I must also thank my lab-mates in the EBDL, and lab alumni who have already left but educated me the most when I was a graduate freshman. At least half of my coding and quantitative skills are leant from them. It's a pleasure to know all of you from a very diverse academic background, and to enjoy the holidays and beautiful seasons together. I also want thank John Shriver and Rishi Prasad from the Science Team of Farmlogs, Ann Arbor, MI, helped design the workflow of Chapter 5; the Backend team at Farmlogs helped for computing support.

Last but not least, I am grateful for the support I received from my parents, who are always supportive for whatever decision I make, and always encouraging whenever I am stuck. I am deeply indebted to my girlfriend, Hui Kong, who has made my life brilliant, and has supported my career track with her wisdom and grace!

TABLE OF CONTENTS

Page

Page

ABSTRACT

Jin, Zhenong. Ph. D., Purdue University, May 2016. Crop Modeling for Assessing and Mitigating the Impacts of Extreme Climatic Events on the US Agriculture System. Major Professor: Qianlai Zhuang.

The US agriculture system is the world's largest producer of maize and soybean, and typically supplies more than one-third of their global trading. Nearly 90% of the US maize and soybean production is rainfed, thus is susceptible to climate change stressors such as heat waves and droughts. Process-based crop and cropping system models are important tools for climate change impact assessments and risk management. As data-science is becoming a new frontier for agriculture growth, the incoming decade calls for operational platforms that use hyper-local growth monitoring, high-resolution real-time weather and satellite data assimilation and cropping system modeling to help stakeholders predict crop yields and make decisions at various spatial scales.

The fundamental question addressed by this dissertation is: How crop and cropping system models can be "useful" to the agriculture production, given the recent advent of cloud computing and earth observatory power? This dissertation consists of four main chapters. It starts with a study that reviews the algorithms of simulating heat and drought stress on maize in 16 major crop models, and evaluates algorithm performances by incorporating these algorithms into the Agricultural Production Systems sIMulator (APSIM) and running an ensemble of simulations at typical farms from the US

Midwest. Results show that current parameterizations in most models favor the use of daylight temperature even though the algorithm was designed for using daily mean temperature. Different drought algorithms considerably differed in their patterns of water shortage over the growing season, but nonetheless predicted similar decreases in annual yield. In the next chapter of climate change assessment study, I quantify the current and future yield responses of US rainfed maize and soybean to climate extremes with and without considering the effect of elevated atmospheric CO_2 concentrations, and for the first time characterizes spatial shifts in the relative importance of temperature, heat and drought stresses. Model simulations demonstrate that drought will continue to be the largest threat to rainfed maize and soybean production, yet shifts in the spatial pattern of dominant stressors are characterized by increases in the concurrent stress, indicating future adaptation strategies will have trade-offs between multiple objectives. Following this chapter, I presented a chapter that uses billion-scale simulations to identify the optimal combination of Genotype × Environment × Management for the purpose of minimizing the negative impact of climate extremes on the rainfed maize yield. Finally, I present a prototype of crop model and satellite imagery based within-field scale N sidedress prescription tool for the US rainfed maize system. As an early attempt to integrate advances in multiple areas for precision agriculture, this tool successfully captures the subfield variability of N dynamics and gives reasonable spatially explicit sidedress N recommendations. The prescription enhances zones with high yield potentials, while prevents over-fertilization at zones with low yield potentials.

CHAPTER 1. INTRODUCTION

1.1 Introduction

Global demand for agriculture crops as food, feed and bioenergy fuels will continue to grow in response to the increasing population, changing diet structure and surging need for alternative energy. For food alone, a recent study relates food consumption to gross domestic production (GDP) has estimated that the production from agriculture systems has to double by 2050 (Tilman et al., 2011). This poses a great challenge to the human society, given the increasing competition for land and water from the need to maintain other essential ecosystem services such as carbon storage and biodiversity (Matthews et al., 2011; Challinor et al., 2014). Concerns on food security have been further raised in face of the climate change (Lobell et al., 2011). Climate changes, especially those increasingly frequent and severe extreme climatic events (ECEs) such as heat waves and drought, are significant threats to the agriculture sector by lowering crop productivity and increasing inter-annual variations in yields (Challinor et al., 2014; Deryng et al., 2014; Rosenzweig et al., 2014). Climate change may also favor outbreaks of pests or pathogens, thus generate secondary damage to the agriculture system (IPCC, 2012).

Maize (Zea mays L.) and soybean (Glycine max Merr.) are two of the most important crops. Specifically, maize accounts for approximately 27% of global cereal

planting area and 34% of cereal production (Shiferaw et al., 2011). Maize is a major source of food calorie and nutrition, especially for millions of people in developing countries (Shiferaw et al., 2011). It is also used extensively as an ingredient in animal feed or as the substrate to produce biofuels. Soybean represents 6% of the world arable land, and is an important source of proteins and oil (Hartman et al., 2011). Climatic threats to the production of maize and soybean vary among regions, yet in general excessive heat and drought are two primary stressors in temperate zones (Schlenker and Roberts, 2009; Lobell and Gourdji, 2012; Harrison et al., 2014; Rosenzweig et al., 2014; Geng et al., 2016; Lesk et al., 2016)

The US agriculture system is the world's largest producer of maize and soybean, and typically supplies more than one-third of their global trading (USDA, 2015). Nearly 90% of the US maize and soybean productions are rainfed (NASS, 2007), thus are susceptible to climate change stressors. The rising temperature and changing precipitation patterns, often in forms of heat waves and droughts, have started to threaten the US agriculture system (Melillo et al., 2014). For example, the 2012 US drought and the co-occurring heat wave severely hit the US Midwest, and reduced the 2012 maize production (which was expected to increase by 20% compared to the previous year) to 13% lower than the 2011 value; soybean production was down by 3% in spite of a 3% increase in the harvested area (USDA, 2013). As extreme heat and drought events are projected to continue in the US with increasing frequency and intensity (Diffenbaugh and Ashfaq, 2010; Mishra et al., 2010), it is compelling to understand the current and future impacts of these weather extremes on the US maize and soybean production, as well as to figure out potential mitigation strategies.

Process-based crop and cropping system models that simulate the crop growth, nutrient cycling as well as water and energy balance on daily or sub-daily time steps are important tools for climate change impact assessments and risk management (Rosenzweig et al., 2014; Ewert et al., 2015). Their ability to understand complex system interactions among water, soil, light, plants and humans offers unique opportunities to evaluate trade-offs when adaptation objectives are to achieve multiple productivity and environmental goals (Boote et al., 2013; Matthews et al., 2013; Holzworth et al., 2014; Ewert et al., 2015). Early applications have shown promising results, such as supporting government policy (Bezlepkina et al., 2010; Mellilo et al, 2014), informing breeding strategies (Lobell et al., 2015; Messina et al., 2015; Hammer et al., 2016; Zheng et al., 2016) and guiding farming practice (Honda et al., 2014; Thompson et al., 2015). Cropping system models are also enlightening to the understanding new physiological mechanisms when impacts of changes in climate factors are not unidirectional. For example, elevated atmospheric CO_2 concentration ($[CO_2]$) is often considered as a benefit to the crop growth indirectly by raising the water use efficiency (Bernacchi et al., 2007; Hussain et al., 2013; Ort and Long, 2014); yet may increase the canopy temperature and crop heat stress as a result of reduced latent heat flux associated with decreased canopy transpiration (Long et al., 2004). In this case, crop models with the inclusion of canopy-scale energy balance can be helpful to quantify the net benefit (Boote et al., 2013; Twine et al., 2013).

As data-science is becoming a new frontier for agriculture growth, the incoming decade is almost certain to witness the surging of operational platforms that use hyper-local growth monitoring, high-resolution real-time weather and satellite data assimilation

and cropping system modeling to help stakeholders predict crop yields and make decisions at various spatial scales. The opportunities, however, are currently impeded by: (i) the poor ability of crop models to quantitatively reproduce what's actually happening in a field with the right scale and decent accuracy; and (ii) the vague conceptual framework to connect the existing advances in geoscience and information technology. From the point view of climate change, traditional cropping system models are far from satisfactory for the purpose of decision-support and risk management, because they are originally designed to capture the average state based on long-term climatology and often lack of scalability beyond the sites where they are developed and validated. Solving these problems will ensure high payoff beyond scientific novelty of the research *per se*.

1.2 Research objectives

The fundamental question discussed by this dissertation is: How cropping system models can be "useful" to the agriculture production? By "useful", it means be able to quantify and predict the risks of climate change, to identify the local optimal management strategy when trade-offs have to be balanced, and to improve the production efficiency. As an early attempt to address this question, I come up with four studies in this dissertation that cover a range of hot topics in the field of agriculture modeling. I start my exploration with a crop model inter-comparison study (i.e. Chapter 2) to mechanistically understand whether or not current generation of crop models is capable to capture the growth response to heat extremes and drought, by comparing existing algorithms from 16 major crop models that simulate the direct heat and drought stress on maize photosynthesis and yield production. I have also documented these algorithms at equation

level based on my review of the documentation and/or source code of these 16 crop models, which can serve as a useful reference manual for the crop modeling community. Next in Chapter 3, I present a climate change assessment study that simulates the US rainfed maize and soybean growth, driven by high-resolution (12km × 12 km) Weather Research and Forecasting (WRF) Model downscaled future climate scenarios, to quantify the spatiotemporal patterns of yield losses caused by heat and drought stress and the gains due to elevated atmospheric CO_2. Chapter 4 moves one step forward to the adaptation and mitigation domain, which investigates how crop modeling can help to identify the optimal farming strategy that minimizes the adverse impact of climate extremes within a nested genotype (G) × management (M) × environment (E) space. Last but not least, Chapter 5 develops a scalable very-high-resolution (5m × 5m) precision fertilization tool by integrating advances in several research areas including digital soil mapping, crop modeling and satellite data assimilation.

Underlining these studies are the recent advancements in high-performance computing and communication technologies, which has made it possible to process massive remotely-sensed or field survey data and to assimilate weather records in near real-time. It has scaled the conventional point-based crop modeling research up to the continental scale. One the other hand, compared with many existing large-scale, coarse-resolution agriculture modeling researches that aim at supporting national or global policy-makers (e.g. Drewniak et al. 2013; Deryng et al., 2014; Rosenzweig et al., 2014; Twine et al., 2013), simulations and projections presented in this dissertation have preserved much spatial heterogeneity, thus are more informative to stakeholders at local scales.

1.3 APSIM description

The Agricultural Production Systems sIMulator (APSIM) is the primary crop model used throughout this dissertation. APSIM is an agricultural system modeling platform that can simulate a number of crops under various climatic, edaphic and management conditions, and hence is used worldwide to address a range of research questions related to cropping systems (Keating et al., 2003; Holzworth et al., 2014). In particular, maize is simulated by the APSIM-Maize module and soybean is simulated by the APSIM-Plant module. The APSIM-Maize module is inherited from the CERES-Maize, with some modifications on the stress representation, biomass accumulation and phenological development (Hammer et al., 2009). The APSIM-Plant module is a generic template that can simulate over 30 crops including soybean, by parameterizing the physiological processes for each species (Holzworth et al., 2014). In recent years, APSIM has been successfully applied in the US to investigate the impact of changing maize canopy structure on yield (Hammer et al., 2009), the sensitivity of heat and drought on maize and soybean production (Lobell et al., 2013, 2014), and the water use efficiency of maize-soybean rotation system (Dietzel et al., 2016). During the course, researchers have started to calibrate and validate the *Maize* and *Plant* modules along with some dependent modules of soil temperature, moisture and nutrient cycling in APSIM for the Midwestern US (Archontoulis et al. 2014a; Dietzel et al., 2016), and accumulated a set of parameterized maize and soybean cultivars in this region (Archontoulis et al. 2014b). For example, based on a set of detailed site-level measurements covering most of the important crop and soil processes, Archontoulis et al. (2014a) calibrated and evaluated

the APSIM Maize, SoilWat (for soil water dynamics and solute transport), SoilTemp (for soil temperature), SoilN (for N cycling) and SurfaceOM (for manure) modules in Iowa.

The flexible and powerful framework of APSIM makes it an ideal tool for incorporating new physiological processes or assimilating algorithms from other models. First, one critical feature of APSIM is the implementation of generic crop model template (Wang et al., 2002). The actual simulation for a given crop is built by calling hierarchical subroutines from the crop process library (CPL) to capture the unifying plant physiologies (e.g. phenology, photosynthesis, carbon allocation, nutrient cycling and environmental stress). All related parameters for thresholds and shapes of physiological response functions are stored in a crop-specific XML file. Since CPL is separately compiled as a dynamic link library, it is very convenient to add new algorithms at process level without changes in other components of the model (Wang et al., 2002). Second, APSIM is highly modularized in a way that a set of common software interfaces (i.e. common modeling protocol) will coordinate the model computation and convey required variables between different modules (Holzworth et al., 2014). Thus, even if incorporating new physiological processes will require additional input data or variables calculated in other modules, developers can easily register these variables in the *Component Interface* module and recompile only a few modules. Last but not least, APSIM provides an immense array of management functionality within the "Management" toolbox via easy-to-command scripting language. The scripting capability allows user to precisely define on-farm management activities, including, but not limited to, controls of fertilization, irrigation, sowing date, seeding rate and cultivar (Holzworth et al., 2014).

CHAPTER 2. CROP MODEL INTERCOMPARISON ON SIMULATING THE IMPACTS OF HEAT AND DROUGHT STRESS ON MAIZE GROWTH

2.1 Introduction

The long-lasting and pervasive 2012 heat wave and drought in the United States damaged a substantial proportion of crop commodities, especially those in the Midwest (Mallya et al., 2013). Such an extreme climatic event (ECEs), however, is only a microcosm of the past decades full of fierce weather extremes (Coumou & Rahmstorf, 2012). These ECEs are projected to continue in the future, with increasing magnitude, duration and frequency (IPCC, 2012). The rising incidence of weather extremes will exacerbate negative impacts on the crop productivity; indeed, critical thresholds are already being exceeded (Hatfield et al., 2014). As many other crops, contemporary maize production is threatened by the changing climate that reduces maize farming efficiency (Bassu et al., 2014). Concerns have thus been raised about maintaining a stable increase rate of the US maize yield, which is vital to the global food security (Bruinsma, 2009; Ort and Long, 2014). Extreme heat and drought are the two dominant constraints to the rainfed maize cultivating system in the US (Schlenker & Roberts, 2009; Lobell et al., 2013; Hatfield et al., 2014).

Process-based crop models that incorporate maize modules are powerful tools for evaluating the potential impacts of climate change on maize yield (Bassu et al., 2014). Combined with hyper-local growth monitoring and assimilation of high-resolution and

real-time weather data, crop models can increasingly help stakeholders predict maize production and make decisions. However, these models remain poorly suited to manage and alleviate the risks from ECEs such as heat and drought. Most current generation of ecosystem models, including crop models, were originally optimized to simulate average conditions based on long-term climatology (Reichstein et al., 2013), and their algorithms that simulate specific stresses are not well parameterized, either due to a lack of natural and experimental records of maize yield responses to high temperature and severe drought with which to train models, or due to a slow pace of updating model parameterizations. While broad agreement exists in terms of the effects of heat and drought on maize growth and development, researchers have abstracted this knowledge into markedly different equations and interactions (Saseendram et al., 2008; Bassu et al., 2014). Differences among algorithms are more prominent for heat than for drought, likely because fewer high-quality datasets have been available to describe heat stress effects on maize biomass production, grain-set, grain fill and yield. There is a clear need to systematically assess the environmental responses of biological processes in crop models, especially those processes that directly determine the simulated crop productivity.

As a critical first step towards model improvement, crop model comparison studies have become popular, especially for climate change scenarios (Rosenzweig et al., 2013). In a review of 5 major crop models, Saseendram et al. (2008) found that these models all use the ratio of actual to potential transpiration or evapotranspiration to indicate water stress, but none of them can accurately represent the coupled processes of carbon assimilation, transpiration, energy balance, and stomatal behavior. Eitzinger et al. (2013) compared responses to heat and drought stress of seven widely used crop models, and

pointed out that even though a general consensus can be reached on the yield trend in response to increased temperatures, these models were not able to capture the direct heat stress impacts that account for substantial yield variations. More recently, the Agricultural Model Intercomparison and Improvement Project (AgMIP) has significantly advanced this field under protocols of coordinated evaluation, intercomparison and improvement of crop models (Rosenzweig et al., 2013). Asseng et al. (2013) observed that variations among crop models account for a greater proportion of the uncertainty in simulating global wheat yields under climate change than variations among future climate scenarios. By evaluating the performance of 23 maize models under four production conditions, Bassu et al. (2014) found that an ensemble of models was more reliable than one single model in capturing the mean yield even with very limited data for model calibration.

These comprehensive assessments advance the operational use of available crop models and shed light on the capability and uncertainty in the tools, but their findings often give only vague guidance to support individual model improvement (Donatelli et al., 2014). This tradeoff is inevitable in studies that compare the output from full models. Since crop models differ substantially in the way they simulate crop physiology, soil physical characteristics and nutrient states, not to mention the differences in input variables and parameter settings, model developers often find it hard to tell which part of their models need to be improved when simply looking at the final results (e.g. yields). Some might argue that modelers can trace sources of uncertainty by examining intermediate variables; for instance by comparing leaf area index (LAI) with observations. Unfortunately, though, any of these intermediate variables themselves are results of

complicated interactions among processes within a model. For a specific crop process (e.g. photosynthesis, phenology and yield formation), there usually exist a number of ways to construct the mathematical algorithms (Bassu et al., 2014; Martre et al., 2014). Thus, to quantitatively understand the uncertainty related to that particular process, comparison should be done in a way similar to a controlled experiment, such that any other processes are isolated.

The idea of focusing on different algorithms or different implementations of the same algorithm for a particular process (defined as "algorithm ensemble" hereafter) when comparing crop models has been tested a few times and proved to be promising for elucidating the target issue (Saseendran et al., 2008; Alderman et al., 2013; Eitzinger et al., 2013; Donatelli et al., 2014; Kumudini et al., 2014). It is favorable also because research advances that can be easily assimilated into models are mostly those at the process level (Donatelli et al., 2014). However, very few studies have performed comparisons in a fully controlled style such that a process ensemble was quantitatively evaluated within a single platform (but see Donatelli et al. (2014) for a pioneering case study on soil temperature simulation). Insufficient modulization, poor documentation of most crop models and intellectual property boundaries are believed to be the three vital obstacles that hinder reimplementation and reuse of alternative algorithms for a specific process (Holzworth et al., 2015).

In this study, we implement the "algorithm ensemble" framework to evaluate the performance of difference algorithms in capturing the impact of heat and drought stress on maize biomass production and yield formation. We first review existing algorithms at the equation level from 16 major crop models that simulate the direct heat and drought

stress on maize photosynthesis and yield formation, and document them for crop modelers. Next, we describe how representative algorithms were extracted from their parent crop models and incorporated into a standard model so that variations among algorithms could be quantified in a controlled manner. We select the Agricultural Production Systems sIMulator (APSIM) as the standard model, because its generic and modularized design allows algorithms to be replaced without changing the model structure. Finally, the revised APSIM with algorithm ensemble is used to simulate maize production at typical farms in the US Corn Belt, and evaluated using the county-level yield statistics from the USDA National Agricultural Statistics Service (NASS). Our goal is to understand why a particular algorithm (if any) performed better than others in capturing the signal of heat and drought, and to offer clear and useful information regarding crop model improvement. We exclude the evaluation of algorithms of indirect heat and drought stresses via leaf elongation/senescence, which are often programed to be more susceptible to adverse growth conditions (e.g. water stress effect in CERES-Maize), because the complex interactions between phenology and photosynthesis will make the results too complicated to interpret. We focus on maize because it is the most important cereal commodity in the United States, but the framework presented in our study can be extended to other crops and any process in a crop model.

2.2 Review of simulating heat and drought stress in crop models

Sixteen major maize models were selected for evaluation and classification with respect to their algorithms of describing heat and drought stress on carbon assimilation and yield production. Although previous literature reviews did an excellent job in

summarizing the physiological knowledge and conceptual models of crop responses to stress factors (Prasad et al., 2008; Saseendran et al., 2008; Parent and Tardieu, 2014; Barlow et al., 2015; Rezaei et al., 2015), quantitative evaluation and comparison at an algorithm level is scarce. Although our focus here is for maize, mechanisms and modeling approaches evaluated can be applied for other cereals.

2.2.1 Heat Stress

The negative impacts of short episodes of high temperature on crop yields have been found with sufficient evidence (Prasad et al., 2008; Schlenker and Roberts, 2009; Lobell, et al., 2013). A number of mechanisms could potentially explain the robust relationship, including but not limited to: sensitivity of anthesis-silking period to heat stress (Bolanos and Edmeades et al., 1996), declines in net photosynthesis (Prasad et al., 2008), hastening leaf senescence (Parent and Tardieu, 2012), and changes atmospheric water demand and soil water supply (Lobell et al., 2013, 2014). Implementations of these many processes are often different between crop models, resulting in complicated interactions and iterations. To evaluate individual stress effects and alleviate the interference of multiple interactions, we exclude the indirect heat stress on maize yields via tuning of the canopy phenology, but only focus on processes that directly affect biomass and yield production. Based on this premise, the formalism of yields response to heat stress in the reviewed models is mainly through placing constraints on 3 aspects of reduction functions, including: (i) photosynthesis, (ii) harvest index, (iii) grain number or grain filling rate (Table 1).

Biomass accumulation via photosynthesis is a common starting point of crop growth, whereas the modeling methods differ among crop models. Simulations of heat

stress on photosynthesis can be further divided into three subgroups. The first one considers limit on the whole canopy light use efficiency (LUE). Models with this type of algorithm are often those origins from the 1980s (e.g. APSIM, CERES, EPIC, STICS and SWAT) or designed for simulating large-scale crop yields responses (e.g. DayCent and PEGASUS). The second subgroup uses more mechanistic ways to describe leaf-level RUE/LUE, and then scales up to the whole canopy based on LAI. The implementations of HYBRID-maize and WOFOST are relatively simple, such that the leaf-level maximum assimilation rate is adjusted with sub-optimal daytime temperature. CSM-IXIM uses much more complicated calculation routines. Designed for improving model accuracy under stresses, CSM-IXIM separates leaf area into sunlit and shaded fractions, and calculates light absorption using a nonrectangular hyperbola function. Temperature effects on assimilation are described by multiplying a cubic function to the parameters of the hyperbola function, while parameters of the cubic function itself need to be calibrated (Lizso et al., 2005). The third group considers limit of the Rubisco activity and/or electron transport at leaf level (i.e. Farquhar photosynthesis model). Representing heat stress at leaf level is more intricate as photosynthesis models at this level are inherently complicated. For instance, AgroIBIS simulates gross primary production through the use of mechanistic photosynthesis and semi-mechanistic stomatal conductance algorithms, within which heat will increase the stomatal resistance and further limit photosynthesis (Kucharik and Brye, 2003). In MONICA, the parameter of maximum saturated Rubisco carboxylation rate is adjusted by a simple temperature function with optimum around 30 to 40 °C (Sage and Kubien, 2007). For the models reviewed above, the limiting function is often a response curve within the suitable range of temperature for biomass

accumulation, and hence heat stress is actually a segment of such response curves when close to the upper limit (Figure 2.1). For the remaining four models (i.e. AquaCrop, CropSyst, GLAM and MAIZSIM), no mechanistic algorithms of direct heat stress on biomass accumulation are detected from publically accessible documentation (but see Challinor et al., 2009 for a reduction in transpiration efficiency due to high temperature).

Once biomass accumulation has established, one simple approach to account for the impact of heat stress on yields is to reduce the harvest index (i.e. the ratio of grain weight to total plant biomass; HI). While in reality HI reduction can be attributed to a failure of reproductive processes, of grain abortion or of photosynthesis-inhibited grain formation on a particular day, modeling efforts to date have largely focus on a short period around flowering (Rezaei et al., 2015). AquaCrop implemented this approach for the whole canopy (Raes et al., 2009), in which high temperature episodes during the flowering period can reduce the daily increment in HI by a fraction weighted on fractional flowering. Challinor et al. (2005) defined the time window of heat stress as -5 to +12 days from the onset of anthesis and when developing the GLAM model, as field research results show that grain yields can be reduced by exposure to heat both before and after flowering (Rezaei et al., 2015). This algorithm was then added to CropSyst by Moriondo et al. (2011) and validated for European winter wheat and sunflower, but so far is not an inclusion to the standard CropSyst. Variations of this algorithm were also incorporated into MONICA and PEGASUS, who shared much with the one presented by Moriondo et al. (2011), but differed slightly in either the time window or the temperature thresholds for identifying the heat stress episode.

As a more mechanistic alternative to the HI approach, calculating final yield according to grain numbers is also popular among cereal models. When high temperature episode occurs, a reduction function can be applied either to the grain number or to the grain filling rate. Theoretically, heat stress could negatively impact not only the grain number through reduced photosynthesis, failure of flowering or pollination, but also the grain filling rate and duration (Razaei et al., 2015). In the model realization, majority models only implemented a reduction factor on the grain filling rate (e.g. CERES-Maize, HYBRID-Maize, MAIZSIM and STICS), so as to avoid double accounting heat stress effects caused by the same signal. The shapes of temperature-dependent grain filling function are very similar to those used for photosynthesis processes (Appendix A, Text A1), where the scalar decreased from 1 at optimal temperature to zero at lower and upper temperature thresholds. In addition to an empirical reduction functions on grain filling rate, APSIM-Maize also considers the heat stress on grain number such that it is reduced proportionally to accumulated degree days above 38 °C (Carberry et al., 1989). STICS considers cold damage to the grain number, but not heat stress (Brisson et al., 2009). It should be noted, however, the process of carbon translocation is implemented in HYBRID-Maize, MAIZSIM and STICS so that when net carbon assimilation exceed the stressed grain filling rate, the surplus will be allocated to a carbohydrate reserve (e.g. stalk) for future translocation.

2.2.2 Drought stress

Drought can adversely affect crop growth and yield (Saseendran et al., 2014), mainly through regulations of leaf expansion and senescence, photosynthesis, carbon allocation, yield formation, and growth of rooting system (Prasad et al., 2008). Maize

production in rain-fed systems is mainly constrained by water deficit, especially during its reproductive stages (Lobell et al., 2014). Again, similar to the review of heat stress, our review will exclude those indirect impacts from drought via phenology and rooting system. Conceptually, drought can be easily defined as water supply in soil fails to meet the plant demand, whereas accurately representing water stress in crop model remains a major challenge to model developers (Parent and Tardieu, 2014). Most crop models simulate water stress according to simple indices such as (i) a function of available soil water content (SWC), (ii) ratio of water supply to demand, (iii) ratio of actual to potential transpiration, and hardly (iv) a function of leaf water potential (Table 2).

Calculating water stress as a function of SWC is conceptually simple and easy to implement. Some models relate soil water deficit (SWD) directly to photosynthesis by limiting LUE (e.g. PEGASUS and STICS) or more mechanistically the stomatal openness (e.g. AgroIBIS). However, these models often only consider the soil water supply while ignore the plant water demand, thus their estimation of water stress should be treated with caution. In AquaCrop, SWD will affect the increase of HI through complex subroutines (Text A1). Water stress before yield formation may counterintuitively increase HI as a result of less energy is spent for vegetation growth, while SWD occurred during pollination and crop transpiration can reduce the final HI (Raes et al., 2009). Although field studies in general support the adaptation mechanism of increased carbon partitioning to the rooting system in response to water shortage (Chaves et al., 2002), only a few models (e.g. CSM-IXIM, DayCent, MAIZSIM) have explicitly simulated the dynamical root vs. shoot ratio as a function of SWC.

APSIM is a typical model using the idea of relating drought to the ratio of water supply to demand. In APSIM, soil water supply (W_s) is simulated as:

$$W_s = \left[\sum_{i=1}^{I-1} KL_i(SW_i - LL_i)\right] + c \cdot KL_I(SW_I - LL_I) \quad (2.1)$$

where i is the soil layer, I is the deepest soil layer where roots are present, SW is the layer specific soil water content, LL is the lower limit of plant-extractable soil water, KL is the coefficient for root water extraction, and c is an adjusting variable for the deepest layer. On the other hand, plant water demand (W_d) is calculated as the amount of water required to support the light-limited biomass production:

$$W_d = \frac{\Delta Q}{TE} \quad (2.2)$$

where ΔQ is the light driven daily biomass production, and TE is the transpiration efficiency inversely proportional to the VPD. Water stress factor is calculated as W_s/W_d, and will reduce ΔQ when $W_s < W_d$. CropSyst and GLAM should also be classified into this group, even though these two models did not explicitly calculate $W_s < W_d$. Instead, daily biomass increment in both models is a product of available water supply and transpiration efficiency, and hence shortage of W_s will directly reduce the dry matter production.

The idea of using AT/PT to indicate water stress is applied by the majority models, although a close check of algorithms may reveal their slight differences on the complexity and the threshold for stress (Text A1). In general, these models will simulate a reference evapotranspiration (ET_0) with variants of the Penman-Monteith method (Penman, 1948; Priestley-Taylor, 1972; Allen et al., 1998), and then partitioning ET_0 into potential plant transpiration (EP_0) and soil evaporation (ES_0) according to the Ritchie

(1972) approach. AT or equivalently plant water uptake is calculated either by sum up the root water uptake throughout the soil profile (e.g. CERES-Maize, CSM-IXIM, DayCent, EPIC, HYBRID-Maize, SWAT) or by multiplying EP_0 to limiting factors, including soil water deficit (e.g. AquaCrop, MONICA. WOFOST), water logging (e.g. AquaCrop, MONICA, WOFOST), or soil salinity stress (e.g. AquaCrop). Once AT/PT is calculated, this ratio will be often set as a linearly reducing factor to the daily increase of biomass or harvest index (Table 2.2).

Stomatal conductance, and hence plant water stress, is often simulated as a function of SWC, yet leaf water potential has been supported to be a more direct indicator of plant water status (Tuzet et al., 2003; Prasad et al., 2008). Tuzet et al. (2003) first implemented this idea and proposed a coupled model of stomatal conductance, photosynthesis, leaf energy balance, and transport of water through the soil-plant-atmosphere continuum. The same algorithm is incorporated into MAIZSIM by Yang et al. (2009) such that the stomatal closure factor $f(\Psi_l)$ is calculated by:

$$f(\Psi_l) = \frac{1 + exp[s_f \Psi_f]}{1 + exp[s_f(\Psi_f - \Psi_l)]} \tag{2.3}$$

where Ψ_l is the bulk leaf water potential, Ψ_f is a reference potential ($= -1.2$ MPa), and s_f is a sensitivity parameter ($= 2.3$). Simulation accuracy of maize transpiration improved with the coupled algorithm that considers the control of Ψ_l on stomatal conductance significantly outcompete the conventional method for drying soil, but trends to be similar when plants were well watered or under minor water stress (Yang et al. 2009). The key variable Ψ_l is calculated iteratively by the 2DSOIL model (Timlin et al. 2002), while the very complicated simulation routine is beyond the scope of this paper.

2.3 Materials and methods

In this section, we first describe a method to quickly screen the behavior of heat stress algorithms. Next, we describe simulations that use an algorithm ensemble for the historical period of 1980-2013 and future scenarios of 2006-2099. A brief introduction to the development and application of APSIM-Maize model and its important engineering features is provided in the Introduction Chapter. Screening of heat stress algorithms was conducted at the AmeriFlux Mead Rainfed station, Saunders, NE (41.18 ^{o}, -96.44 ^{o}), where hourly meteorological and fluxes variables were archived. Screening of drought stress algorithms was performed at Agricultural Engineering and Agronomy Research Farms of Iowa State University, Boone, IA (42.02^{o}, -93.78^{o}). The ensemble simulation was conducted at the Iowa farm as well as at two other sites: (i) the AmeriFlux Bondville station, Champaign, IL (40.01^{o}, -88.29^{o}); (ii) Purdue Agronomy Center for Research and Education, West Lafayette, IN (40.47^{o}, -86.99^{o}). For brevity, we mainly focus on the Indiana farm for the ensemble simulation, while present similar results from the other two farms in the Appendix A.

2.3.1 Screening of heat and drought stress

To understand the behavior of representative heat and drought response functions, we pulled out these algorithms from their parent models and reprogrammed each in R language. Such a "lightweight" method allowed fast screening of these algorithms, while avoiding the "heavy" task of running crop models, which usually requires extensive preparation.

For heat stress, we selected the temperature response curve of photosynthesis and/or carbon assimilation from AgroIBIS (Quadratic; Kucharik & Brye, 2003), APSIM

(piecewise linear; Keating et al., 2003), CERES (piecewise linear; Jones et al., 2003), DayCent (Generalized Poisson; Parton, 1993), EPIC (Sinusoidal; Sharpley & Williams, 1990), MAIZSIM (Exponential; Yang et al., 2009), SWAT (Exponential; Neitsch et al., 2011) and WOFOST (piecewise linear; Supit et al., 1994). These 8 representative selections cover all different shapes of temperature response curves for the 16 crop models reviewed in this paper (Table 2.1), and detailed descriptions for each can be found in Text A3. These temperature response curves were compared to the observed ratio of gross primary production (GPP) to absorbed photosynthetically active radiation (APAR) at different temperatures from the AmeriFlux Mead Rainfed station (Text A2). Next, we calculated the mean annual heat stress factors by integrating daily values over either the growing season. Daily weather inputs, including maximum and minimum air temperature at a spatial resolution of 1km × 1km were downloaded from the Daymet website (http://daymet.ornl.gov/). During our preliminary analysis, we observed that models such as DayCent, SWAT and WOFOST that use daily mean temperature to force the heat stress algorithm predicted almost no heat stress on annual basis, while the CERES model that uses daylight temperature (approximated by $\frac{T_{max}+T_{mean}}{2}$ hereafter) was more sensitive to excessive heat. Therefore, we also tested the effect of using daylight temperature to simulate heat stress. The simulation results were compared to growing season extreme degree days (EDD, which is cumulative daily mean of hourly temperature above 30 °C; Lobell et al., 2013) and killing degree days (KDD, which is the cumulative daily mean temperature above 29 °C; Butler et al., 2013), both of which are indicators of excessive heat for crops (details of our implementation are given in Text A3).

For drought stress, we evaluated the three dominant algorithms that cover more than 80% of the crop models we reviewed (Table 2.2): functions of average soil moisture content (SWC), water supply to demand ratio (Ws/Wd) and actual to potential transpiration ratio (AT/PT). It should be noted that although Ws is close to AT because soil water supply largely determines the actual transpiration in many models, the denominators of Wd and PT are quite different, such that the former is based on the concept of transpiration efficiency (Hammer et al., 2010) and the latter directly reflects daily weather conditions (Allen et al., 1998). For simplicity, we used the APSIM SoilWat module (a tipping-bucket model) to simulate daily state variables and fluxes that were not directly observed. We calculated mean annual drought stress factors by averaging daily values over the growing season for each year. To reduce the uncertainty in hydrological modeling, we reused the APSIM simulation configuration and parameters from the well-calibrated site in Boone, IA (Archontoulis et al., 2014). We again used meteorological inputs from the Daymet dataset.

2.3.2 Ensemble simulation

The algorithm ensemble for each site consisted of 30 simulation runs (i.e. 10 simulations of heat stress algorithms for different processes × 3 varieties of drought stress algorithms). For heat stress, we constructed ten simulations (SM) that covered (i) two vapor pressure deficit (VPD) calculation methods, (ii) four different representations of heat stress on biomass production, (iii) two heat stress modifiers on grain-filling, (iv) three harvest index (HI) models, and (v) one leaf-level photosynthesis model (Figure 2.1). Specifically, SM1 is the reference simulation that used the default APSIM algorithms of heat stress on photosynthesis, grain number development and grain filling. SM2 replaced

the default APSIM VPD algorithm, which is purely based on maximum and minimum daily temperature and is hence occasionally criticized for overestimating drought stresses during hot days (Basso and Ritchie, 2014), with the more common method that requires either daily dew point temperature or relative humidity as input data (Abtew & Melesse, 2013). SM3, SM4 and SM5 replace the APSIM multi-linear temperature stress function on the radiation use efficiency (RUE) with its counterpart in STICS, SWAT and WOFOST, respectively. It should be noted that STICS uses canopy temperature, which can be calculated by an empirical relation model, instead of air temperature to force the stress function (Text A1). SM6 was a simulation using the algorithm of high temperature effect on grain filling from MAIZSIM. SM7, SM8 and SM9 retained the APSIM photosynthesis and biomass production routines, but estimated yield based on the simulation of HI instead of the original grain number × grain-filling rate method. SM7 incorporated the PEGASUS HI method (also used in CropSyst and GLAM), in which potential HI can be reduced due to heat stress around the silking-anthesis stage (i.e. flowering stage). SM8 used the SWAT HI method, which first develops potential HI according to the accumulation of daily heat units, and then calculates the actual HI based on the average water deficit over the growing season. SM9 adopted the HI model from AquaCrop, in which the potential HI can be adjusted either upward or downward by a number of environmental stress factors (Raes et al., 2009). To compare the performance of RUE-based biomass production models with the more mechanistic model of leaf-level CO_2 assimilation processes, we incorporated the coupled photosynthesis-stomatal conductance model for C4 plants according to Collatz et al. (1992) as SM10 (Text A4). Similar leaf-level photosynthesis models have been implemented in more recently

developed crop models (e.g. AgroIBIS, CSM-IXIM, MAIZSIM and MONICA). Since SM1 - SM10 are not fully orthogonal, results from these simulations should not all be compared against each other. The effect of changing the APSIM default VPD algorithm can be observed by comparing SM1 vs. SM2. If the focus is on different parameterizations of heat stress on biomass production, then compare SM1 vs. SM3, SM4 and SM5. Comparing SM1 and SM6 illustrates the difference between two heat stress functions on grain-filling. Different implementations of HI algorithms can be evaluated by looking at SM7, SM8 and SM9, while the difference between grain filling vs. the HI method can be compared by looking at the group of SM1 and SM3-5 vs. the group of SM7-9. The effect of replacing an RUE model with leaf-level photosynthesis can be seen by comparing results from SM1 and SM10. On top of each simulation with a particular heat stress algorithm, we further nested three varieties of drought stress algorithms that describe water deficit as a function of SWC, Ws/Wd or AT/PT. More detailed theoretical backgrounds for each of these algorithms are given in Text A1. Simulations of maize phenology, soil moisture, temperature and nutrient dynamics were still carried out by the default APSIM platform.

To evaluate the APSIM-Maize performance on yield prediction, we compared model simulations with the NASS county-level rainfed maize yield data (e.g. Tippecanoe County for the farm from West Lafayette, IN). We used Daymet meteorology variables, as mentioned above, to run APSIM. Soil parameters, such as layered soil hydraulic properties and soil organic matter fractions, were extracted from the SSURGO database (Web Soil Survey: http://websoilsurvey.sc.egov.usda.gov). A detailed description for each of these soil parameters is presented in Archontoulis et al. (2014). When a farm had

several soil types according to SSURGO, we simply selected the one that accounted for the largest fraction, to reduce the computational cost. As a result, we derived Flanagan silt loam soil for the Illinois farm, Chalmers silt clay loam soil for the Indiana farm and Webster clay soil for the Iowa farm. Management history is critical for models to reproduce the historical trend in maize yield. In rainfed fields, the required management information includes: (i) sowing date, seeding rates and cultivar; (ii) fertilizer type, amount and timing. We derived most of the information from the NASS survey report, with state-specific details provided in Table A1.

2.3.3 Analysis

To quantitatively understand the sensitivity of model-simulated biomass and/or yield to heat and drought stress, we further calculated the relative contributions of each stress over the historical period of 1980-2013 and in two future climate scenarios. Simulations were conducted by the standard APSIM-Maize (i.e. SM1) for the Indiana farm. The APSIM framework allowed us to switch on and off a certain stress by setting the corresponding stress function equal to 1 (Text A1). The sensitivity of biomass reduction (%) to drought was calculated as:

$$\mathrm{S_{Drought}} = \frac{\left(B_{Drought} - B_{Potential}\right)}{B_{Potential}} \times 100\% \quad (2.4)$$

where $B_{potential}$ is the simulated biomass from SM1 when stresses that directly limit photosynthesis and grain development are excluded, and $B_{Drought}$ is the value from the simulation that includes drought stress. Likewise, we calculated the sensitivity of biomass accumulation to high temperature as:

$$S_{H\_RUE} = \frac{\left(B_{Temperature} - B_{Potential}\right)}{B_{Potential}} \times 100\% \quad (2.5)$$

in which $B_{Temperature}$ is the value from the simulation that only applied the temperature response curve to the RUE. The sensitivity of grain growth, and hence yield, to extreme heat was quantified as:

$$S_{H\_Grain} = \frac{\left(Y_{Heat} - Y_{potential}\right)}{Y_{Potential}} \times 100\% \quad (2.6)$$

where $Y_{potential}$ is the potential yield that considered stresses on biomass accumulation but not heat stress on grain set and grain fill, and Y_{Heat} was the actual yield. To run APSIM-Maize under a projected future climate, we used daily projections from 2006 to 2099 provided by The NASA Earth Exchange Global Daily Downscaled Projections (NEX-GDDP). This downscaled dataset in a spatial resolution of 0.25 degrees was derived from the general circulation models (GCMs) participating in the Coupled Model Intercomparison Project Phase 5 (CMIP5) under two of the four representative concentration pathways (RCPs). The effect of elevated CO_2 on maize growth was not simulated here, since it is beyond the scope of this study and the magnitude of maize yield response to CO_2 is controversial (Leakey et al., 2009). To reduce the computational cost, we selected projections for RCP4.5 and RCP8.5 from 8 representative GCMs (Table A2). The simulations conducted here were enough to extend the quantification of relative contributions of heat and drought stress into the future.

2.4 Results

2.4.1 Screening of heat stress functions

Temperature response curves of maize carbon assimilation differ markedly among selected crop models (Figure 2.2a). While some models use a single optimum temperature in their response curve (e.g. AgroIBIS and DayCent), others specify a wider range of temperatures (i.e., a plateau) for optimum or near optimum growth. AgroIBIS, EPIC and SWAT specify 25 °C as the optimal temperature for maize, beyond which heat stress starts to reduce photosynthesis. APSIM, DayCent and WOFOST use approximately 30 °C as the maximum optimal temperature. CERES and MAIZSIM, using daylight and hourly temperature as the forcing data, have even higher maximum optimal temperature of 33 °C and 32 °C, respectively. The upper limit temperature at which stress reaches its maximum differs substantially among models (Figure 2.2a). These differences are also reflected by the observed temperature responses of GPP to APAR ratio (as an approximation of RUE) (Figure A1). The optimal temperature range for hourly GPP/APAR is roughly 20 -31 °C, and the response curve is more like a piecewise linear function. For daylight GPP/APAR, the optimal temperature range is roughly 28-31 °C; this is probably why our simulations produce similar results when using daylight and hourly temperature to drive the algorithms. The optimal temperature for the daily mean GPP/APAR occurs around 25 °C (which agrees with Agro-IBIS, EPIC and SWAT), and the response curve is more like a quadratic function.

The predicted growing season average reduction in photosynthesis due to heat stress did not exceed 2% for most algorithms when forced by daily mean temperature, even in the years of 1988 and 2012, in which severe heat waves were recorded (Figure

2.3). Such predictions are likely unrealistic given the negative relationship between excess heat indicators (e.g. EDD and KDD) and maize yield. When heat stress is simulated using daylight temperature instead of mean daily temperature, yields simulated using all of the algorithms vary interannually with the heat stress factors, and become negatively correlated with EDD or KDD (Figure 2.3). Algorithms from APSIM, DayCent, EPIC, MAIZSIM and WOFOST have very high correlations ($r < -0.95$), followed by AgroIBIS ($r = -0.87$). The magnitude of reduction due to heat stress typically remained less than 5%, except for the EPIC simulation, which decreased by up to 10%. We also tested the effect of increasing simulation time frequency, in which the daily stress is calculated by averaging the every 3-hours prediction, and obtained results very close to simulations that use daylight temperature (not shown).

2.4.2 Screening of drought stress function

During the moist year of 2010 (May-August precipitation was 878 mm), algorithms that calculate stress factor as a function of SWC or Ws/Wd (SWC method and Ws/Wd method hereafter) predicted almost no drought stress, while the algorithm based on AT/PT (AT/PT method) predicted substantial stress over the growing season (Figure 2.4a). During the dry year of 2012 (May-August precipitation was 301 mm), all three methods indicated severe drought during the summer, although the magnitude of water shortage predicted by the Ws/Wd method was much greater than the other two methods (Figure 2.4b). The more severe drought predicted by Ws/Wd starting in July was likely caused by both the steady decrease in soil water supply and the persistent high transpiration demand (Figure A2).The AT/PT method indicated occasional water deficit in the early growing season, while the other two methods were unresponsive (Figure

2.4b). Mean annual drought stress varied substantially across years, fluctuating between 0.7 and 1.0 for years 1980-2013 (Figure 2.4c). The stress calculated by the SWC method closely resembled results from the Ws/Wd method ($R^2 = 0.9$), whereas the AT/PT method differed ($R^2 = 0.53$ with the SWC method and $R^2 = 0.67$ with the Ws/Wd method), consistently predicting more severe drought stress.

2.4.3 Comparison between algorithm ensembles

The ensemble simulations generally captured the inter-annual yield variability for the years 1980-2013 (Figure A3), with R^2 varying between 0.39 and 0.67, RMSE ranging from 1.089 to 1.557 t/ha, and Spearman correlation ranging from 0.2 to 0.6 (Figure 2.5). Compared to the very limited long-term historical simulations reported in peer-reviewed journals, our results are significantly better in matching the county-level yield statistics than Lobell et al. (2014) for Johnson, Iowa, using APSIM-Maize and Drewniak et al. (2013) for the whole US using CLM-Crop, but are close to the simulations given in Elliot et al. (2013). The improvement is mainly because we explicitly customized the simulations with yearly management information (e.g. planting date, density and fertilizer amount) according to the NASS database. Interestingly, using different drought stress algorithms had little effect on the model predictability, except that the AT/PT method produced slightly worse performance (e.g. SM2 and SM10; Figure 2.5a,b). Although mainstream drought stress algorithms produced quite different predictions for the seasonal pattern of water deficit (Figure 2.4), they displayed similar capability to represent drought on an annual basis.

Simulations from SM2, with the updated VPD algorithm, generally gave the worst model predictions (smallest R^2 and Spearman correlation, largest RMSE; Figure 2.5), but

outperformed all other simulations for the extreme drought year of 2012. Other simulations with the default VPD algorithm substantially underestimated yield by as much as 2.9t/ha in that year (Figure A3). Such systematic biases could be a result of the overestimation of VPD and hence crop water demand. In the current version of APSIM, the daily water-limited dry matter production, calculated as soil water supply × transpiration efficiency (TE), is inversely proportional to VPD (Text A3). The overestimation of VPD may lead to unrealistically high water demand and thus greatly overstates water deficits on exceptionally hot days (Basso and Ritchie, 2014). On the other hand, underestimating soil water supply when high VPD continuously depletes soil water could also overestimate the drought stress. Take the extreme dry year of 2012 as an example: weekly maximum VPD was almost 1.1 kPa higher when simulated by the default method than with the conventional method (Figure A6), which lowered TE and reduced biomass, as water supply was coincidently also exceptionally low. However, because the APSIM-Maize model has long been calibrated with the default VPD calculation route, simply changing the VPD algorithm will not guarantee an improvement in the overall model performance.

Using canopy temperature (SM3) instead of daily mean temperature to calculate heat stress lowered model performance at farms from Indiana (Figure 2.5) and Illinois (Figure A4) and slightly improved model predictions for the Iowa farm (Figure A5), possibly because the empirical canopy temperature model we adapted from STICS is only valid under a limited set of conditions. The simulated mean daily canopy temperature was generally higher than the air temperature measured at 2 m height, but mostly no more than 3°C (Figure A7), whereas the difference observed in rainfed fields

ranged from -2 to 7.5°C (Siebert et al., 2014). Switching between heat stress algorithms made little difference for predicted yield variability (i.e. SM1 vs. SM4-6), confirming that current crop models are insensitive to heat stress. Although it is difficult to recommend any algorithm over the others under contemporary climate conditions, crop modelers should keep in mind that these algorithms may diverge substantially when being used for future projections.

Simulations with the HI method consistently outperformed the others in terms of capturing the yield variability ($R^2 > 0.64$) and minimizing the prediction error (Figure 2.5). SM8 and SM9 performed slightly better than SM7, which used the PEGASUS algorithm, possibly because PEGASUS does not include water stress like the former two algorithms, but only considers heat stress around the silking-anthesis period when calculating the actual HI (Deryng et al., 2014). Potential HI for AquaCrop can be more conservative (e.g. 0.5 in this study), because AquaCrop has incorporated a mechanism through which crops generally produce excessive flowers to help recover once environmental constraints on pollination are ameliorated (Raes et al., 2009; Text A1). The parameter of potential HI for SWAT should be set slightly higher than for the other two models in order to get acceptable results (e.g. potential HI=0.55 in this study), since the HI in SWAT is often stressed more than that in the PEGASUS model and will not be compensated by additional flowers as in AquaCrop.

Last but not least, the leaf-level photosynthesis algorithm had a similar prediction bias (RMSE = 1.272 t/ha) and yield variability (R^2 = 0.54) as the RUE-based simulation (SM1 vs. SM10; Figure 2.5), despite its more complex model structure and heavier computational load (if solving coupled equations uses a numerical iteration method). It

should be noted that the Collatz model does not explicitly consider N limitation when calculating the gross CO_2 assimilation (Collatz et al., 1992), and is thus less responsive to the historical increase in fertilizer applications (Figure A3).

2.4.4 Past and projected heat and drought stress on yield

Yield losses at the Indiana farm due to climatic stress were attributed more to water deficits than sub-optimal temperatures (hot or cold; Figure 2.6), and thus the losses caused by excess heat were even smaller. The direct losses from higher-than-optimal temperature were mostly trivial and accounted for no more than 6% even in the notoriously hot years of 1988 and 2012, while the losses from water stress were more than 10% in several years and peaked at 30% in 2012. However, part of the water stress impact could be an indirect effect of high temperature, since warming increases water demand via elevating the VPD and at the same time decreases soil water storage by accelerating transpiration over short time periods (Lobell et al., 2013). Under projected future climates, the models suggest drought will continue to play a critical role in reducing the maize production at the Indiana farm, and the stress will intensify faster under the high emission scenario (Figure 2.7). Average biomass reduction due to drought will increase from 15% in the 2000s to 20% and 27% at the 2090s under RCP4.5 and RCP8.5 scenarios, respectively. The influence of high temperature on biomass accumulation is predicted to be small under RCP4.5, but becomes increasingly prominent after 2050s under RCP8.5. In a few years warmer climates increase yields, possibly because the positive effect of moderate warming on the rate of grain filling overcomes the negative effect on other processes. Extreme heat only occasionally damages simulated maize production in the first half of the 21st century, but reduces grain number and yield

with greater frequency and intensity after the 2050s, especially under the RCP8.5 scenario (Figure 2.7c). It should be noted, however, the relative importance of drought vs. heat is specific to the US Midwest, and may differ in more humid regions such as Europe.

2.5 Discussion

2.5.1 Lessons from review of algorithms

Heat stress functions can be effective when based on T_{mean}, daylight, or hourly temperature as long as they are parameterized correctly. However, it is very likely that a few models that base their temperature responses of RUE on T_{mean} actually have functions that were parameterized based on an hourly (or instantaneous) temperature response. For crop models that use daily T_{mean} to calculate heat stress factors, the optimal temperature threshold for algorithms should be smaller than algorithms using daylight or hourly temperature. The likely maximum optimal temperature for a T_{mean} function is around 25°C, which is smaller than the critical temperature threshold for maize growth (i.e. ~30°C) derived from large-scale statistics by Schlenker & Roberts (2009) and Lobell et al. (2013). Nonetheless, the literature-suggested temperature threshold is very close to the maximum optimal daylight or hourly temperature for RUE of 31-32°C. One follow-up concern is that these temperature thresholds may vary across space, given that the cultivars planted could be different from one place to another as a result of years of breeding and selection. While the spatial pattern of an optimal temperature threshold deserves further investigation, we also suggest that crop modelers consider replacing this type of hard-coded temperature threshold with uncertain parameters, to increase model agility (Mendoza et al., 2015).

The use of daylight temperature instead of instead of T_{mean} improves model performance by making heat stress algorithms responsive, likely because the current parameterizations of heat stress algorithms in most crop models that use daily mean temperature happen to be close to the RUE response curve to daylight temperature (Figure 2.2a and Figure A1). This simple modification is very easy to implement, and is further justified when the difference between 3-hr simulations and the use of $\frac{T_{max}+T_{mean}}{2}$ is very small on either a daily or an annual basis. Shortening the simulation time step certainly works because it allows the algorithm to reproduce the diurnal cycle of air temperature and hit those time points when temperature is significantly higher than the threshold. To control the computational cost, crop modelers would not have to run the whole model with higher time frequency, but could simply run the subroutine used to calculate stress factors.

The behaviors of drought stress algorithms were close to our expectations. In general, predictions made by the SWC method were less severe but smoother, possibly because the use of a multi-layer tipping-bucket model in the APSIM. As maize roots can normally penetrate to 1.5-2 meters depth and withdraw water throughout the whole soil profile (Hochholdinger, 2009), crop models often calculate water stress by averaging stress factors across all of the layers. However, simulated soil moisture of deep layers in many crop models normally had very small fluctuations, therefore minimizing simulated water stress for the whole soil column. The AT/PT method, which calculates potential transpiration with the Priestley-Taylor equation (Priestley & Taylor, 1972), showed substantial daily fluctuation, and tended to overestimate drought stress when there was no or mild soil water shortage. Sau et al. (2004) also reported that the use of Priestley-Taylor

equation tends to overpredict potential ET measured under irrigated and rainfed conditions in southern Spain, which reduces stress factors when AT is fixed, and therefore underestimates LAI, biomass and grain yield. The use of the FAO56 ET method (Allen et al., 1998) has been shown to perform better than the Priestley-Taylor method (Saseendran et al. 2008), but requires more detailed ground observational data as input. However, even if the calculation of PT can capture daily weather fluctuations well, how fast crops can respond to those fluctuations remains an open question. The Ws/Wd method, which is based on the concept of transpiration efficiency (Text A1), predicted little water stress during the cool early growing season, likely because Wd is small as a result of: (i) low VPD at low temperature and hence high TE; (ii) low dry matter accumulation rates given the low temperatures and less radiation interception in the early season. During the drought year of 2012, the Ws/Wd method predicted substantially more severe drought than the AT/PT method due to both high Wd values and low Ws (Figure A2). On the water demand side, APSIM tends to overestimate VPD during hot summers (Basso et al., 2014), thus results should be interpreted with caution during severe summer droughts.

2.5.2 Lessons from the ensemble simulation

The consistent underestimation of the yield increase trend by all simulations may be a consequence of simulating a single cultivar for the whole study period and in all of the different locations (Figure 2.5a). It is well established that farmers change cultivars very frequently, and cultivars vary substantially in their yield potential as a result of differences in traits such as relative maturity (Kumudini et al. 2014), light use efficiency (Tollenaar and Aguilera, 1992; Singer et al., 2011) and genetically modified stress-

tolerance (Xu et al., 2013). While such cultivar information is more difficult to obtain, crop modelers can inversely estimate spatiotemporal variations of cultivar-specific parameters against in-situ measurements. Given the very limited number of existing case studies (Sakamota et al., 2010; Jones et al., 2011; Archontoulis et al. 2014), this area deserves more research effort in the future.

Contrary to our expectations, the seemingly simple HI method outperformed more mechanistic methods that account for grain numbers and grain filling. A possible explanation is that the HI method has been parameterized based on historical agronomic data, and therefore can reproduce county-level yield statistics better than mechanistic approaches derived from field experiments. Moreover, when simulating maize yield with more mechanistic algorithms, climate variability has already been largely represented in the biomass estimates, so that additional steps to simulate grain number and grain-filling based on the concept of carbon source and sink lead to a greater uncertainty than obtained with the HI method. On the other hand, models that explicitly simulate kernel development can provide estimates of grain number, sugar and oil content, all of which are commercially valuable information (Borrás et al., 2002). In short, more complex and mechanistic algorithms are not necessarily better than simpler alternatives. The pros and cons of simple algorithms largely depend on the model application scale and variable of interest.

Although the leaf-scale photosynthesis model showed no apparent advantages in terms of predicting yield, it should be considered as a research frontier for next generation model development (Boote et al., 2013). The conventional RUE-based crop models have hit a bottleneck, in that they lack leaf-level physiological processes, and

hence cannot disentangle interactions between photosynthesis and many well-known regulating factors such as light, CO_2, leaf energy, leaf water and enzyme status (Lizaso et al., 2005). For example, elevated atmospheric CO_2 is believed to mitigate water stress in maize by reducing stomatal conductance and improving water use efficiency (Leakey et al., 2006; Hussain et al., 2013), but how much this will truly benefit yield is open to debate (Leakey et al., 2009; Boote et al., 2013; Urban et al., 2015). In fact, a negative feedback exists between improved water use efficiency and canopy temperature and VPD, because lower transpiration will reduce latent heat flux from canopy to the atmosphere, causing foliage temperatures to rise, which could again increase transpiration (Lobell et al., 2013). Improved crop modeling at the leaf scale that couples CO_2, water and energy is thus needed.

2.5.3 Reflections on crop model improvements

Overall, our analysis shows that algorithms from representative maize models do not adequately capture the impact of climate extremes on maize photosynthesis and yield. These conclusions are consistent with several other model comparison studies for cereal crops under various growth conditions (e.g. Asseng et al., 2013; Eitzinger et al., 2013; Bassu et al., 2014). Knowledge gaps and promising research frontiers for improving the predictability and credibility of current crop models have been discussed in a number of review papers (Boote et al., 2013; Parent and Tardieu, 2014; Barlow et al., 2015; Rezaei et al., 2015). Based on our analyses, we highlight the following three features that have not been well addressed in existing crop models.

First, crop models need better mechanisms to handle climate and weather extremes. Existing temperature and moisture response functions of many physiological processes

used by crop models to capture the climate variability are mainly summaries of observed historical statistics (Reichstein et al., 2013), and hence are questionable when used to fit novel climate conditions. For instance, the extremely high yield reduction predicted by the standard APSIM in the 2090s should be treated with caution, since it has not been validated at those novel bioclimatic scenarios. Regarding time scale, heat waves may happen very quickly – within a window of a few hours – and therefore is beyond the current simulation capacity of most crop models. CropSyst has recently incorporated a mechanism to discount biomass production when high temperatures last for more than 4 hours (Alderman et al., 2013). In addition, a perspective from ecosystem modeling suggests defining extreme climatic events as "an episode or occurrence in which a statistically rare or unusual climatic period alters ecosystem structure" (Smith, 2011). In this sense, crop models should go beyond the current continuous reduction functions and incorporate mechanisms to capture heat and drought stress that occurs singly, coincidently or when one follows another, and whose impact may or may not be reversible. Existing models only have very limited implementations for events-based simulation. For example, in APSIM-Maize high temperatures immediately following emergence will kill a fraction of plants. The implementation of a response of grain number set to heat extremes in APSIM and DSSAT is an early attempt to account for the carryover effect, although its parameterization is not adequately reliable due to limited experimental data. Other models, including CropSyst, GLAM, MONICA and PEGAUS, implement a reduction in HI when there is heat stress around the flowering stage.

Second, although the importance of considering canopy temperature in quantifying the heat stress impact has been emphasized quite often in recent years (Siebert et al.,

2014; Rezaei et al., 2015), potential losses from increasing nighttime temperature also deserve adequate attention. Nighttime warming has been shown to negatively affect plant growth across the Northern Hemisphere, because it boosts nighttime plant respiration that consumes carbon accumulated during daylight photosynthesis (Peng et al., 2013). Evidence also suggests that damage from nighttime heat stress is amplified during the reproductive phases, and that nighttime warming was partly responsible for the lower productivity and reduced kernel quality observed across the US Corn-Belt in 2010 and 2012 (Hatfield et al., 2014). With the number of hot nights projected to increase by as much as 30%, yield reductions will become more prevalent (Hatfield et al., 2011). However, none of the models we reviewed explicitly considered the direct impact of nighttime warming. Crop models with leaf-level photosynthesis algorithms can be easily adapted to account for nighttime heat (e.g. AgroIBIS, CSM-IXIM and MAIZSIM), although they have not been well parameterized and tested. MONICA also uses a mechanistic photosynthesis model, but its daily time step certainly obscured the signal of high nighttime temperature (Appendix A, Text A1). For models using the RUE approach, the nighttime temperature effect could be considered by incorporating a new limiting factor as a function of nighttime temperature when calculating the daily biomass accumulation, or by adding a reduction term elsewhere (e.g. when allocating the dry matter to grains).

Finally, the best way to coordinate multiple stresses needs further investigation. For those RUE-based models, the minimum of heat and drought stress factors is normally used to limit potential biomass production (e.g. APSIM-Maize, CropSyst, CSM-CERES

and SWAT), while a product of both is applied in PEGASUS and STICS. In some cases, VPD is further used to adjust the potential RUE or TE (e.g. APSIM, CropSyst, SWAT and GLAM). For leaf-level photosynthesis models, the temperature effect is supposed to be captured by the temperature dependency of each parameter, and water stress is reflected in the stomatal conductance. But AgroIBIS also adjusts maximum photosynthetic rate by a water stress factor, and MAIZSIM limits stomatal conductance by a function of leaf water potential. This variety of approaches begs the question: Do any or all of these forms lead to double accounting of heat and drought stresses? To our knowledge, no studies have answered this question. When simulating yield formation, either via grain development or the HI method, some models purely use heat or drought stress alone and some models use both (Table 2.1 and Table 2.2). Given that these crop models are individually developed and their main purpose is to predict biomass or yield variability, the inconsistency in the organization of these stress factors is quite understandable. However, this question should be answered because: (i) current models may give the right result but for the "wrong reasons", i.e., despite being based on unrealistic algorithms, and (ii) the lack of an answer hinders the assimilation of newly discovered stress mechanisms. One possible solution for mechanistic models is to compare intermediate model outputs (such as LAI, canopy level assimilation) to intermediate measurements (Boote et al., 2013), while for RUE-based models more efforts are needed.

In short, our study identifies the model formulations that best predict the impacts of heat and drought stress on maize biomass production and yield, and recognizes gaps to further reduce the prediction uncertainty. The framework presented here can be applied to

modeling other crop physiological processes and factors (e.g., phenology, chill and canopy transpiration), and used to improve yield predictions of other crops in a wide variety of crop models, thus is a significant advance in the crop modeling research.

Table 2.1 Summary of heat stress algorithm on maize photosynthesis, grain set/fillings and harvest index.

Model	Process	Model type	Input	Key parameters	Reference
AgroIBIS	Stomatal resistance	Quadratic	Tleaf	Topt[a]=25	Kucharik & Brye, 2003
APSIM	RUE	Multilinear	Tmean	Tbase[b]=8, Topt1=15, Topt2=30, Tlim[c]=44	Keating et al., 2003
	Grain number	Linear	Tmax	Tlim=38, Sensitivity=0.05	Carberry et al., 1989
	Grain filling	Linear	Tmean	Tcrt[d]=c(6, 10, 16, 22, 30, 56.3)	
AquaCrop	Harvest index	Logistic	Tmean	Topt2=30, Tlim=35	Raes et al., 2009
CERES-4.0	RUE	Multilinear	Teff	Tbase=6.2, Topt1=16.5, Topt2=33, Tlim=44	Jones et al., 2003
	Grain filling	Multilinear	Tmean	Tbase=5.5, Topt1=16, Topt2=39, Tlim=48.5	
CropSyst	Flowering	Multilinear	Thr	Tcrt=31, Tlim=44	Stöckle et al., 2013
DayCent	GPP	GPoisson	Tsoil	Topt=30, Tlim=45, Sleft=1, Sright=2.5	Parton, 1993
EPIC	RUE	Sinusoidal	Tground	Tbase=8, Topt=25	Sharpley & Williams, 1990
GLAM	Flowering	Multilinear	Tam	To be calibrated	Challinor et al., 2005
HYBRID-maize	Assimilation rate	Multilinear	Tday-time	Tbase=8, Topt1=18, Topt2=30	Yang et al., 2013
	Grain filling	Quadratic	T3hr	Topt=26	
CSM-IXIM	Assimilation rate	Complex	Thr		Lizaso et al., 2005
MAIZSIM	Carbon supply	Exponential	Thr	Td=48.6	Yang et al., 2009
	Grain filling	Quadratic	Thr	Topt=26	Grant 1989
MONICA	Assimilation rate	Multilinear	Thr		Sage & Kubien, 2007
	Flowering	Multilinear	Tday-time	Tcrt=30, Tlim=40	Moriondo et al., 2011
PEGASUS	LUE	Quadratic	Tmean	Tbase=0, Topt1=15, Topt2=40, Tlim=65	Deryng et al., 2011
	Flowering	Multilinear	Teff	Tcrt=32, Tlim=45	Deryng et al., 2014
STICS	RUE	Quadratic	Tleaf	Tbase=2.5, Topt1=10, Topt2=30, Tlim=30	Brisson et al., 2009
	Grain filling	Multilinear	Tleaf	Tbase=5, Topt1=6, Topt2=26.5, Tlim=27.5	
SWAT	RUE	Exponential	Tmean	Tbase=8, Topt=25	Neitsch et al., 2011
WOFOST	Assimilation rate	Multilinear	Tday-time	Tcrt=c(0, 9, 16, 18, 20, 30, 36, 42)	Supit et al., 1994

[a]Topt: optimum temperature above or below which stress will occur; a non-stress plateau is assume for curves with two optimum temperatures (e.g. Topt1 and Topt2). [b]Tbase: base temperature below which full stress is assumed. [c]Tlim: limiting temperature threshold at which full heat stress is reached. [d]Tcrt: critical temperature threshold at which heat stress starts.

Table 2.2 Summary of drought stress algorithm on maize photosynthesis, grain set/fillings and harvest index.

Model	Process	Conceptual	Function type	Reference
AgroIBIS	Photosynthesis rate (Vmax)	SWC	exponential	Kucharik & Brye, 2003
APSIM-Maize	RUE	Ws/Wd	linear	Keating et al., 2003
	Grain filling	Ws/Wd	linear	
AquaCrop	Stomatal closure	SWC	convex curve	Raes et al., 2009
	Harvest index	Complex subroutines		Raes et al., 2009
CERES-Maize	RUE	AT/PT	linear	Lopez-Cedron et al, 2005
	Grain filling	AT/PT	quadratic	Lopez-Cedron et al, 2008
CropSyst	Water dependent growth	Transpiration efficiency		Stöckle et al., 2013
	Harvest index	Stage-dependent average water stress	linear	
DayCent	GPP	Available water to PET	linear	Parton et al., 1993
	Carbon allocation	Soil water content	empirical	
EPIC	RUE	Wu/PT	linear	Sharpley & Williams, 1990
	Harvest index	Wu/PT	convex curve	
GLAM	Transpiration efficiency	Transpiration efficiency		Challinor et al., 2004
HYBRID-maize	Assimilation rate	AT/PT	linear	Yang et al., 2013
CSM-IXIM	Carbon allocation	AT/PT	exponential	Lizaso et al., 2011
MAIZSIM	Stomatal conductance	Leaf water potential	logistic	Yang et al., 2009
	Carbon allocation	SWC	linear	Acock et al., 1982
MONICA	Assimilation	AT/PT	linear	Sage & Kubien, 2007
PEGASUS	LUE	SWC	exponential	Deryng et al., 2011
STICS	RUE	SWC	linear	Brisson et al., 2008
SWAT	RUE	AT/PT	linear	Neitsch et al., 2011
	Harvest index	AET/PET	linear	
WOFOST	Assimilation rate	AT/PT	linear	Supit et al., 1994

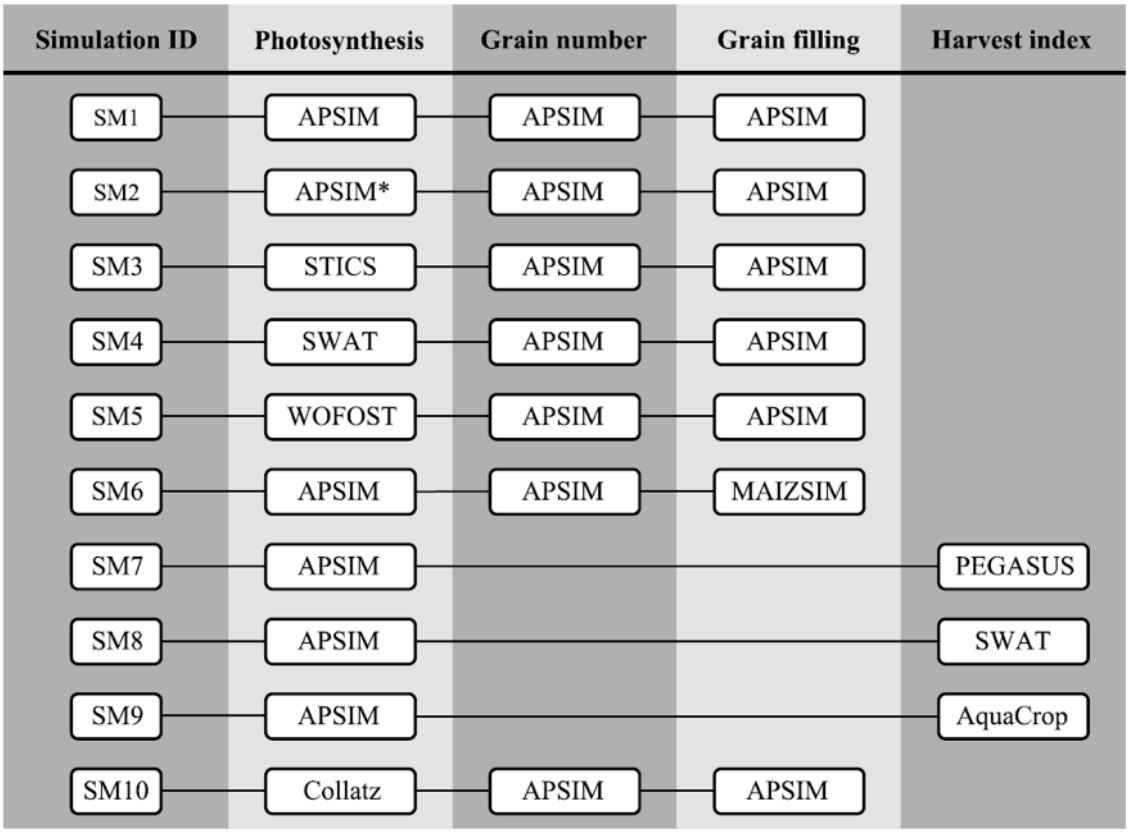

Figure 2.1 Framework for using ensemble simulations to compare algorithms at the process level. Heat stress algorithms for each process (i.e. photosynthesis, grain number development, grain-filling rate and harvest index increment) are listed as bricks. The combination of different bricks for all processes evaluated leads to a simulation (SM).

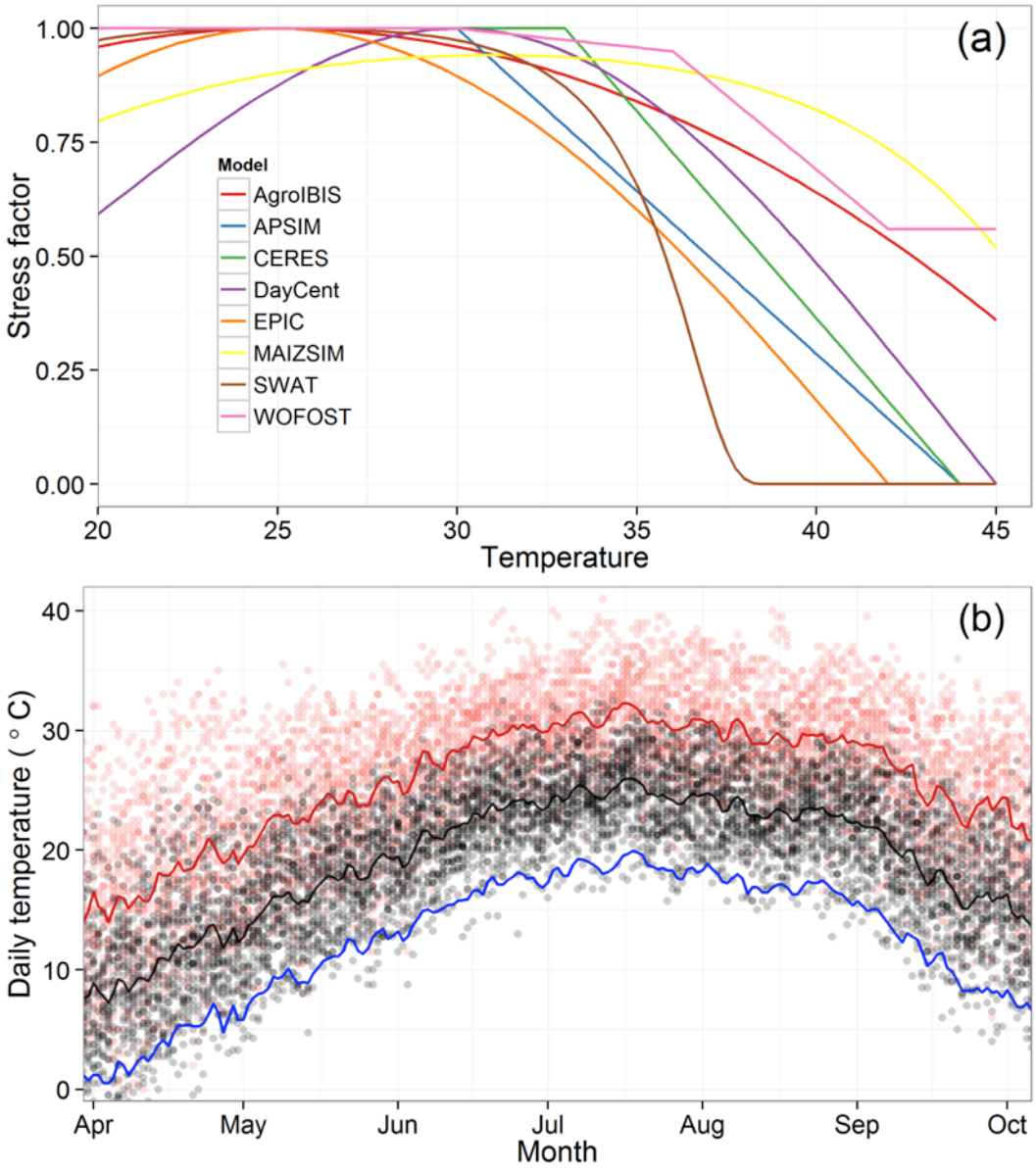

Figure 2.2 (a) Temperature response curves used in representative crop models. (b) 34-year (1980-2013) averaged growing season daily maximum (red line), mean (black) and minimum (blue) temperature for the Indiana farm in this study. Red and black dots are daily maximum and mean temperatures for all years, respectively.

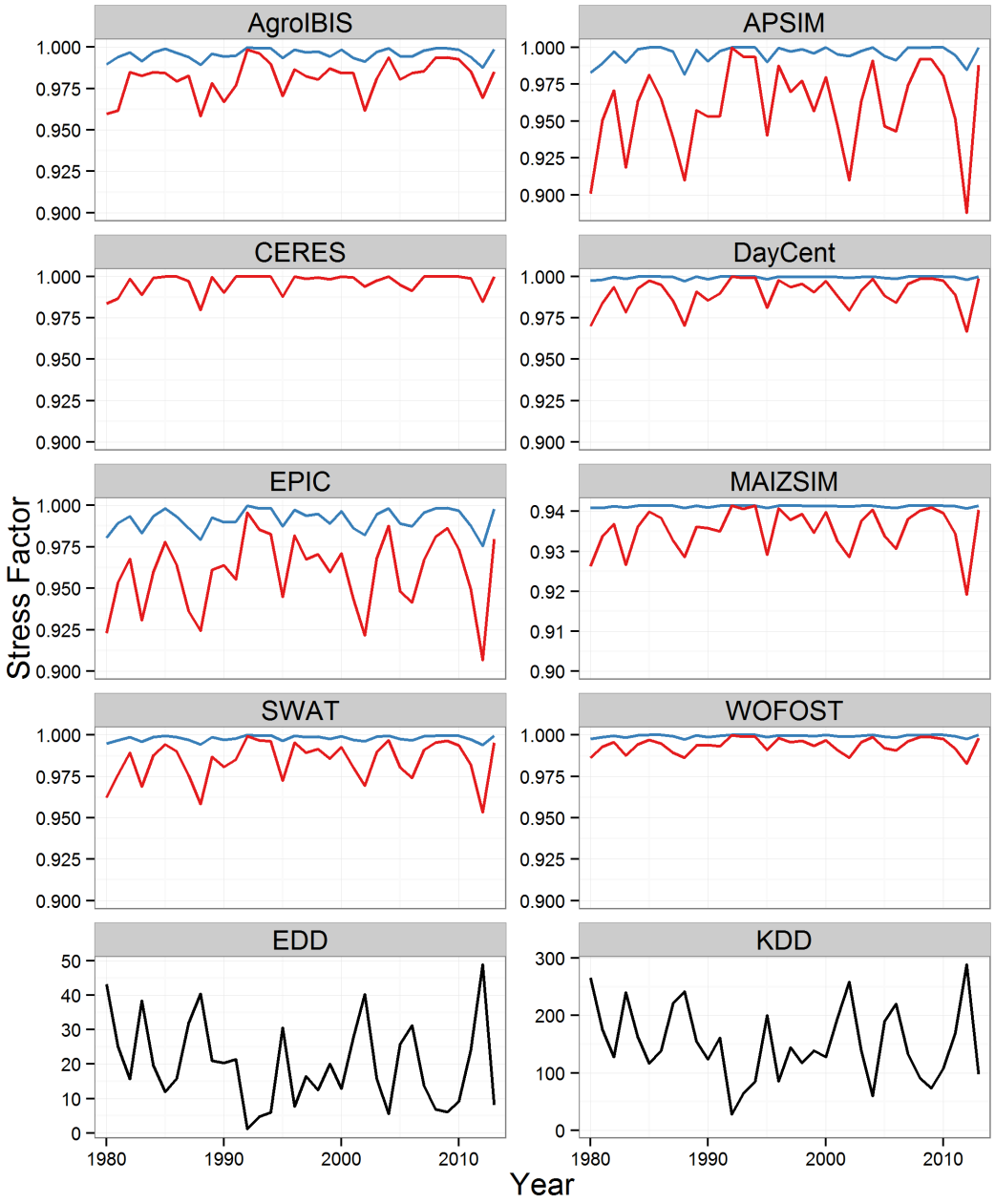

Figure 2.3 Effect of the temperature forcing data of algorithms on their predictions of mean annual heat stress (1 for no stress and 0 for full stress) for the Indiana farm. Simulations using daily mean temperature are shown as blue lines, and simulations with daylight temperature are shown as red lines. Note that AquaCrop's algorithm is on a different scale than those from the other models. Indexes of excessive heat, namely extreme degree days (EDD) and killing degree days (KDD) (Text A3), are given for reference.

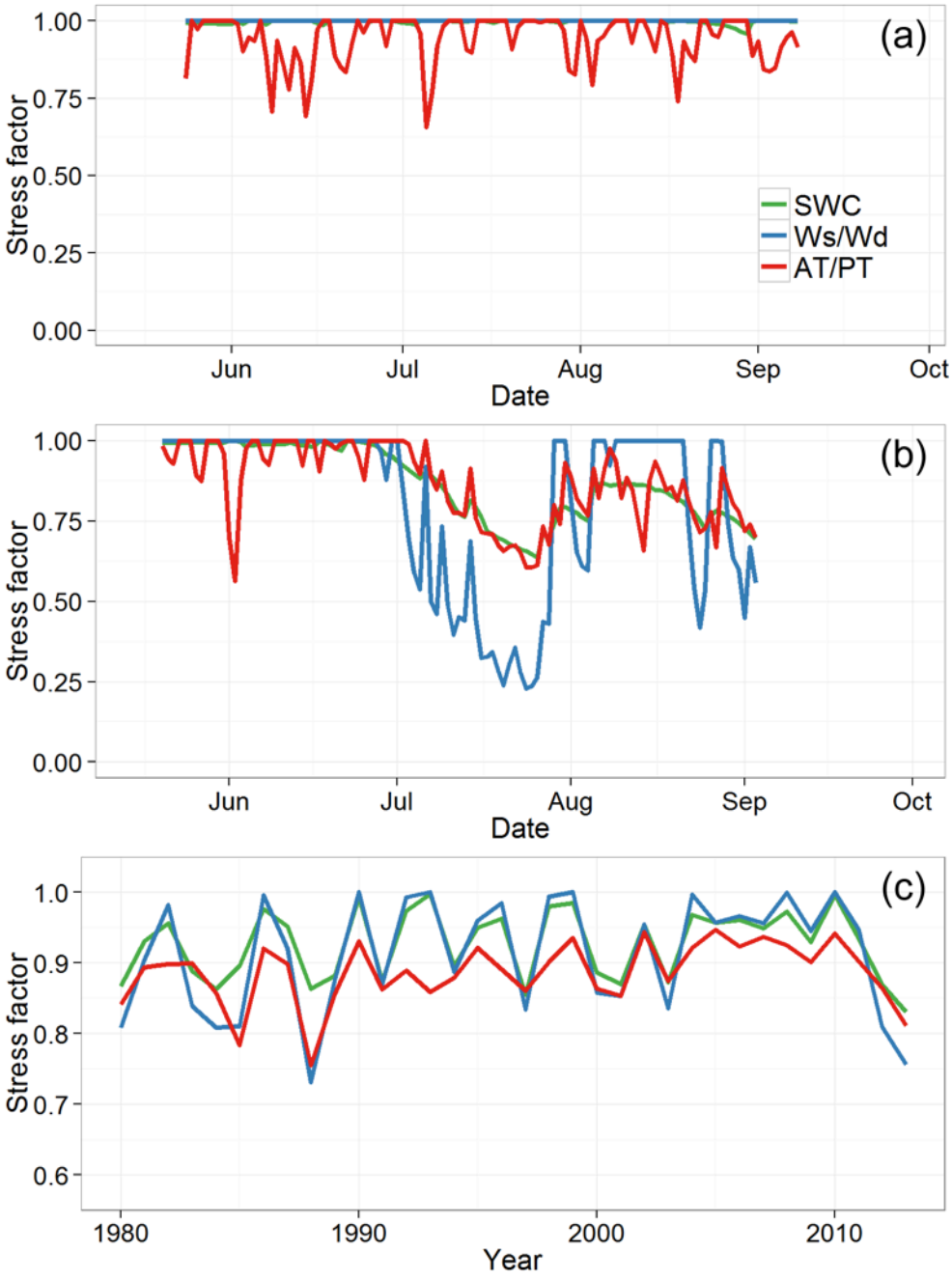

Figure 2.4 Drought stress (1 for no stress and 0 for full stress) for the Iowa farm as predicted by different drought stress algorithms. Seasonal dynamics of daily stress factors for the moist year of 2010 (a) and the drought year of 2012 (b). (c) Inter-annual variability of mean growing season stress factors from 1980 to 2013.

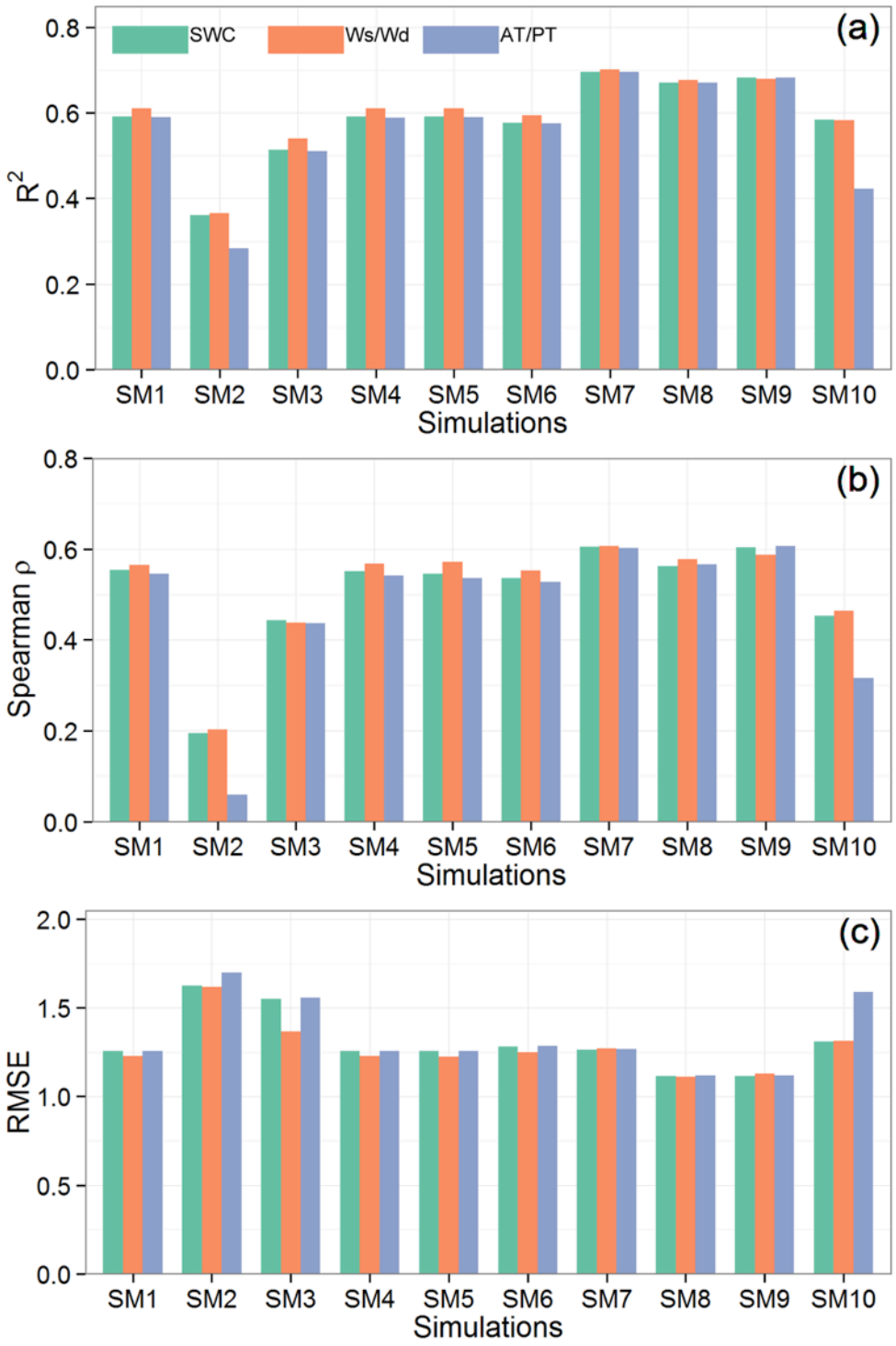

Figure 2.5 Simulated annual yields by 30 simulation trials (10 heat × 3 drought stress algorithms) for the Indiana farm from 1980 to 2013. See Figure 2.1 for detailed algorithm combinations for each ensemble. Yield trend derived from USDA NASS county level statistics is denoted by the black dashed line.

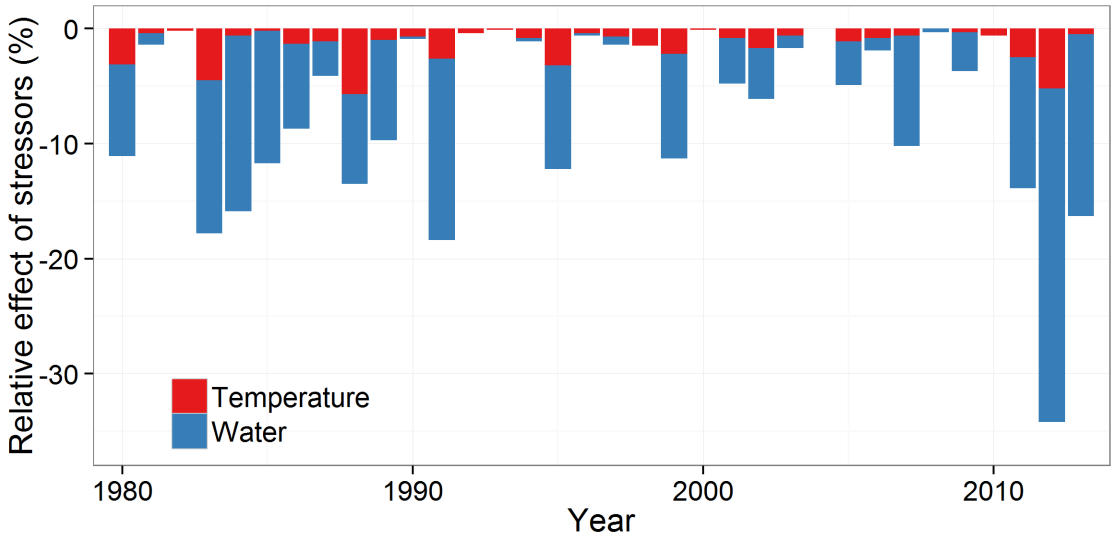

Figure 2.6 Percentage yield reduction attributed to temperature and water stress on the Indiana farm from 1980 to 2013, as simulated using the standard APSIM-Maize model.

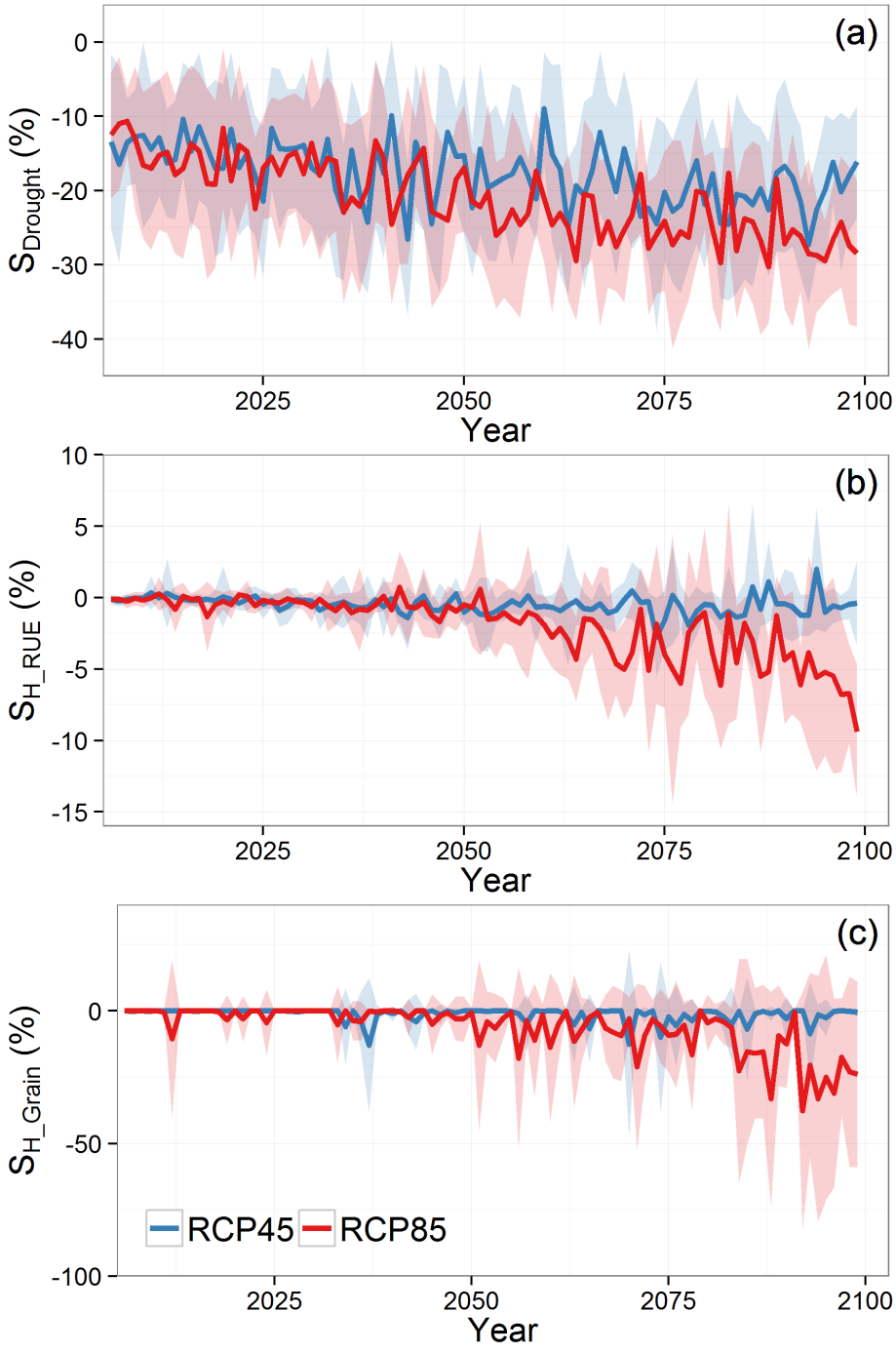

Figure 2.7 The effects of drought (a), high temperature via photosynthesis (b) and heat via grain development (c) on maize yield for the Indiana farm under two Representative Concentration Pathway (RCP) scenarios. Solid lines are mean predictions from eight General Circulation Models (GCMs), and shaded areas represent one standard deviation.

CHAPTER 3. ASSESSING THE IMPACTS OF HEAT AND DROUGHT STRESS ON THE US MAIZE AND SOYBEAN PRODUCTION

3.1 Introduction

The negative impact of high temperature on crop production, commonly referred to as "heat stress", has been identified for maize and soybean with sufficient evidence (Prasad et al., 2008; Schlenker and Roberts, 2009; Djanaguiraman et al., 2011; Lobell, et al., 2013; Rezaei et al., 2015). A number of mechanisms could potentially explain the observed relationship, including but not limited to: sensitivity of anthesis-silking period to high temperature (Bolanos and Edmeades et al., 1996), declines in net photosynthesis (Prasad et al., 2008; Rezaei et al., 2015), hastening leaf senescence (Parent and Tardieu, 2012), and changes atmospheric water demand and soil water supply (Lobell et al., 2013, 2014). Drought, often defined in an agronomic perspective as insufficient water supply for plant growth demand, can adversely affect crop growth and yield through limiting leaf expansion and senescence, photosynthesis, carbon allocation, yield formation, and growth of rooting system (Prasad et al., 2008; Saseendran et al., 2014). The productions of maize and soybean in the US rainfed system are susceptible to heat and drought stress (Mellilo et al., 2014), although maize in the US Midwest has become more sensitive to drought than soybean for the past two decades as a result of a higher increasing trend in the seeding rate (Lobell et al., 2014). Substantial increase in concurrent heat and drought has been observed in the contiguous US since 1950s (Mazdiyasni & Aghakoucha, 2015),

causing greater agricultural risks compared with years when these events occur singly or one follows another. The critical role of extreme heat for the US maize and soybean appears to be a result of its nonlinear effect on vapor pressure deficit (VPD), as high VPD not only exacerbates short-term water demand but also lowers future soil water supply (Lobell et al., 2013, 2014; Urban et al., 2015). Although heat and drought stress seems to be intertwined with each other, distinguishing whether the yield losses are due to heat or drought is important for developing comprehensive strategies for breading and field management when farmers have to cope with between both stresses (Lobell et al., 2015).

Elevated atmospheric carbon dioxide (CO_2) further complicates the quantification of heat and drought stress on maize and soybean growth. By reducing the stomatal openness, elevated CO_2 leads to decreased crop transpiration and increased soil moisture storage (Long et al., 2006; Bernacchi et al., 2007; Leakey et al., 2009; Bunce, 2014; Madhu & Hatfield, 2014), thus ameliorating the potential drought stress and benefit the yield (Leakey et al., 2006; Hussain et al., 2013; Lobell et al. 2015; Urban et al., 2015). Nonetheless, the reduction in canopy latent heat as a result of less water fluxes will elevate the leaf temperature and stress the photosynthetic apparatuses (Bernacchi et al., 2005; Long et al., 2006; Twine et al., 2013). Crops grown under elevated CO_2 may express higher thermotolerance of photosynthesis, but are more likely for C3 (e.g. soybean) rather than C4 (e.g. maize) species (Taub et al., 2001; Wang et al., 2007). On the other hand, CO_2 directly stimulates the C3 photosynthesis and compensates a portion of the climate-induced yield losses (Long et al., 2006; Bishop et al., 2015). This so called CO_2 fertilization effect is anticipated because major C3 crops are CO_2-starving under the

current atmosphere (Chapin et al., 2011), and elevated CO_2 can increase their radiation utilization and net photosynthesis by raising the intercellular CO_2 substrate and inhibiting the competing photorespiration (Long et al., 2006; Dermody et al., 2008; Leakey et al., 2009). For C4 crops that are CO_2-saturated under current atmosphere, the effect of rising CO_2 on yield is more controversial, such that earlier enclosure studies reported significant fertilization effect and more recent Free-air concentration enrichment (FACE) experiments concluded small responses (Long et al., 2006; Ainsworth et al., 2008). The stimulation of maize yield is likely to be prominent only under drought conditions (Leakey et al., 2006; Twine et al., 2013).

Process-based crop models are powerful tools for investigating the complex interactions among heat, drought and elevated CO_2, although the quantitative relationships between yield and these factors remain uncertain (Lobell et al., 2013; Bassu et al., 2014; Rosenzweig et al., 2014). Twine et al. (2013) simulated the surface energy budget of maize and soybean in the US Midwest with the Agro-IBIS model, and found elevated CO_2 from 375 to 550 ppm suppressed canopy latent heat flux but increased sensible heat flux for both crops, which ameliorated drought stress and stimulated soybean yield of ca. 10% averaged over 30 years and maize yield of ca. 10% during dry years. A recent study that applied the PEGASUS model with 72 climate change scenarios showed that elevated CO_2 substantially counteracted the extreme heat stress during the crop reproductive phase by the 2080s (Deryng et al., 2014). By using the Agricultural Production Systems Simulator (ASPIM) at representative sites in the Northeastern Australian, Lobell et al. (2015) concluded that elevated CO_2 increased sorghum (a C4 species) transpiration efficiency (TE) and partially offset the drought exacerbated by the

concurrent rising VPD during the 21st century; warming relieved spring drought for winter wheat (a C3 species) by hastening the phenological progress, while elevated CO_2 further benefit the yield by increasing both radiation-use efficiency (RUE) and TE. However, existing modeling studies are too limited to draw robust conclusions on the crop responses to future heat and drought stresses. More efforts are thus needed to quantify these complex interactions at different geographic domains and with various spatial details.

In this study, we use the APSIM, driven by high-resolution (12 km) Weather Research and Forecasting (WRF) Model (version 3.3.1) downscaled future climate scenarios, to investigate the impacts of future climate extremes on the US maize and soybean production. Specifically, we answer the following questions: (i) How do future climate extremes affect the US corn and soybean yield? (ii) How do climate extremes shift in their relative importance and geographic distributions? (iii) How much can CO_2 fertilization compensate the yield loss caused by climate extremes? (iv) How do the high resolution-driven APSIM simulations differ from existing estimates driven by coarse resolution climate model?

3.2 Materials and methods

3.2.1 Quantify heat and drought stress

In APSIM, heat and drought stress can cause yield losses through limiting the photosynthesis and reproductive growth, while indirectly through affecting other physiological processes such as phenology development, canopy expansion, and nitrogen cycling. The feedbacks among these processes can be complex and hard to coordinate

(Parent & Tardieu, 2014), and often lack of empirical data to verify. Therefore in this study, we only focus on the direct impact of heat and drought stress on maize and soybean production.

As the start point of yield modeling, daily biomass accumulation (ΔB) is the minimum of light (ΔB_r) and water (ΔB_w) limited photosynthesis. The light-limited biomass production based on the concept of radiation use efficiency (RUE) is calculated:

$$\Delta B_r = I \times RUE \times min\{f_{T,photo}, f_{N,photo}, f_{P,photo}\} \tag{3.1}$$

where I ($MJ\ m^{-2}$) is the solar radiation intercepted by the canopy, RUE ($g\ MJ^{-1}$)is crop-specific and stage-dependent constants; $f_{T,photo}$, $f_{N,photo}$ and $f_{P,photo}$ are temperature, nitrogen and phosphors stresses on photosynthesis, respectively. The temperature stress, $f_{T,photo}$, is a trilinear function of the daily mean temperature:

$$f_{T,photo} = \begin{cases} 0, & otherwise \\ 1 - \dfrac{T_{opt1} - T_{mean}}{T_{opt1} - T_{min}}, & if\ T_{min} < T_{mean} < T_{opt1} \\ 1, & if\ T_{opt1} \le T_{mean} \le T_{opt2} \\ \dfrac{T_{max} - T_{mean}}{T_{max} - T_{opt2}}, & if\ T_{opt2} < T_{mean} < T_{max} \end{cases} \tag{3.2}$$

in which parameter values for the US Midwest based on literatures (Prasad et al., 2008; Schlenker & Roberts, 2009; Parent & Tardieu, 2014; Rezaei et al., 2015) are [T_{min}, T_{opt1}, T_{opt2}, T_{max}] = [8, 15, 29, 44] for maize and [T_{min}, T_{opt1}, T_{opt2}, T_{max}] = [10, 20, 30, 40] for soybean. Water stressed biomass production is calculated as:

$$\Delta B_w = \Delta B_r \times min\left\{\frac{W_s}{W_d}, 1\right\} \tag{3.3}$$

where W_s is the potential daily soil water uptake through the multi-layer soil profile, and W_d is the transpiration water demand calculated as the ratio of ΔB_r ($gC \cdot m^{-2}$) and TE

($gC \cdot m^{-2} \cdot mm^{-1}$). TE is determined by the VPD and a crop-specific transpiration efficiency coefficient (TE_c):

$$TE = TE_c / VPD \tag{3.4}$$

in which TE_c is a constant of 0.009 KPa for maize and 0.005 KPa for soybean when atmospheric CO_2 is 350 ppm. Since the calculation of VPD is temperature dependent, a strong interaction between temperature and water stress exits in the model structure.

The yield production is then estimated based on the dry matter supply (i.e. biomass allocation) and demand (determined by the kernel number and kernel filling rate) for maize, and the harvest index (HI) for soybean. In the *Maize* module, heat stress reduces the kernel number per ear in proportion to the accumulated degree days above 38 °C during the flowering phase (Carberry et al., 1989). High temperature also slows down the kernel filling rate, with optimal filling at 30 °C and complete stop at 56.3 °C. The kernel filling rate is further reduced by a soil water stress factor ($f_{SW,kernel}$), such that:

$$f_{SW,kernel} = 0.45 + 0.55 \times min\left\{\frac{W_s}{W_d}, 1\right\} \tag{3.5}$$

For soybean, the daily potential increase in HI is adjusted by an energy cost to synthesize the oilseeds but not any direct heat stress. In this study, we add a stress factor (f_{HSA}) to account for the impact of heat stress during the flowering period on the HI following Deryng et al. (2014):

$$f_{HSA} = \frac{1}{TSP} \sum_{1}^{TSP} f_{HSAd} \tag{3.6}$$

where TSP is the thermal sensitive period from $min\{0.45\ GPL,\ flowering\}$ to

$max\{0.7\ GPL,\ flowering\}$; GPL is growing period length defined as emergence to maturity; the daily heat stress scalar, f_{HSAd}, is calculated as:

$$f_{HSAd} = \begin{cases} 1, & if\ T_{eff} < T_{cr} \\ 1 - \dfrac{T_{eff} - T_{cr}}{T_{lim} - T_{cr}}, & if\ T_{cr} \le T_{eff} < T_{lim} \\ 0, & if\ T_{eff} > T_{lim} \end{cases} \quad (3.7)$$

in which T_{cr} and T_{lim} is 35 and 40 °C, respectively; T_{eff} is the daytime effective temperature approximated by the average of daily mean and maximum air temperature.

To quantify contributions of heat and drought stress to yield losses, we regroup these stresses and introduce three switches to control the inclusion of each group. The first switch regulates the inclusion of high temperature stress (f_{Temp}), which refers to the condition with higher-than-optimal temperature that reduces the RUE of both crops and kernel filling rate of maize. The second switch controls the inclusion of heat stress around the flowering phase (f_{Heat}), which imposes restriction on the development of maize kernel number and soybean HI. The third switch is for drought stress ($f_{Drought}$), which limits the RUE of both crops and the kernel filling of maize. For a give group of stress, its impact is calculated by:

$$Stress\ impact(\%) = \left(Yield_{S,off} - Yield_{potential}\right)/Yield_{potential} \quad (3.8)$$

where $Yield_{S,off}$ is the simulated yield after switching off the corresponding stress, and $Yield_{potential}$ is the simulated yield when switching off all stresses.

3.2.2 Simulate maize and soybean responses to elevated CO_2

The projected atmospheric CO_2 by 2090 is 534 ppm under the Representative Concentration Pathway 4.5 (RCP4.5) scenario (Wise et al., 2009), and 845 ppm under

RCP8.5 (Riahi et al., 2007). Accordingly, we adjust the maize transpiration efficiency coefficient to 0.0106 KPa for RCP4.5 scenario and 0. 0135 KPa for RCP8.5 following Lobell et al. (2015), which approximately equals 10.6% increase per 100 ppm. We use the multi-year averaged values from soybean FACE (SoyFACE) (Bernacchi et al., 2005, 2007) to derive soybean TE_c and RUE by 2090 under RCP4.5, because the CO_2 manipulation of 550 ppm at SoyFACE is very close to the CO_2 value of 534 ppm by 2090. In this case, TE_c increases by 9.2% to 0.00546 KPa and RUE increases by 16.7% to 1.02 g/MJ. For RCP8.5 scenario, we interpolate values from the mean of multiple enclosure experiments that have raised CO_2 level closer to the projected value of 845 ppm (Table 3.1). Because TE_c and RUE are not directly measured by most of the SoyFACE and enclosure studies, we derive the values from two conceptually similar measures that are available from the literature. Specifically, we approximate the percentage change of stomatal conductance to water vapor (g_s) for TE_c, and changes in the none-stressed leaf photosynthesis rate (A_{sat}) for RUE (see discussion for justification). In this case, TE_c increases by 36.1% to 0.0068 KPa and RUE increases by 39% to 1.22 g/MJ.

3.2.3 APSIM regional simulation

The point-based APSIM was run for both rainfed maize and soybean at a spatial resolution of 10km for two contrasting time slices: (i) 1995-2004; (ii) 2085-2094 (under RCP4.5 and RCP8.5 scenarios, respectively). Geographic distributions of non-irrigated maize and soybean are derived from the 5 arc-minute resolution M3-Cropland data (Ramankutty et al., 2008). To reduce the computational load, we only include grid cells if maize or soybean covers more than 5% of the area. In total, we obtain 33254 grids for maize and 29019 grids for soybean.

Meteorological inputs for the APSIM, including daily maximum and minimum temperature, precipitation and solar radiation, are generated by a 12 km regional climate model (WRF) which uses the original Community Climate System Model version 4 (CCSM4) data from the fifth phase of the Coupled Model Intercomparison Project (CMIP5) archive as the initial and boundary conditions (Wang & Kotamarthi, 2015). We name the regional climate model as WRF-CCSM4 hereafter. As is noted by Wang & Kotamarthi (2015), driving the WRF with the bias-corrected CCSM4 did not always outperform the downscaling without bias-correction, especially for the precipitation over the US Midwest where most of the rainfed maize and soybean grow.

Spatially explicit information on soil, crop cultivar and management is critical for APSIM regional simulations. Soil parameters, such as soil texture, layered soil hydraulic properties and soil organic matter fractions, are extracted from the 1:250,000 U.S. General Soil Map (STATSGO2) database. The description for each of these required soil parameters is documented in Archontoulis et al. (2014a). For a given grid, it may cover multiple soil map units according to STATSGO2, and each map unit normally contains more than one component that stores layer specific soil parameters. To balance the computational cost and soil heterogeneity, we only consider soil map units that take more than 5% of the 10×10 km grid area, and the largest component within each soil map unit. When doing the simulation, our script will run APSIM for each of major soil map units and calculate the area weighted average yield for the grid. Management activities for the historical period of 1995-2004, includes seeding rates and fertilizer amount, are from the USDA National Agricultural Statistics Service (NASS) survey report at state level (Table A1). Crop sowing date is derived from the Crop Calendar Dataset (Sacks et al., 2010).

For maize, we select the Pioneer_P04612XR_106, a representative cultivar in the US Midwest that was parameterized by Archontoulis et al. (2014a), for the whole study area. For soybean, APSIM version 7.7 provided totally 54 US cultivars for major production states, which are parameterized by Archontoulis et al. (2014b). We assume the same spatial information for future scenarios of 2085-2094 as the baseline simulation, thus excluding the potential of agronomic improvement on crop adaptation and mitigation.

3.2.4 Analysis

To validate the regional APSIM application, we aggregate the simulated annual maize and soybean yield into county average and compare to the NASS reported county-level rainfed crop yield for years 1995-2004. Because of the bias that WRF-CCSM4 has, it is not surprising that the WRF-CCSM4 driven APSIM shows bias from historical survey data as well. To further check the performance of APSIM over the US Midwest, we compared the baseline simulation for the US core Corn Belt (i.e. Illinois, Indiana and Iowa) to another set of historical simulations using the Daymet reanalysis data (http://daymet.ornl.gov/). We use quantile regression (Koenker & Bassett, 1978) instead of the ordinary least square regression to quantify the sensitivity of maize and soybean yields to future climate extremes. Such an implementation is essential in order to identify the sensitivity and vulnerability of crop yield to climate change cross a large geographic span. For example, places with high yield losses may have higher sensitivity to excessive heat due to the interactions between crop water supply (approximated by precipitation) and demand (regulated by temperature induced VPD change).

3.3 Results

3.3.1 Model evaluation

The simulated mean decadal maize yield for 1995-2004 ranges from 2.9 to 13.1 t/ha, with high yield occurs at some counties from the core Corn Belt and low yield occurs at the edge of the Midwest (Figure 3.1). For soybean, the simulated yield ranges from 0.6 t/ha at the US Southeast to 4.2 t/ha at the core Corn Belt. In general, our simulations successfully capture the spatial pattern of NASS reported county-level rainfed maize and soybean yield. The maize simulation slightly underperforms the soybean simulation in capturing the NASS variations (R^2=0.44 for maize versus R^2=0.61 for soybean), but is 30% less biased in terms of the relative root mean squared error (RRMSE) (RRMSE=0.19 vs. RRMSE=0.26).

Simulated maize and soybean yields are less satisfying in reproducing the NASS survey data for all location × year combinations (R^2=0.26 for maize versus R^2=0.3 for soybean), but can be substantially improved by substituting the WRF-CCSM4 climate data with Daymet (Figure B1) when doing the regional simulation. The improvements indicate that APSIM is able to reproduce both the mean yield and interannual variability given high quality climate forcing data, whereas using downscaled global climate model (GCM) outputs inflates the simulation uncertainty. Since the focus of this study is to assess changes in current and future crop yield, and APSIM simulations can reasonably reproduce the decadal surveyed data, we believe the analysis presented in the following sections based on the APSIM model driven by WRF-CCSM4 data is reasonable.

3.3.2 Projected changes in climate and yield

Compared with the period of 1995-2004, decadal mean maximum growing season temperature (*Tmax*) during 2085-2094 is projected to increase by 1.5-4.5 °C under RCP4.5 scenario and 3.5-6 °C under RCP8.5 scenarios (Figure 3.2a,b). Warming is most prominent at the US Midwest under both scenarios, thus strikes much of the major maize and soybean planting area. Projected summer precipitation (*sumPrec*) regime differs between two scenarios for the Midwest (Figure 3.2c,d), where rainfall decreases up to 150 mm under RCP4.5 and increases roughly 50-150 mm under RCP8.5. Wet trend is projected for the Northeast and Southeast under both scenarios, with RCP8.5 projecting roughly 100 mm more precipitation amount than RCP4.5. Changes in maximum weekly mean VPD (*VPDmax*) are slightly higher under RCP8.5 than under RCP4.5. Possibly due to the drying trend occurred at the Midwest under RCP4.5, the core Corn Belt states (especially Iowa) experience the most substantial increase in *VPDmax*; whereas for RCP8.5, regions with maximum change move towards southwest.

In response to the spatial pattern of projected climate change, maize yield under RCP4.5 decreases mostly by 10-40% at the Midwest where warming and drying are concurrent, and increases by 0-20% for states eastern than Illinois where the magnitude of warming is moderate and wetting is projected (Figure 3.1 and Figure 3.3a). Maize yield gain is on average 10% higher under RCP8.5 than RCP4.5, and yield loss under RCP8.5 is less for states at the western part of the Midwest (e.g. Illinois, Iowa and Minnesota) (Figure 3.3b). Interestingly, although RCP4.5 projects less rainfall at some part of eastern Midwest (i.e. Indiana, Michigan and Ohio), these states still receive a slight yield gain at the late 21st century. We argue that it is because water supply is

excessive for these states, whereas temperature is limiting the historical maize production. Moreover, since the yield of US maize increases with temperature up to 29 °C, moderate warming under this threshold may benefit maize growth (Schlenker & Roberts, 2009). Region with yield losses is accompanied by increases of interannual yield variation for both climate scenarios (Figure 3.3c,d), indicating future agricultural challenges not only include the drop in absolute predictability but also the loss of yield stability.

Most of the soybean producing area suffers from yield losses of more than 20% under both RCP4.5 and RCP8.5 scenarios (Figure 3.4a,b). The spatial distribution of negative trends is primarily dominated by the increase of heat extremes and atmospheric transpiration demand (indicated by VPD), with decreased precipitation plays a secondary role. In general, the increase of interannual yield variability under RCP4.5 is higher for regions with more yield losses, but not comparable with yield changes under RCP8.5 (Figure 3.4c,d).

3.3.3 Effects of elevated CO_2 on yield

For maize, elevated CO_2 alleviates the yield loss under RCP4.5 and shifts some regions with yield loss into yield gain, but does not benefit regions that have already showed yield gain (Figure 3.3). This phenomenon is further verified by the violin plot (Figure 3.5a,b), in which the distribution of yield change under RCP4.5 shrinks at low quantile but is almost the same at high quantile. A possible explanation is that regions with yield gain when excluding the CO_2 effect are not stressed by drought, and hence CO_2-induced water conservation does not benefit the yield production. This finding is consistent with the empirical evidence that maize has little to gain in the absence of water stress (Leakey et al., 2006). The CO_2 fertilization effect is more prominent under RCP8.5,

which reduces the proportion of high yield losses and raise the number of pixels with yield gain from 29% to 61% at the core Corn Belt (Figure 3.5a,b). Elevated CO_2 also moderates the decadal yield coefficient of variations (CV) under both climate scenarios, and is more effective in reducing the magnitude of variability (Figure 3.3).

For soybean, the positive effect of elevated CO_2 on yield is apparent, especially for the RCP8.5 scenario (Figure 3.4a,b,e,f). A noticeable feature is that rising CO_2 benefits regions that have already showed yield gain. These results are as expected, since elevated CO_2 not only increases soybean's canopy transpiration but also directly boosts the photosynthesis potential. Statistically, including CO_2 effect in the simulation increases pixels with positive yield response from 7% to 42% under RCP4.5, and from 10% to 95% under RCP8.5 (Figure 3.5c,d). The distribution of yield change under RCP4.5 diverges from the 50% quantile when CO_2 is considered in the simulation, suggesting the effect of elevated CO_2 is nonhomogeneous across different quantiles. In contrast, the distribution shrinks more at 0-25% quantile, indicating that elevated CO_2 will benefit more for regions with high climatic yield gaps. However, rising CO_2 seems to have little effect on mitigating the interannual variability of soybean yield, and even exacerbates CV changes under the RCP4.5 scenario (Figure 3.4). Maintaining a stable soybean production remains a challenge for the US Midwest at the late 21st century.

Overall, elevated CO_2 has higher influence under RCP8.5 for both crops, which is consistent with the much higher CO_2 level under RCP8.5 (845 ppm versus 534 ppm). The projected benefits of elevated CO_2 on reducing the yield losses and variability are comparable to the results from studies that use multiple process-based crop models driven

by multiple GCM outputs (Deryng et al., 2014; Rosenzweig et al., 2014), and to the conclusions from an empirical analysis for the US maize (Urban et al., 2015).

3.3.4 Sensitivity of yield changes to climate extremes

As we expect, changes in crop yields are negatively correlated with *Tmax*, and positively correlated with *sumPrec*, with *VPDmax* adjusting sensitivity to *sumPrec* (Table 3.1). Given that our analysis covers a large geographic span, we further investigate these relationships for different quantiles of the data. For both maize and soybean, high yield losses (i.e. <10% quantile) are associated with higher-than-average sensitivity to *Tmax* and high yield gains (i.e. >90% quantile) are less sensitivity to *Tmax*, especially for soybean under RCP8.5 (Figure 3.6). Yield sensitivity to water is collectively determined by the regression slope of *sumPrec* and its interaction with *VPDmax*. Quantiles of high yield losses in maize are characterized with greater slopes for *sumPrec* and smaller slopes for *VPDmax*, and a reverse trend in slopes is identified for soybean. Such interactions between *sumPrec* and *VPDmax* may indicate that drought stress on maize is mainly determined by water supply from the precipitation, while the transpiration demand as determined by *VPDmax* is more important for soybean drought. Including the CO_2 effect into simulations almost uniformly lowers the yield sensitivity to drought, either through reducing the slopes *sumPrec* or increasing the slopes for *VPDmax*. Interestingly, elevated CO_2 increases the soybean yield sensitivity to *Tmax*, in particular for yield changes at low quantiles. We believe this is likely a result of the additive benefit with the stimulation CO_2 on soybean RUE, which causes greater yield response per unit change in *Tmax*.

3.3.5 Shifts in the influence of heat and drought stress

For maize, the regional mean climatic yield gap derived from the baseline simulation is ~6%, and can be almost fully attributed to drought (Figure 3.7a). At the late 21st century, the yield gap increases substantially to 19% under RCP4.5 and 23% under RCP8.5. Although drought is still the dominant stress, f_{Temp} and f_{Heat} calculated by Eqn-8 collectively accounts for 20% and 30% of the climatic yield gap under RCP4.5 and RCP8.5, respectively. Including the CO_2 fertilization effect into simulations markedly reduces the climatic yield gap, mainly because the alleviation of drought in response to higher transpiration efficiency (Figure 3.7b). One noticeable feature of the change is that f_{Temp} and f_{Heat} in combination contribute almost equally as drought to the yield gap under the RCP8.5 scenario, indicating agronomic adaptation and mitigation strategies will need to simultaneously consider heat and drought stresses.

For soybean, the baseline simulation gives a much higher climatic yield gap of ~13%, among which a quarter is contributed by f_{Temp} and three quarters can be attributed to drought (Figure 3.7c). Over the time, the projected yield gap increases slightly to 18% under RCP4.5 and 20% under RCP8.5, and the dominance of drought gives way to the heat constraints. f_{Temp}, f_{Heat} and $f_{Drought}$ comprise almost one-third for each under RCP4.5, while f_{Temp} and f_{Heat} in total contribute to 60% of the yield gap under RCP8.5. In contrast to maize, considering the CO_2 effect does not lower the relative importance of drought stress for soybean, but even increases the drought share under RCP4.5 (Figure 3.7d). We believe this is because drought, compared to high temperature and heat stress, not only directly offsets the benefit of higher transpiration

efficiency for soybean but also constrains the benefit from CO_2-stimulated RUE when high water demand is not satisfied.

Given that the shift of different stresses may not be uniform across the region, and the potential implications for breeding and variety selection, we further investigate the spatiotemporal dynamics in geographic distributions of climatic stressors to potential crop yields (Figure 3.8). The baseline simulation for maize suggests that climatic stresses of more than 5% mainly occur at the west of the US Midwest, and is almost purely in the form of drought (Figure 3.8a). In response to climate change, areas that exhibit yield gaps of more than 5% expand, especially in the core Corn Belt and the eastern US. A mixture of f_{Heat} and $f_{Drought}$ is identified for the northern part under RCP4.5 (Figure 3.8b), while a mixture of f_{Temp} and $f_{Drought}$ is observed in the eastern US under RCP8.5 (Figure 3.8c). Simulations with the CO_2 effect included project less expansion of the area of more than 5% yield gaps, and less influence by drought, especially under RCP8.5 (Figure 3.8d,e). For soybean, there is a clear West-to-East transition from drought-dominant to heat-dominant in the baseline simulation (Figure 3.8f). Climate scenarios at the late 21st century lead to expanded stresses in the Southeast that causes more than 5% yield gaps, mostly in forms of f_{Temp} or a mixture of f_{Temp} and $f_{Drought}$. Including the CO_2 effect increases the relative impacts of drought under RCP4.5, but has little influence on the spatial dominance of different stresses under RCP8.5. Future projections also reveal a consistent spatial pattern of the geographic distribution of different stressors, that is f_{Temp} dominant at the Southeastern US, f_{Heat} dominant at the Western part of study area, and $f_{Drought}$ dominant at the North, with mixtures of stresses lie in between.

3.4 Discussion

By using the very-high-resolution downscaled climate projections by a regional scale climate model and the modified APSIM, this study quantifies the yield responses of US rainfed maize and soybean to future climate extremes by the late 21st century, and for the first time characterizes dynamics in the relative importance of temperature, heat and drought stress in this region. We demonstrate that climatic yield gaps and interannual variability of maize and soybean are greater in the US core production areas than the remaining parts. The effect of elevated CO_2 is partially offsetting the yield losses and interannual variability caused by climate extremes, and is more prominent in soybean than in maize under RCP8.5 scenario. Our results show that drought will continue to be the largest threats to maize and soybean production in this region, although the magnitude of damages depend on the current vulnerability and its dominant role may gradually give way to the other two stresses in response to the combination of rising CO_2 and associated climate changes. We also reveal that shifts in the geographic distributions of the stress dominance are characterized by increases in the concurrent stresses, especially for the core Corn Belt. Collectively our findings imply the importance of considering drought and extreme heat simultaneously for future agronomic adaptation and mitigation strategies, particularly for breeding programs and seeding management.

Yield responses to future climate extremes are not unidirectional in this region. For instance, places with drastic drying and moderate warming trends may still gain yield for maize irrespective of the inclusion of CO_2 fertilization effect. One explanation based on our results is the greater sensitivity to temperature and moisture change for soybean (Figure 3.6). But it is also likely that climate vulnerability is heterogeneous within this

region. A recent systems modeling analysis for a typical research farm in the US Midwest showed that the optimal water use efficiency for maize and soybean occurred with 430 and 317 mm seasonal rainfall, respectively, whereas yields did not benefit from additional precipitation above these levels (Dietzel et al., 2016). Similar hydroclimatic threshold that determines the drought susceptibility was also identified for global tropical forests (Guan et al., 2015). The exact precipitation threshold may vary from one place to another, as a result of interactions with other climatic and edaphic factors. Our analysis of the spatial pattern of stress dominance (Figure 3.8) can be viewed as an early attempt to qualitatively identify spatial heterogeneities in the vulnerability of the regional cropping systems. Given that the disaster potentials of extreme heat and drought depends not only on the severity of the event *per se* but also on the sensitivity and vulnerability of the exposure system, more detailed quantitative assessments are need in the future.

Future climate extremes are likely to strike crop growth as concurrent heat and drought events, thus set higher demand for agricultural adaptations since the optimal breeding or management strategy may differ among stresses (Lobell et al., 2015). A number of crop traits can be potentially adopted to ameliorate drought stress, including the limited-transpiration trait that can stabilize or even lower transpiration rates of both maize and soybean under high VPD conditions (Sinclair et al., 2010; Messina et al., 2015; Shekoofa et al., 2015). Yet limiting transpiration may bring the side effect of burning leaves, as canopy transpiration is a major pathway for latent heat flux. For example, Messina et al. (2015) showed that the benefit of limited-transpiration trait was more prominent for drought-prone environments, while yield penalty was simulated for wet conditions. The trade-off between drought-tolerance and heat-tolerance for breeding

programs may vary with geographic locations, and deserve more research efforts. Simulation studies will continue to provide valuable references to find the optimal strategy, yet more detailed genetic variability need to be incorporated into the current generation of crop models (Boote et al., 2013).

As the first caveat, it should be noted that the climate forcing data is one major but inevitable source of uncertainty in our projections, as is the case for many other crop modeling studies (Ruane et al., 2013; Asseng et al., 2013; Deryng et al., 2014). The use of WRF-downscaled climate scenarios that capture more detailed spatiotemporal climate variability (Wang & Kotamarthi, 2015) allows us to assess the climate change impact on maize and soybean yields at a county level. But it also introduces uncertainty derived from the choice of GCM outputs that provide the boundary conditions for the WRF simulation. While climate model projects generally agree with the direction and magnitude of temperature changes, they are less concordant in terms of precipitation change (IPCC, 2013). Our analysis shows that heat stresses become more influential at the late 21st century, yet drought stress is still the dominant threat to crop yields in most cases. In this case, the uncertainty around the projections of precipitation is likely to be more critical than temperature in determining the simulated yield uncertainty. In this study, we used a dataset that drives WRF with CCSM4 outputs. Previous evaluations confirmed that CCSM4 has moderate bias versus historical precipitation data for the Contiguous US and smaller spread for extreme precipitations when compared to other CMIP5 models (Wang & Kotamarthi, 2015). While VPD (normally derived from RH) is also a critical meteorological variable that affects the crop yield response, its model projections have not been adequately evaluated. Moreover, VPD is often not delivered by

high-resolution downscaled climate data product, thus hinders the inclusion of these variables into modeling and analysis. Ideally, our APSIM simulation should include more WRF outputs driven by additional GCMs to understand the associated uncertainty. Thus we are open to share our data with researchers who would like to compare our results with additional modeling studies using different crop models and climate models.

The projected compensations of elevated CO_2 on stress-induced yield losses are highly dependent on the parameterization of crop physiological response. Uncertainty may be less for maize than for soybean, because the latter not only adjusts TE but also RUE in response to the rising CO_2. Interestingly, a 50% increase in maize TE by CO_2 under RCP8.5 only led to a 13.5% more yield, while a combination of 36.1% increase in RUE and 39% increase in TE benefited soybean yield by 49%. The disproportional yield responses may indicate that the direct increase in photosynthetic potential will benefit more than conserving waters, although the nitrogen fixation ability of soybean is likely to further feedback positively to the biomass production. Compared to the general agreement on maize TE (Lobell et al., 2015), the response of soybean TE and RUE to elevated CO_2 are far less consistent among literatures (Ainsworth et al., 2002). SoyFACE often predicted much more conservative soybean physiological responses than enclosure experiments (Long et al., 2006; Ainsworth et al., 2008), possibly because enclosure experiments were not able to realistically reproduce the soil–plant–atmosphere continuum (Long et al., 2006). For both crops, however, none of the current FACE has manipulated CO_2 level close to the scenario of RCP8.5 (> 800 ppm) at the late 21st century, making the parameterization more uncertain under high emission scenarios.

The rising land surface ozone concentration ([O_3]) further complicates the quantification of CO_2 fertilization effect. O_3 is a global threat to crops (Long et al., 2005; Mills et al., 2007; Tai et al., 2014), and has reduced the US rainfed maize and soybean yields by ~10% and 5%, respectively, based on historical observations since 1980s (McGrath et al., 2015). Elevated CO_2 may partially offset the negative effect of high [O_3] exposure (Long et al., 2005; Ainsworth et al., 2012), but cannot prevent O_3-induced accelerated leaf senescence that lowers canopy light interception and reduces crop yield (Dermody et al., 2008). Therefore our projection of yield gain from the rising CO_2 is prone to overestimation by excluding the O_3 effect. The magnitude of O_3 damage varies with crops and environmental conditions (Ainsworth et al., 2012). Yield sensitivity to elevated [O_3] is generally considered to be less for the maize than soybean, given the intrinsically lower stomatal conductance of C4 crops (McKee et al., 2000; Mills et al., 2007), but is likely to be higher for the US rainfed maize than soybean (McGrath et al., 2015). The projected drought relief as a result of higher transpiration efficiency by our simulations maybe diminished when including the O_3 effect. There is evidence showing that exposure to high [O_3] impairs the functioning of abscisic acid (ABA) signaling (one critical mechanism that regulates the stomatal response to soil drying and changes in VPD), thus causing continued water loss despite the possibility of crop dehydration (Wilkinson & Davies, 2010). ABA signaling also interacts with temperature (Wilkinson & Davies, 2010), and partially explains the observed exacerbation of O_3 damage by high temperatures (Tai et al., 2014; McGrath et al., 2015). Representation of these complex interactions in crop models is still in nascent stage. The impacts of elevated [O_3] on tulip polar can be reasonably simulated with the Community Land Model (CLM) by directly

modifying the maximum rate of carboxylation and stomatal conductance in a coupled Farquhar/Ball-Berry model (Lombardozzi et al., 2012). This version of CLM was later parameterized for all plant functional types and used to assess the global carbon and water cycles in response to chronic ozone exposure (Lombardozzi et al., 2015). Similar idea can be applied to crop models that are built on the concept of RUE (e.g. APSIM), such that parameters of RUE and TE are dynamically reduced according to the cumulative O_3 exposure metrics. However, the parameterization of either stomatal or RUE based models at crop species level is currently restricted by the progress in high-quality experimental data, and should receive more research efforts.

Finally, we acknowledge that our projection may overestimate the benefit of higher TEc, because APSIM does not explicitly simulate the canopy energy balance feedback that higher TEc reduces transpiration but also causes the canopy temperature and VPD to rise, which in turn pushing transpiration and soil water depletion up. As a result of this negative canopy energy balance feedback, the reduction in canopy transpiration is often considerably smaller than the magnitude of reduction in stomatal conductance, with greater differences observed in soybean than in maize (Boote et al., 2013). In this study, we approximate the percentage change in g_s as the change in TE_c mostly because a direct measure of TE_c is unavailable in most enclosure or FACE experiments. The more often reported change in canopy transpiration is not equal to the change in TE_c, since the transpiration calculated in APSIM also depends on VPD. As most crop models does not truly include the canopy energy balance or feedbacks that requires simulating evapotranspiration with hourly or even higher time frequency, even compensatory approaches are applausive for future model improvement (Boote et al.,

2013), if not turning the model into a mechanistic manner that demand extensive computational cost on simulating instantaneous energy balances. In fact, a recent study on multi-model comparison of simulating canopy temperature suggested that empirical algorithms are competitive to mechanistic algorithms in their ability to reproduce the crop canopy temperature (Webber et al., 2015), although their parameters need to be localized when applied to a novel region. For example, STICS uses an approach that simulate canopy temperature according to a relationship between daily maximum temperature and daily evapotranspiration, while further adjusting the simulation with net daily radiation and canopy height (Brisson, 2008).

Table 3.1 Literature reported changes in soybean transpiration efficiency (TE) and radiation use efficiency (RUE) under elevated CO_2

Study	Ambient	Elevated	TE	scaled TE	RUE	scaled RUE
Acock et al. (1985)	330	800	-24%	-17.9%	+40%	+29.8%
Jones et al. (1985)	330	800	-18%	-13.4%		
Bunce (1996)	350	700	-37%	-37%		
Booker et al. (1997)	364	726			+56%	+54%
Duga et al. (1997)	359	705	-57%	-57.7%		
Luo et al. (1998)	350	700			+46%	+46%
Serraj et al. (1999)	350	700	-25%	-25%		
Allen et al. (2003)	350	700	-9%	-9%		
Bernacchi et al. (2005)	375	550	-10%		+18%	
Bunce (2014)	380	560			+28%	

Notes: (1) according to the meta-analysis, Ainsworth et al. (2002), A_{sat} on average increases by 39% across all [CO_2] treatments, and is not significantly affected by [CO_2] level. g_s decreased by 36% at 600-800 ppm, and 51% at [CO_2] > 850 ppm. These conclusions can be viewed as an upper limit.
(2) scaled TE/RUE is values for an increase in CO_2 of 350 ppm.

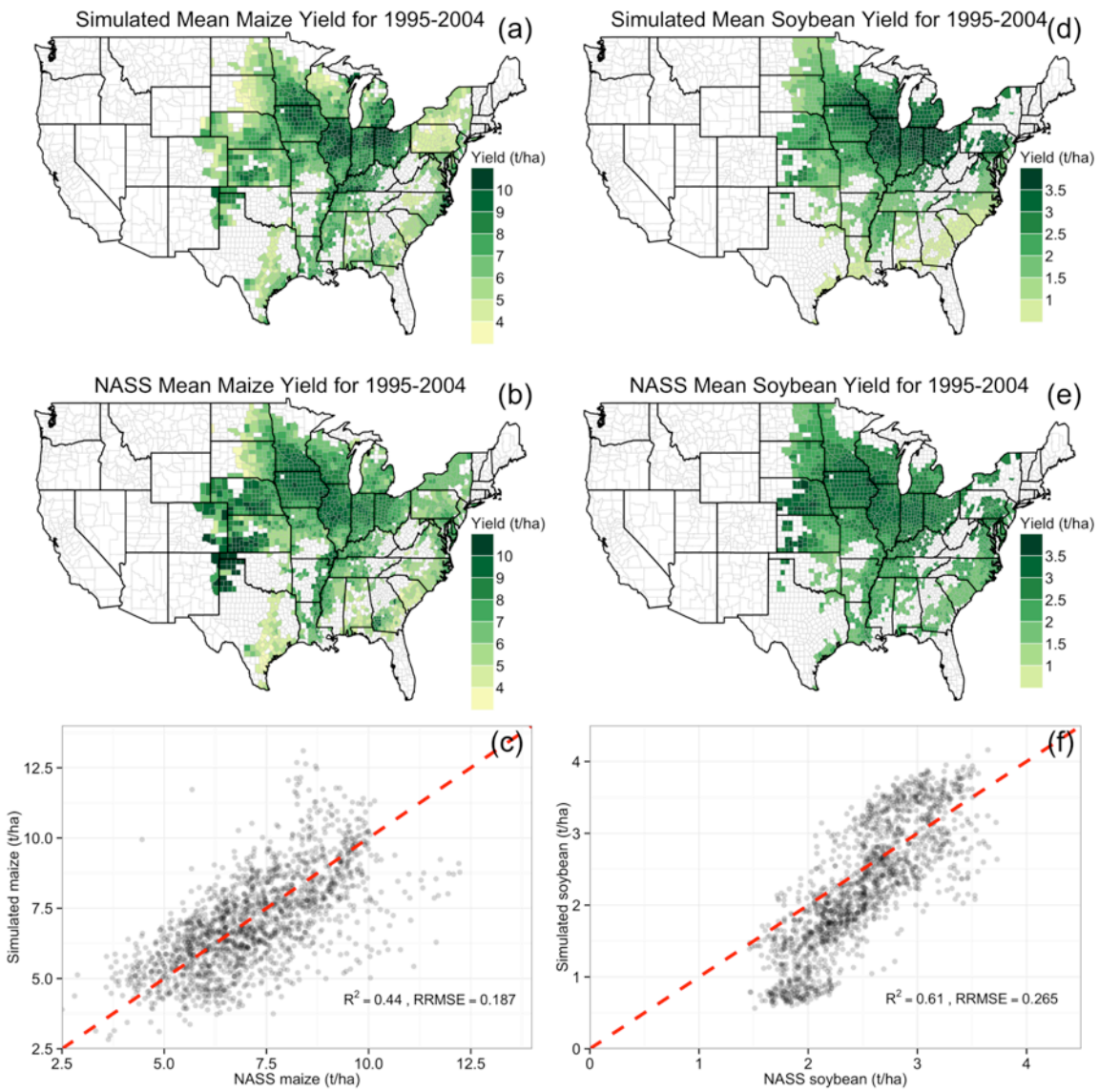

Figure 3.1 Validation of APSIM simulated baseline (1995-2004) mean maize (a, b, c) and soybean (d, e, f) yield against the USDA National Agricultural Statistics Service (NASS) reported rainfed crop yield at county level.

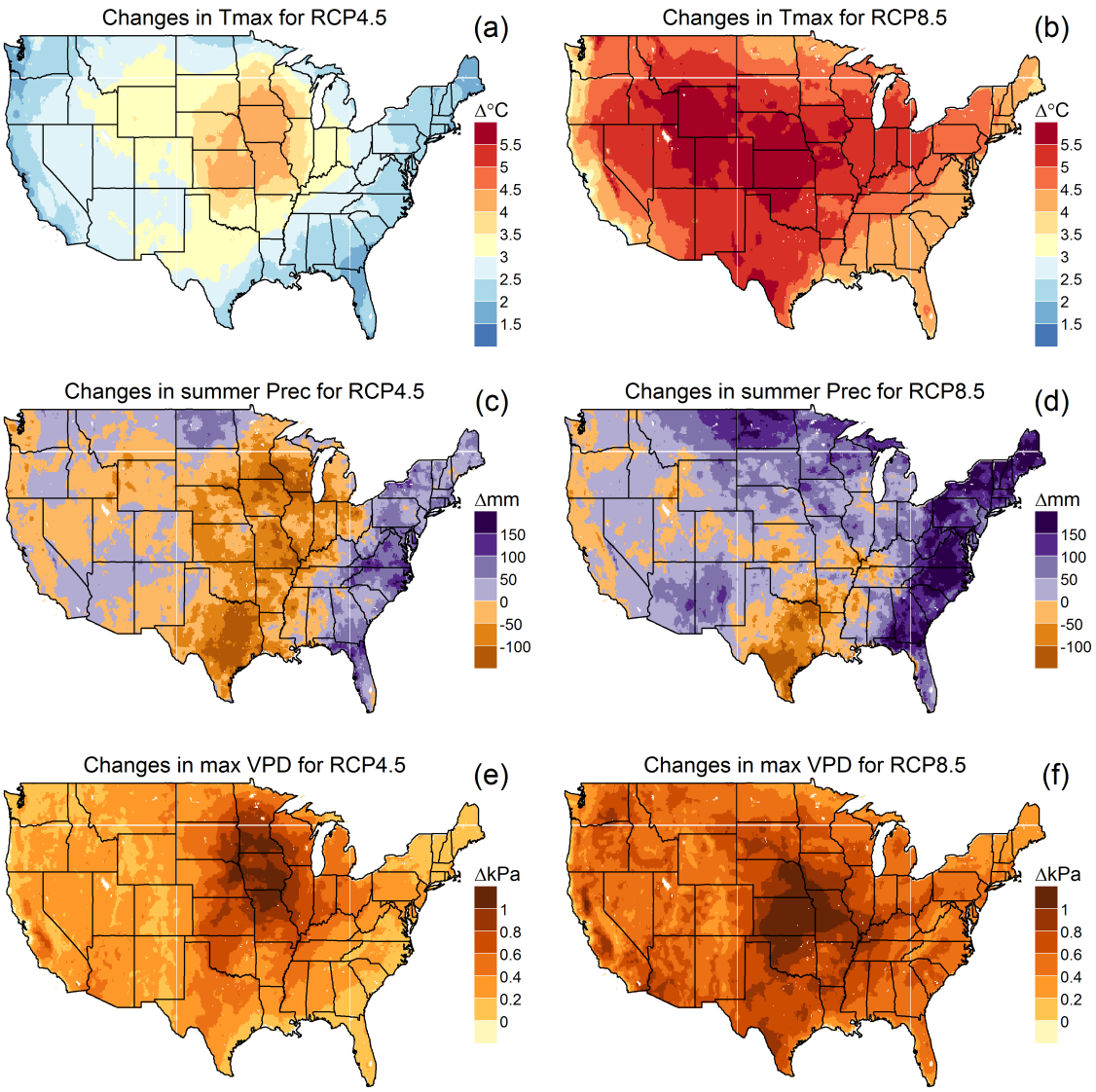

Figure 3.2 Changes in the WRF projected decadal mean maximum growing season temperature (*Tmax*), cumulative summer precipitation (*sumPrec*) and maximum weekly vapor pressure deficit (*VPDmax*) by the late 21st century (2085-2094) compared to the baseline condition of 1995-2004.

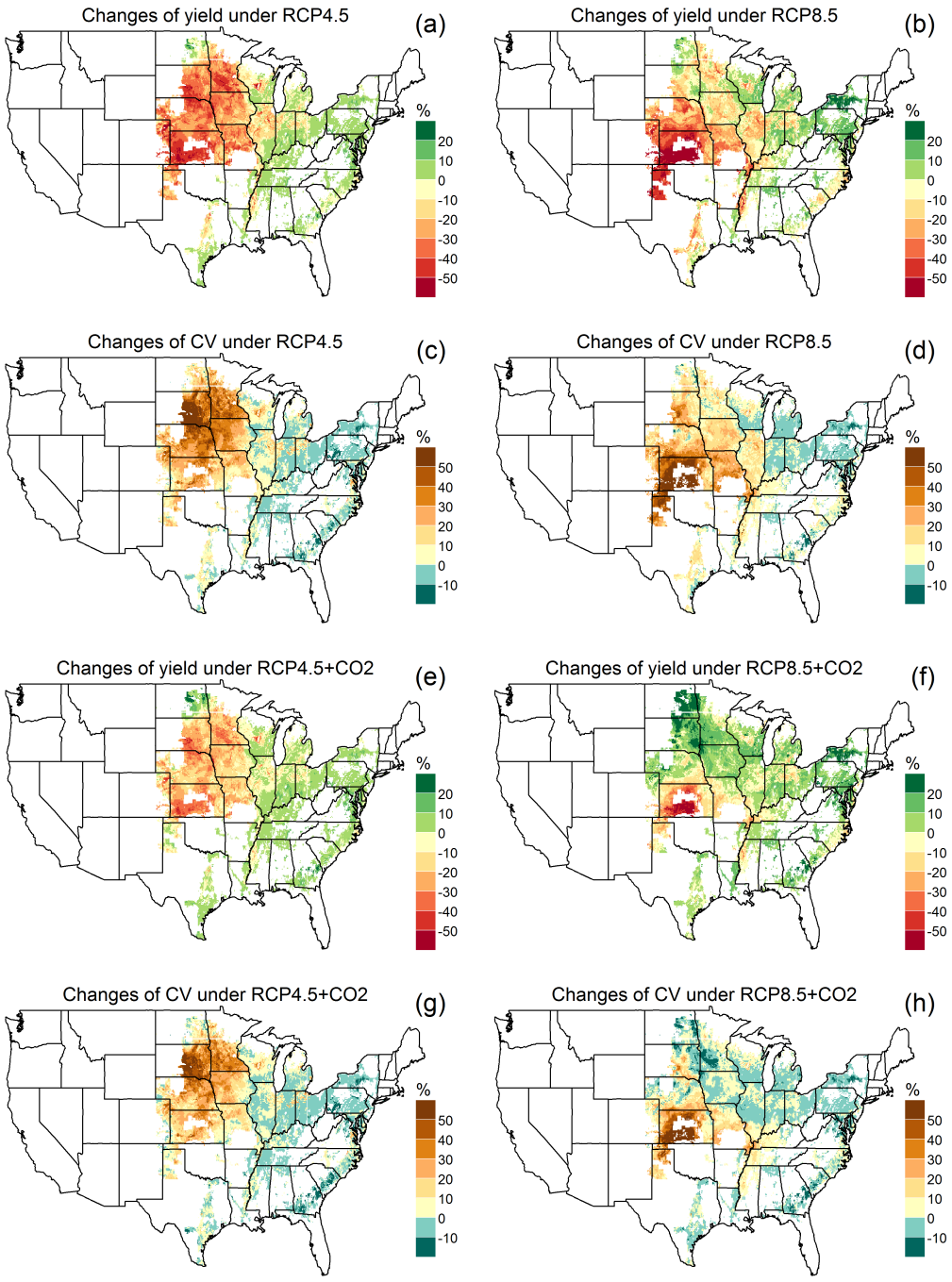

Figure 3.3 APSIM projected changes in decadal mean maize yields and coefficient of variations (CV) by 2085-2094 in comparison to the baseline of 1995-2004, with (a-d) and without (e- h) considering the effect of elevated CO_2 on maize transpiration efficiency.

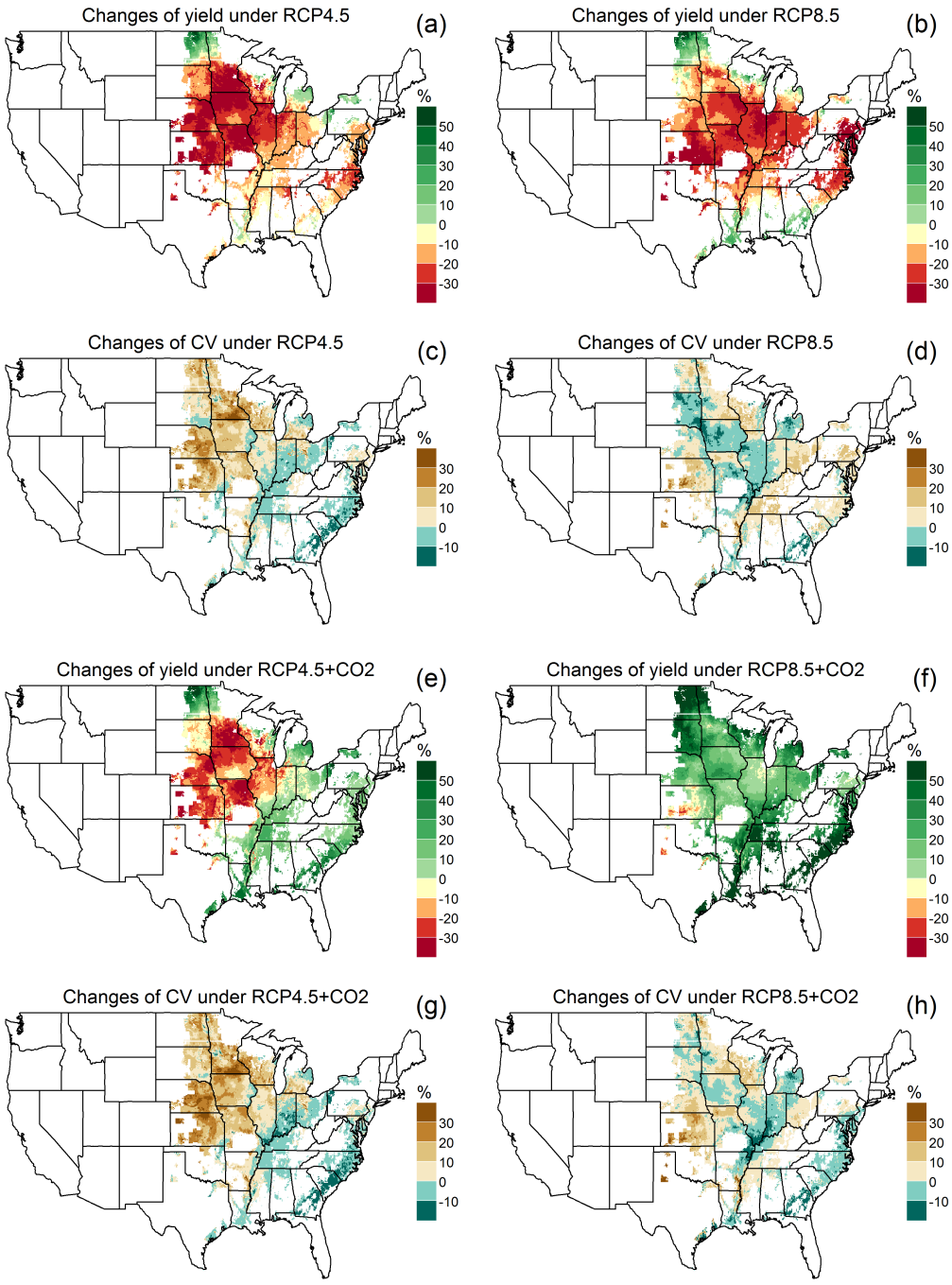

Figure 3.4 APSIM projected changes in decadal mean soybean yields and coefficient of variations (CV) by 2085-2094 in comparison to the baseline of 1995-2004, with (a-d) and without (e-h) considering the effect of elevated CO_2 on maize transpiration efficiency.

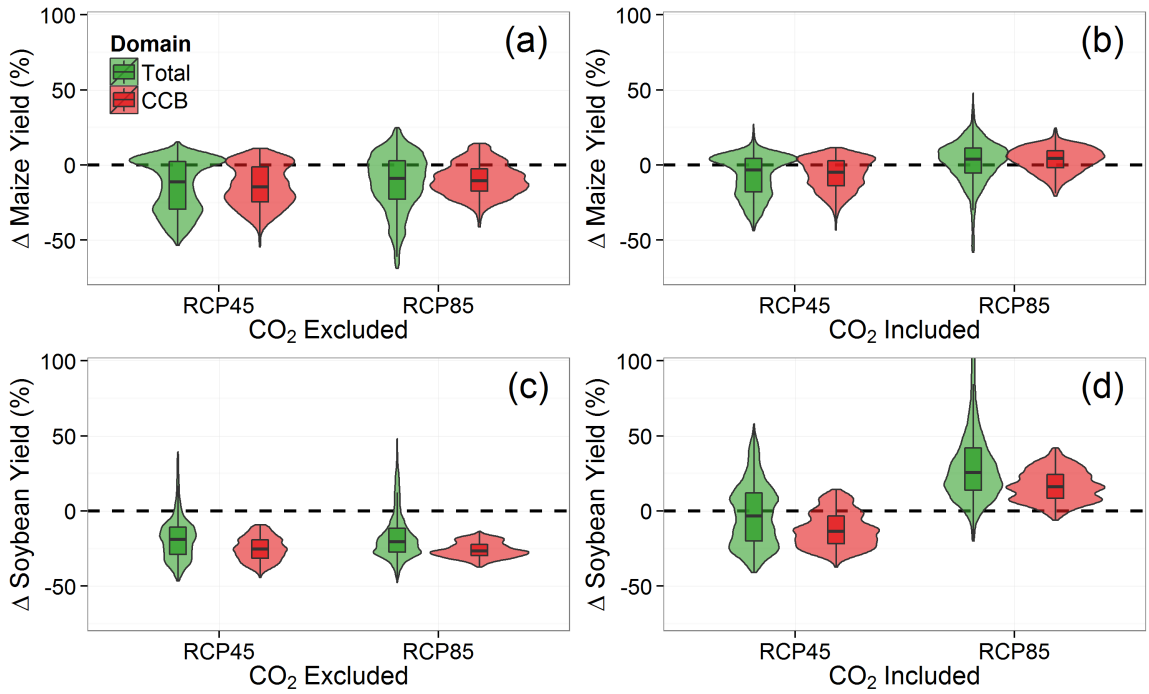

Figure 3.5 Distributions of changes in the decadal mean maize (a, b) and soybean (c, d) yield with and without considering the effect of elevated CO_2. Summary is for both the whole US (total) and the core Corn Belt (CCB; i.e. Illinois, Indiana and Iowa).

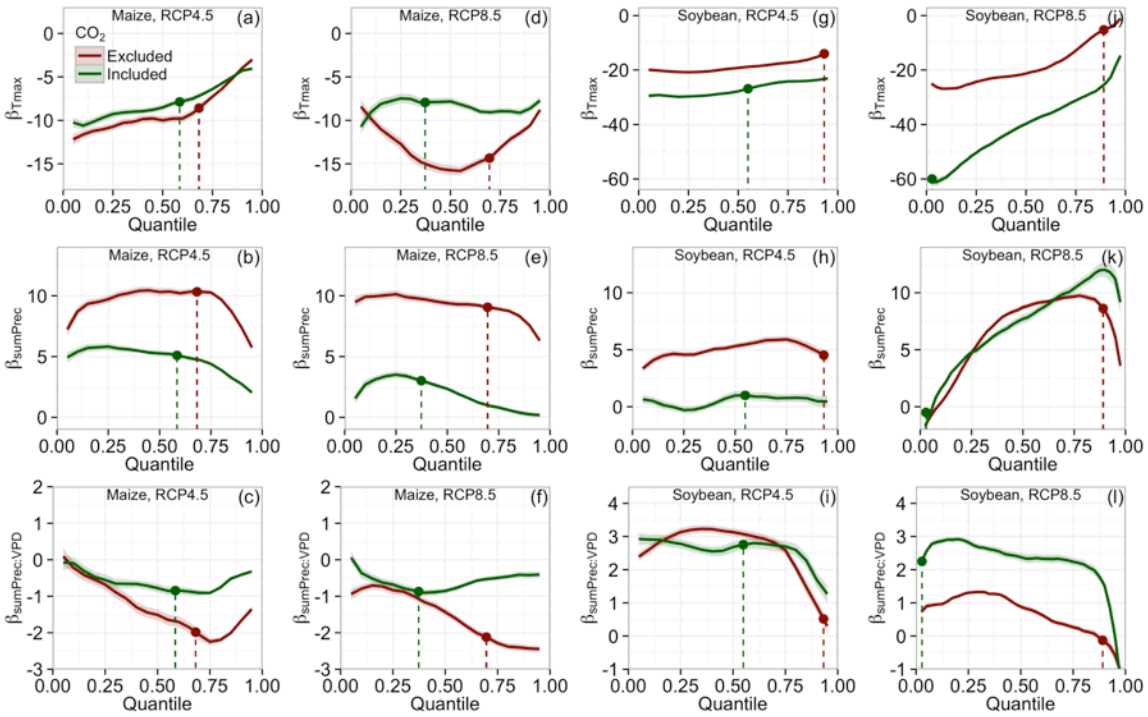

Figure 3.6 Yield response (i.e. yield change in Figure 3.5) of maize (a-f) and soybean (g-l) to mean maximum growing season temperature (*Tmax*), cumulative summer precipitation (*sumPrec*) and maximum weekly vapor pressure deficit (*VPDmax*) under multiple climate scenarios with and without considering the effect of elevated CO_2. Regression coefficients (i.e. the slopes) are derived from quantile regression for each 5% quantile interval. Shaded area represent the 95% confidence interval for the slopes. Intersections of dashed lines and the X-axis are the corresponding quantile where yield responses equal zero (also shown in Figure 3.5).

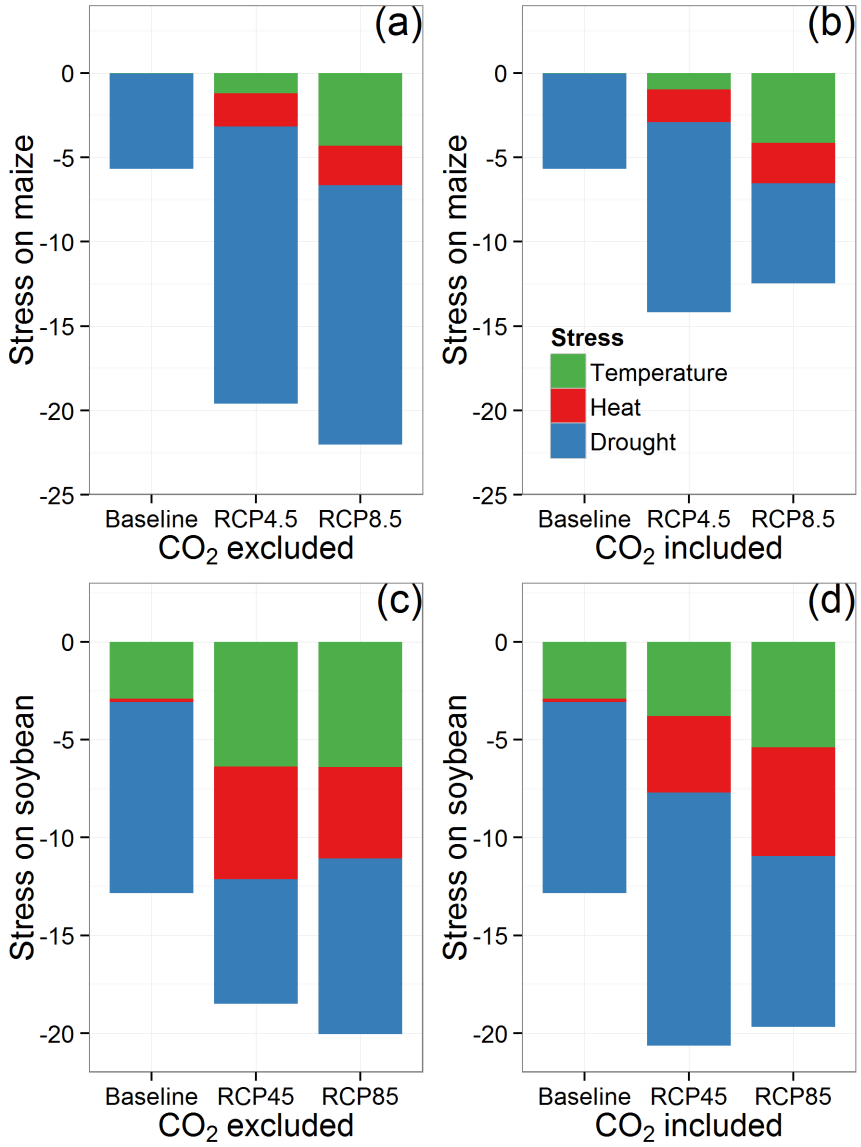

Figure 3.7 Simulated climatic yield gaps and attributions to high temperature, heat and drought stresses for maize (a, b) and soybean (c, d) under multiple climate scenarios with and without considering the effect of elevated CO_2.

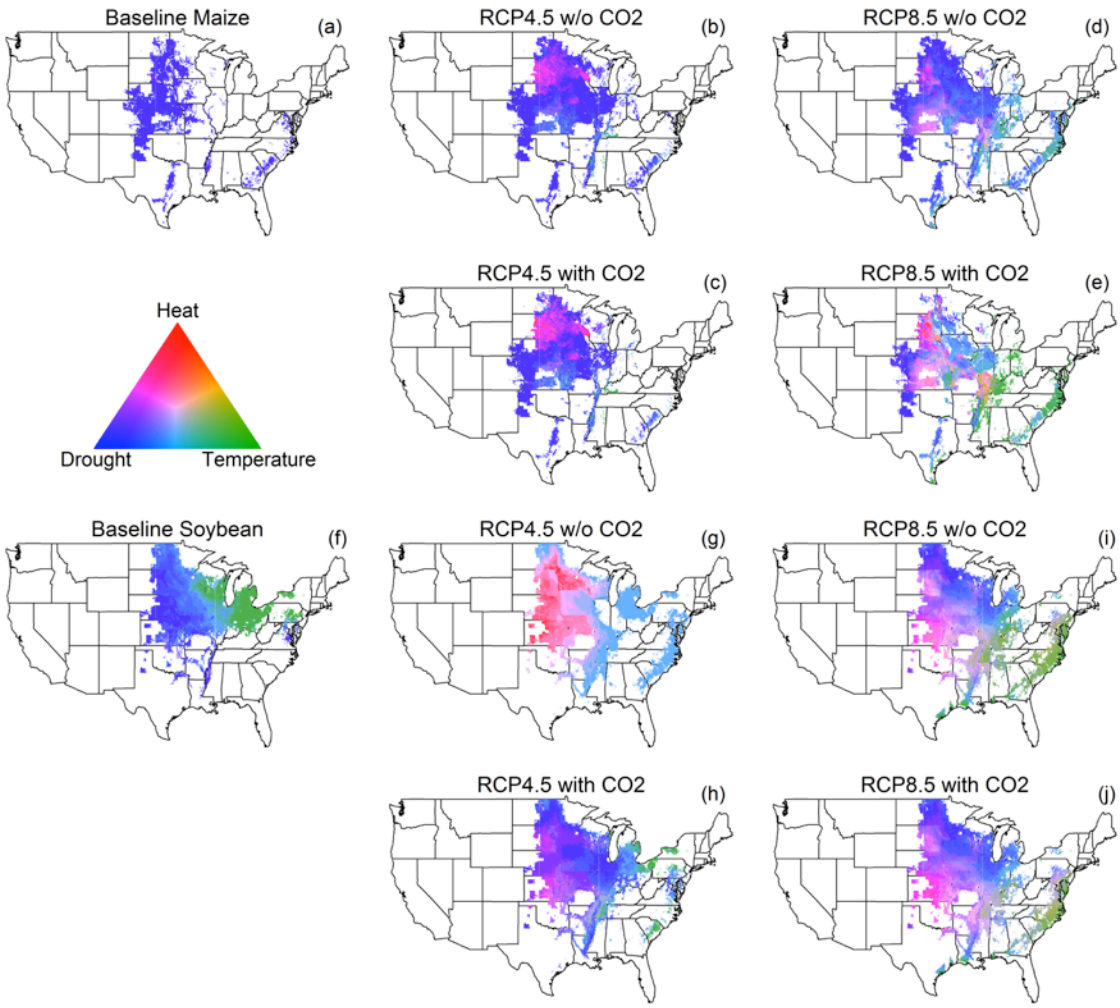

Figure 3.8 Projected shifts in the geographic distribution of relative influence of climate extremes (i.e. high temperature, heat and drought stresses) on maize (a-e) and soybean (f-j) yield under multiple climate scenarios with and without considering the effect of elevated CO_2. Only grid cells with more than 5% climatic yield gaps are shown in the plots.

CHAPTER 4. ADAPTATION POTENTIAL OF THE US RAINFED MAIZE BASED ON GENOTYPE, ENVIRONMENT AND MANAGEMENT ANALYSIS

4.1 Introduction

Global demand for agriculture crops as food, feed and bioenergy fuels poses a great threat to the human society, given the increasing competition for land and water from the need to support other essential ecosystem services such as carbon storage and biodiversity (Karp & Richter, 2011; Challinor et al., 2014). The ongoing and incoming climate changes, especially in forms of increasingly frequent and severe climate extremes such as heat waves and droughts, have further exacerbated the risks on the agriculture system by lowering crop productivity and increasing inter-annual variations in yields (Deryng et al., 2014; Rosenzweig et al., 2014). Such a systematic challenge calls for agronomic adaptations that can overcome the current yield limits and improve the crop production efficiency (Matthews et al., 2013).

In a recent review study, Matthews et al. (2013) identified four broad areas of adaptation for private entities, including: (a) shifting the locally optimal crops; (b) breeding new traits or varieties of existing crops; (c) evolving agronomic management practices and (d) coping with climate uncertainty through the provision of information. While the introduction of some traits, for example, pest resistance (Tabashnik et al., 2013) and modified canopy structure (Drewry et al., 2014), has little apparent negative effects on other aspect of a cropping system, many of other adaptation options involve uncertain

trade-offs and possibly synergies that may or may not be static across space and time (Matthews et al., 2013; Rippke et al., 2016). Correspondingly, developing the optimal adaptation strategy often means to identify favorable combinations of genotype (G) and management (M) for a specific environmental (E) that is characterized by its soil and climate conditions (Hammer et al., 2014).

A number of G attributes have been documented as successful adaptation options for the rainfed maize system, although the consequences of a particular manipulation will differ among E types or associated with a cost for grain yield through interactions with other physiological processes (Matthews et al., 2013). For example, crop maturity is one such genetic trait that can be used for mitigating the negative effect of climate change (Liu et al., 2013; Hammer et al., 2014; Harrison et l., 2014). Selecting early-mature variety may help to avoid the heat and/or drought stress that often occur at late summer, whereas using longer-maturing variety may benefit from the longer growing season to assimilate more carbon. The root structure, in particular the root angle, is a genetic trait that determines the vertical and horizontal root distribution in soil profiles, and hence the ability of plant to extract soil water (Hammer et al., 2009). While steeper and deeper root systems with access to deep soil in general benefit water and nutrient uptake in some maize production environments (Lynch, 2013), the water uptake efficiency of a given root phenotype still differs following soil compactness and hydrologic conditions (Messina et al., 2011; Leitner et al., 2014). A limited transpiration rate (TR_{lim}) is a recently found trait based on the evidence of variations among maize hybrids in their response to high vapor pressure deficit (VPD) at high temperature (Yang et al., 2012; Shekoofa et al., 2016). The expression of TR_{lim} is to maintain a restricted amount of

transpiration once some VPD threshold is reached, thus offering an approach to conserve soil water and improve yield under drought-prone environment (Messina et al., 2015). Yet the net gains from TR_{lim} need to be evaluated by simultaneously considering the potential change in canopy energy balance, since limiting transpiration could increase canopy temperature as a result of reduced latent heat flux (Long et al., 2006).

The effect of a new G attribute on rainfed maize growth is often analyzed in conjunction with contrasting M scenarios, such as the sowing date (Grassini et al., 2009; Liu et al., 2013; Tsimba et al., 2013), levels of seeding rate (Borras et al., 2003; Hammer et al., 2009; Messina et al., 2015) and fertilizer application (Trachsel et al., 2013; Gerde et al., 2016), and row configuration (Borras et al., 2003; Testa et al., 2016). This is typically done using nested experiment design, with a limited number of replicates in space and time, to benchmark the yield of new genotypes against yield of existing genotypes under a few M scenarios (Messina et al., 2011; Hammer et al., 2014). Results from these trials are plausible in understanding the best average performance of adapted genotypes under simple $E\times M$ interactions, but may miss some benefits of adaptation since they do not search the full spectrum of potential $G\times E\times M$ combinations (Hammer et al., 2014).

The demand for searching among the myriad of possible combinations has led to an increasing interest in the use of process-based crop models as key tools for adaptation research (Matthews et al., 2013). By their nature, crop models provide a framework to modify single or multiple genetic traits, management activities and simulated environments, to assess the marginal or joint effect on crop growth and yield (Boote et al., 2013). Crop models can make greater contribution when there is a trade-off associated

with a target trait (Matthews et al., 2013), or when the advantageous for a particular trait may vary depending on the environments. More importantly, the recent advent of high performance computing system has made it easy to evaluate millions of $G \times E \times M$ combinations over an entire region within a short time (Hammer et al., 2014; San Martin et al., 2014), and offers potential to further explore the adaptation space at billion scales. This type of massive simulation approach has been applied successfully to investigate the adaptation potential of several cereal crops (Rotter et al., 2013; Hammer et al., 2014; San Martin et al., 2014; Lobell et al., 2015; Messina et al., 2015), although most of existing studies are for cereals in Europe or Australia. For the US maize production system, which typically supplies nearly 40% of the global maize commodity, a comprehensive study that explores the favorable adaptation strategy in response to the climate change is in urgent need.

The objective of this study is to identify the optimal sowing strategy (i.e. $G \times M$) over a wide range of genetic adaption options, and to project the shifts of successful strategies in space and time. To archive these goals, we designed a modeling experiment of massive scenario simulations using the APSIM platform. Climate change scenarios are constituted by projections generated from a 12km resolution regional climate model (RCM) for 4 time slices (i.e. 1995-2004, 2025-2034, 2045-2054 and 2085-2094). One feature that distinguishes our simulation experiment with existing studies is that we confine the selection of sowing date to those suitable fieldwork days (SWD), which aimed to consider the probability of field inaccessibility when the soil was either too cold or too wet. The complete combinations of $G \times E \times M$ factors for the core Corn-Belt (CCB) states in the US Midwest (i.e. Illinois, Indiana and Iowa) result in approximately 500

million single year simulations. While this study only focuses on the adaptation of rainfed maize, the framework presented here can be extended to other US major crops such as wheat and soybean.

4.2 Materials and methods

4.2.1 Setting APSIM for $G \times E \times M$ analysis

The APSIM infrastructure provides a very convenient framework to perform scenario simulations by supporting customized scripting of management activities and genotypic traits (Hammer et al., 2014; Holzworth et al., 2014), thus allowing us to enumerate the ensemble of yield-adaptation strategies using a plausible range of G and M factors over the spatiotemporally dynamic E scenarios. Attributes for G employed in the simulations included three levels of maturity (Liu et al., 2013) and four levels of TR_{lim} trait (Messina et al., 2015). The setting of different maturity in APSIM can be achieved by varying the thermal time from emergence to end of juvenile stage (i.e. the parameter $tt\_emerg\_to\_endjuv$); the larger this parameter is, the longer it takes a variety to reach the critical flowering stage (Liu et al., 2013). Our maturity adjustment was based on the well-calibrated cultivar, Pioneer_P04612XR_106, against the observed phenology data from Iowa by Archontoulios et al. (2014). Specifically, we set $tt\_emerg\_to\_endjuv$ equals 150, 200 and 250 °C for early-, medium- and late-mature variety, respectively. In addition to changing the length of growing season, varying $tt\_emerg\_to\_endjuv$ also leads to a change in the total leaf number and hence the progress of leaf area index (Hammer et al., 2014). Levels of TR_{lim} trait were implemented by setting different thresholds following Messina et al. (2015). The lowest threshold (and the strongest TR_{lim}

trait expression) is 1.5 kPa, which means maize canopy no longer increase transpiration when the atmospheric VPD rises above this threshold. The remaining three levels are 2.0, 2.5 and 10 kPa. Since it is almost impossible for atmospheric VPD to reach 10 kPa for the temperate zone, this highest threshold actually means no expression of $TR_{\lim}$ trait. For the dimension of M, we also considered four different levels of seeding rates (i.e. 3, 5, 7 and 9 plants/m^2) and a series of possible planting date (see Section 2.3 for the selection among suitable working days). We didn't consider the CO_2 fertilization effect because it is still controversial for the maize in the absence of severe drought (Leakey et al., 2006).

4.2.2 Revise model for canopy energy balance

While elevated [CO_2] can benefit the maize growth by reducing the stomatal conductance and canopy transpiration thus ameliorating water deficit in drought years (Leakey et al., 2006), it may increase the likelihood of heat stress since decreased transpiration lowers the latent heat flux and leads to higher canopy temperature (Long et al., 2004). As many other crop models with a daily time step for transpiration, APSIM does not consider the canopy-scale energy balance (Lobell et al., 2015), thus is not able to evaluate the trade-offs caused by the responses to elevated CO_2 without incorporating mechanisms in this aspect. In this study, we added a simple empirical model for simulating canopy temperature based on the difference between potential and actual crop transpiration (Seguin & Itier, 1983; Brisson et al., 2008). Daily mean canopy temperature (T_c) is calculated as:

$$Tc - Ta = \left(PT \times cover_{green} - AT\right) / \frac{1.68}{ln\frac{1}{0.13 \times h_c}} \tag{4.1}$$

where Ta is air temperature, PT is the potential evapotranspiration calculated by the Priestley-Taylor equation, AT is the actual canopy transpiration calculated based on the transpiration efficiency (TE) method (Lobell et al., 2013), $cover_{green}$ range from 0 to 1 is the canopy faction to intercept radiation, h_c is the canopy height (m), 1.68 and 0.13 are two empirical parameters following the STICS model (Brisson et al., 2008). The underlining assumption is that canopy temperature is lower than ambient Ta when canopy transpires more water than demand and higher than Ta when crop is water stressed. Based on the observed relationship between Tc and Ta for rainfed maize in Siebert et al. (2014), Tc is limited to the range of $[Ta - 6, Ta + 6]$.

4.2.3 Suitable fieldwork days

The SWD is determined based upon soil temperature and soil moisture. In general, maize will not germinate when soil temperature is below 10 °C, thus sowing date should be set when soil temperature is approaching or above this threshold to avoid poor emergence. On the other hand, soil is generally considered not suitable for machinery operations if the soil moisture level deviates too much from the field capacity, although the optimal moisture threshold could vary by soil texture (Rotz and Harrigan, 2005). In this study, we limit the planting window to the Julian days of 61-180 (i.e. from March to late June), and define a day to be suitable for fieldwork when: (i) the 7-day moving-average soil temperature at 5cm is above 10 °C, and (ii) the daily mean soil moisture of the topsoil (0-10cm) is between LL15 and 1.05*DUL, where LL15 and DUL are the notation for wilting point and field capacity in APSIM. Soil temperature and moisture are simulated by the APSIM considering a fallow soil.

Our selection criteria often result in more than 80 SWDs within the planting window for a specific year. To reduce the computational cost for retrieving the optimal sowing date, a hierarchical sampling method is applied. We first divide the planting window of 120 days into twelve 10-days intervals, and identify the optimal interval by comparing the yields from APSIM simulations of which the sowing date are the median SWD within each of the twelve intervals. Next, we loop the APSIM simulation through every other SWD within the optimal interval, and pick up the one with highest yield as the global optimal sowing date. It should be noted that APSIM-Maize considers frost damage by senescing a faction of LAI in proportion to the air temperature below 2 °C.

4.2.4 WRF climate scenarios

Daily climate inputs for the APSIM, including maximum and minimum temperature, precipitation and solar radiation, were generated by a 12 km resolution Weather Research and Forecasting Model (WRF v3.3.1) that used the Community Climate System Model version 4 (CCSM4) outputs for the Representative Concentration Pathways 8.5 scenario from the fifth phase of the Coupled Model Intercomparison Project (CMIP5) archive as the initial and boundary conditions (Wang & Kotamarthi, 2015). The CCSM4 data was corrected for the bias in long-term climatology following Bruyere et al. (2013), which corrected the mean errors but retained the climate variability. The WRF simulations were performed over a very large domain (7200 km × 6180 km) covering the North America (Wang & Kotamarthi, 2015), although only the subset of CCB states was used in this study.

4.2.5 Regional simulation and analysis

Geographic distribution of non-irrigated maize is derived from the 5 arc-minute resolution M3-Cropland data (Ramankutty et al., 2008), resulting in 5799 grids for the CCB states. Spatially explicit information on soil, crop cultivar and management is critical for APSIM regional simulations. We extract soil parameters, such as soil texture, layered soil hydraulic properties and soil organic matter fractions from the 1:250,000 U.S. General Soil Map (STATSGO2) database. The description for each of these required soil parameters is documented in Archontoulis et al. (2014a). To reduce the computational cost, we simply use attributes of the dominant soil component within in the largest soil map unit of each grid cell for our simulations. Management activities for the baseline time slice of 1995-2004, includes seeding rates and fertilizer amount, are from the USDA National Agricultural Statistics Service (NASS) survey report at state level. We assume that the same spatial information for future time slices is the same as the baseline conditions, thus excluding the potential of agronomic improvement on crop adaptation and mitigation.

We calculated the yield benefit from changing the planting date as the ratio (%) of maximum and mean attainable yield for all possible SWDs that have been tested. Assuming optimal planting date, the adaptation potential by changing the remaining $G\times M$ attributes for a given time slice is calculated as:

$$Adaptation\ potential = \frac{Y_{90}{}'}{Y_{90}ref} \tag{4.2}$$

where $Y_{90}{}'$ is the 90% quantile mean yield for a specific future time slice among all $G\times M$ combinations, and $Y_{90}ref$ is the 90% quantile mean yield for the reference time slice (i.e.

1995-2004). All metrics are initially calculated for each grid on annual basis and then summarized into decadal means or other metrics.

4.3 Results and discussion

4.3.1 Climate change and optimal planting date

The projection of future climate changes for the CCB region by our RCM are characterized collectively by the warming and wetting trends (Figure 4.1). KDD, an indicator of excessive heat by accumulating temperature above the critical threshold of 30 °C for maize yield (Lobell et al., 2013) is growing fast over the time, indicating potentially higher risks of heat stress. Although the cumulative rainfall during the growing season on average increases by 140 mm for the 2045-2054 and 118 mm for the 2085-2094, water availability for this region is still uncertain given the simultaneously increased maximum growing season VPD; high VPD level can exacerbate drought by stimulating the short-term canopy transpiration and depleting soil water storage in the longer term (Lobell et al., 2013). These novel yet adverse climate patterns thus call for adaptive managements to prevent failures in maize growth.

An intuitive expectation in management change from the warmer springtime climate conditions (Table 4.1) is the earlier planting date. However, our analysis shows that the probability for the CCB region to be suitable for fieldwork only increases slightly by up to 20% on March and April (Figure 4.2a), suggesting that the potential for advancing the planting date is limited. In fact, the bonus of less thermal constraint on SWD over time (Figure 4.2b) is offset by the increased springtime precipitation that leads to more days with muddy soil and unfavorable condition for machine operations,

especially for the 2085-2094 (Figure 4.2c). Admittedly, the aforementioned result about SWD is partially determined by the projection on precipitation regime and should be interpreted with uncertainty in mind, yet it challenges most existing $G \times E \times M$ analyses (e.g. Martin et al., 2014), which simply use prescribed time intervals to select the optimal planting date, because their proposed optima may not be feasible.

The optimal planting date has advanced consistently for the early-mature maize, but not for the medium- and late-mature varieties (Figure 4.3a). By the late 21st century, early-mature variety ends on average 20 and 30 days earlier than the medium- and late-mature group, respectively (Figure 4.3b). Differences in the number of days to reach maturity become smaller over time (Figure 4.3c), most likely because warming have fastened the phenology progress. These patterns contradict the speculation in Kucharik (2006) that switches to hybrids with a longer growing season could benefit yield gains. We believe the earlier planting for the early-mature variety can be explained as the successful strategy to avoid terminal heat and/or drought stress on August and early September (Lobell et al., 2013). In contrast, the likelihood for medium- and late-mature varieties to be hit by climatic stress is higher given their longer growing season, thus may require more radical inter-annual changes in the optimal planting date (reflected by the wider quantile distributions in Figure 4.3a).

4.3.2 Adaptation potential

The 10-year mean yield benefits from the optimization of planting date are similar among four time slices, mostly distributed within the range of 6-20% (Figure C1a). On the other hand, the distribution of maximum annual yield benefit varies significantly over time (Figure C1b). The maximum yield benefits reach the highest level in 2045-2054,

and then drop slightly back to the level of 20-40% in 2085-2094 regardless of the more radical inter-annual shifting in planting date at the late 21st century (Figure 4.3a). These features in the distribution change indicate that: (i) shifting the planting date, as an adaptation option, is likely most effective around 2050s, and (ii) the adaptation potential from changing the planting date is limited when climate stressors are too severe (Figure 4.1). Spatially, high benefits often occur at the southern and western part of the CCB region, corresponding to the places where climate change is more drastic (Figure 4.4). The maximum yield benefit reaches the highest level (i.e. >50%) in more than one-third of the Iowa during 2045-2054, thus farmers in this sub-region should more caution with the choice of planting date.

It should be noted, however, achieve the full potential of changing planting date as projected here is likely unrealistic, because our selection of the optimal planting date is based on model simulations that "knowing" the meteorological condition for the whole growing season. Yet in reality, farmers will have to decide the timing of planting activities based on weather forecast that may only be reliable for next couple of days, and may lead to the adoption of more conservative strategy on adjusting planting date. According to Rotter et al. (2013), the majority of farmers choose to start planting on average 1 week later than would be climatically possible. To obtain the full bonus of changing the sowing date, weather forecast need to go beyond the window of fewer days and deliver robust projections about the likelihood of spring frost and summer heat and drought several months in advance. Some private entities (e.g. The Weather Trends International, Inc) have claimed to be able to give trustable one-year-ahead projections, but their algorithm is not documented or peer-reviewed.

Even assuming that the planting date is optimized, other adaptation methods (i.e. change the population density and select adapted crop traits) in combined are still not likely to help retain the historical yield level in most of the CCB region (Figure 4.5). Specifically, the decadal optimal adaptation combinations are only able to retain on average 97%, 95% and 90% of the baseline yield level for the period 2025-2034, 2045-2054 and 2085-2094, respectively. Applying annual optimal adaptation significantly increased the adaptation potential on average by 5% (Figure 4.5), especially for sub-regions with less severe climate stressors. The contrast between the effects of decadal and annual optimal adaptation demonstrates that the favorable $G\times M$ strategy is instable for this region, and may vary from year to year depending on E. This highlights the difficulty in identifying broad adaptation when the production environment is highly variable (Hammer et al., 2016).

4.3.3 The $G\times E\times M$ landscape and adaptation recommendation

Figure 6 presents the yield adaptation landscapes that summarize the regional mean and minimum yield (which indicates the risks of crop failure) across different levels of seeding rates, TR_{lim} trait and variations among maturity. In response to the climate change over time, mean yield decreases towards the late 21st century. Medium- and late-mature varieties in general have higher mean and minimum yield than the early-mature group, possibly because of the former two groups has longer growing seasons for carbon assimilation (Figure 4.3c). Preserving TR_{lim} has little benefit on the mean yield, but in contrast has apparent effects on improving the low yield for all future time slices (Figure 4.6). Likely because the negative feedback of elevating canopy temperature is marginal in our simulations, preserving low TR_{lim} threshold always performs better in

formulating grain yield. Since the highest yield always occurs with high seeding rate and the preserve of low $TR_{\lim}$ threshold, it seems the $TR_{\lim}$ trait could help further intensify the cropping system in drought-prone regions (Messina et al., 2015). Higher seeding rate almost consistently results in higher yield, which is understandable yet not in line with the results in Borras et al. (2003) and Hammer et al. (2014). Therefore we speculate that competition for growth resources such as water or nutrient in the CCB region is not significant over the time we evaluated, thus in general high seeding rate is recommended.

There are no consistent trends in the spatial pattern of different G and M attributes (Figure 4.7). Early- and medium-mature varieties are favorable choices for most of the CCB region, except the period of 2025-2034 during which sub-regions with moderate warming favors late-mature variety. Using the highest seeding rate of 9 plants/m^2 is suggested in most circumstances, although the southern and western parts of the study area show some variations in different time slices. $TR_{\lim}$ with the lowest threshold (i.e. 1.5 kPa) dominates the whole region, except the southern Illinois and Indiana during the period of 2085-2094 where high transpiration demand and relatively low soil water availability (Figure 4.1) requires higher $TR_{\lim}$ threshold to be more conservative on retain soil water.

4.4 Conclusions

In this study, we investigated the adaptation potential of rainfed maize yield under climate change at the US CCB region by optimizing the $G \times E \times M$ combinations. Our massive simulations demonstrate that changing the planting date is the most effective adaptation method, although the trend of earlier planting due to warmer spring climate

may be restricted when there is too much springtime precipitation. Assuming optimal planting date, our analysis shows that optimizing the remaining $G\times M$ attributes on decadal basis is not sufficient to maintain the baseline yield for this region, unless annual optimal adaptation strategy is implemented. This contrast implies the difficulty of finding a broad adaptation mode when the inter-annual variation in weather is high. Therefore greater value from adaptation would be received if it is based on relation between $G\times M$ and E rather than geography (Hammer et al., 2014). Low TR_{lim} threshold and high seeding rate show consistent advantage on improving the yields, indicating the cost of implementing TR_{lim} trait and cropping intensification is not high enough to outweigh the benefit. It is likely because our study region is not large enough to include much heterogeneity, thus further research should consider expanding the spatial coverage in order to see some trade-offs associated with certain adaptation methods.

A further consideration is whether or not the full adaptation potential as suggested by model simulations can be achieved. In fact, the choice of favorable adaptation strategy depends highly on the climate projection. Knowing the weather a few months in advance is currently unrealistic, while existing $G\times E\times M$ studies are mostly take it for granted to have the meteorological data for the whole growing season. Transferring the useful information obtained from $G\times E\times M$ analysis thus requires more robust techniques for weather projection. As a final caveat, the factorial nature of $G\times E\times M$ analysis calls for more efficient algorithm of searching the adaptation landscape. Although the use of high-performance computing infrastructure offers the opportunity to explore millions or even billions of $G\times E\times M$ combinations, the current framework of enumerating every

combination is computationally inefficient and only allows the search of a small amount of G or M variables with a limited number of levels. Future research could consider introducing the theory of global or local optimization into the $G \times E \times M$ analysis.

Table 4.1 Projected changes in temperature, precipitation and vapor pressure deficit at 10%, 50% and 90% quantiles.

	1995-2004			2025-2034			2045-2054			2085-2094		
	10%	50%	90%	10%	50%	90%	10%	50%	90%	10%	50%	90%
Temperature (°C)												
Spring mean	8.7	11.3	13.6	9.1	12.8	15.4	11.3	13.7	16.1	13.2	15.3	17.8
Growing season mean	19.5	21.0	22.7	21.3	22.6	24.2	21.9	23.2	25.2	24.0	25.5	27.3
Killing degree days	3	22	67	35	73	182	39	97	234	120	247	443
Precipitation (mm)												
Spring total	300	458	587	336	462	614	319	501	663	359	576	771
Growing season total	443	690	889	457	672	918	469	830	1060	520	808	1083
Vapor pressure deficit (kPa)												
Maximum weekly VPD	1.39	1.57	1.83	1.53	1.73	2.22	1.61	1.86	2.30	1.70	2.06	2.71

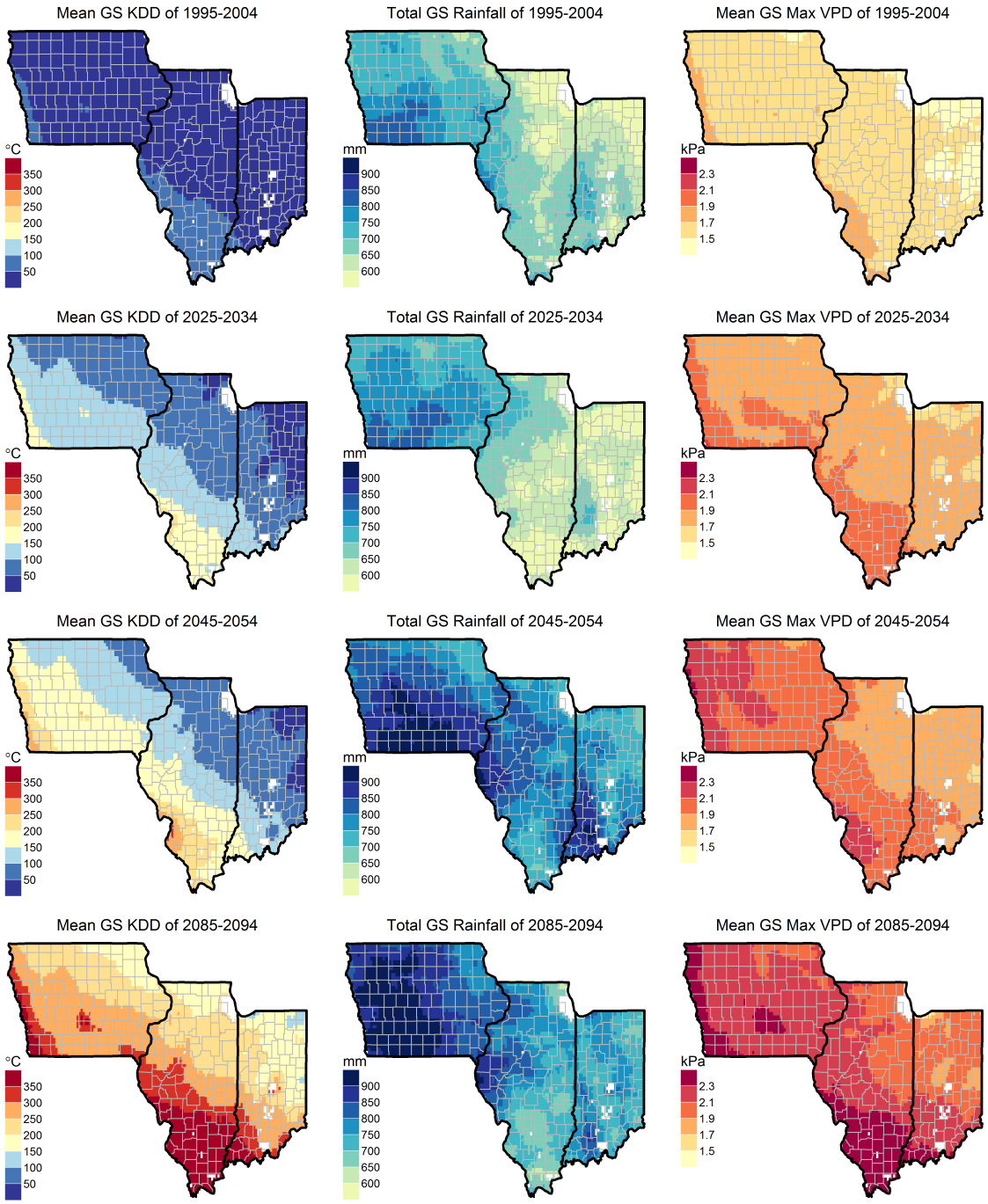

Figure 4.1 Spatial pattern of mean growing season (GS) killing degree days (KDD), rainfall and maximum weekly-mean vapor pressure deficit (VPD) during four time slices.

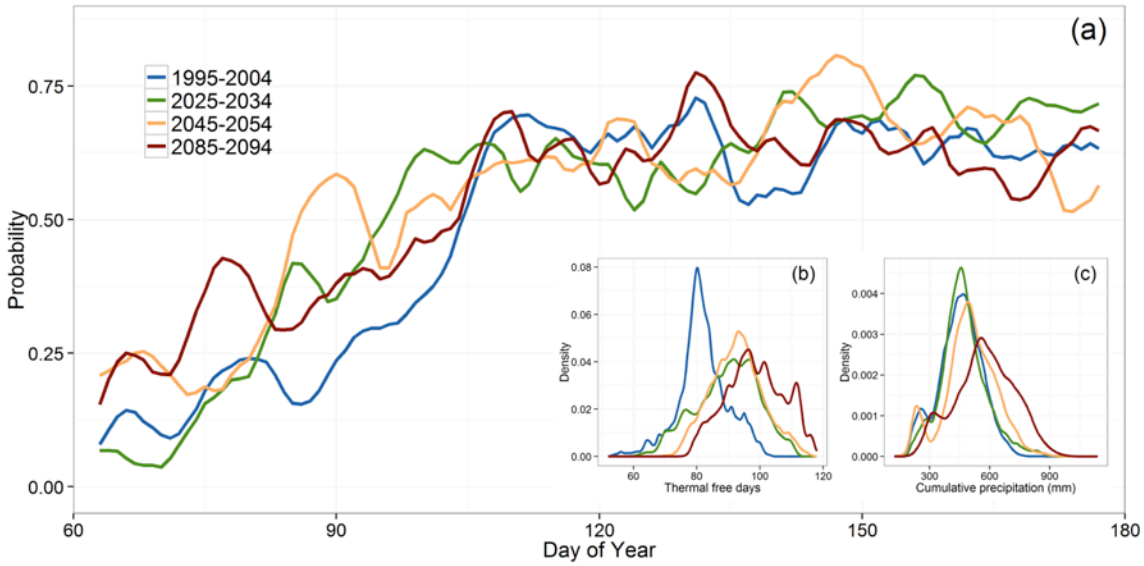

Figure 4.2 The probability of each day to be suitable for fieldwork across the region (a). Distributions of thermal free days (i.e. days with soil temperature above 10 °C) (b) and cumulative precipitation (c) over the planting window from Julian day of 61 to 180.

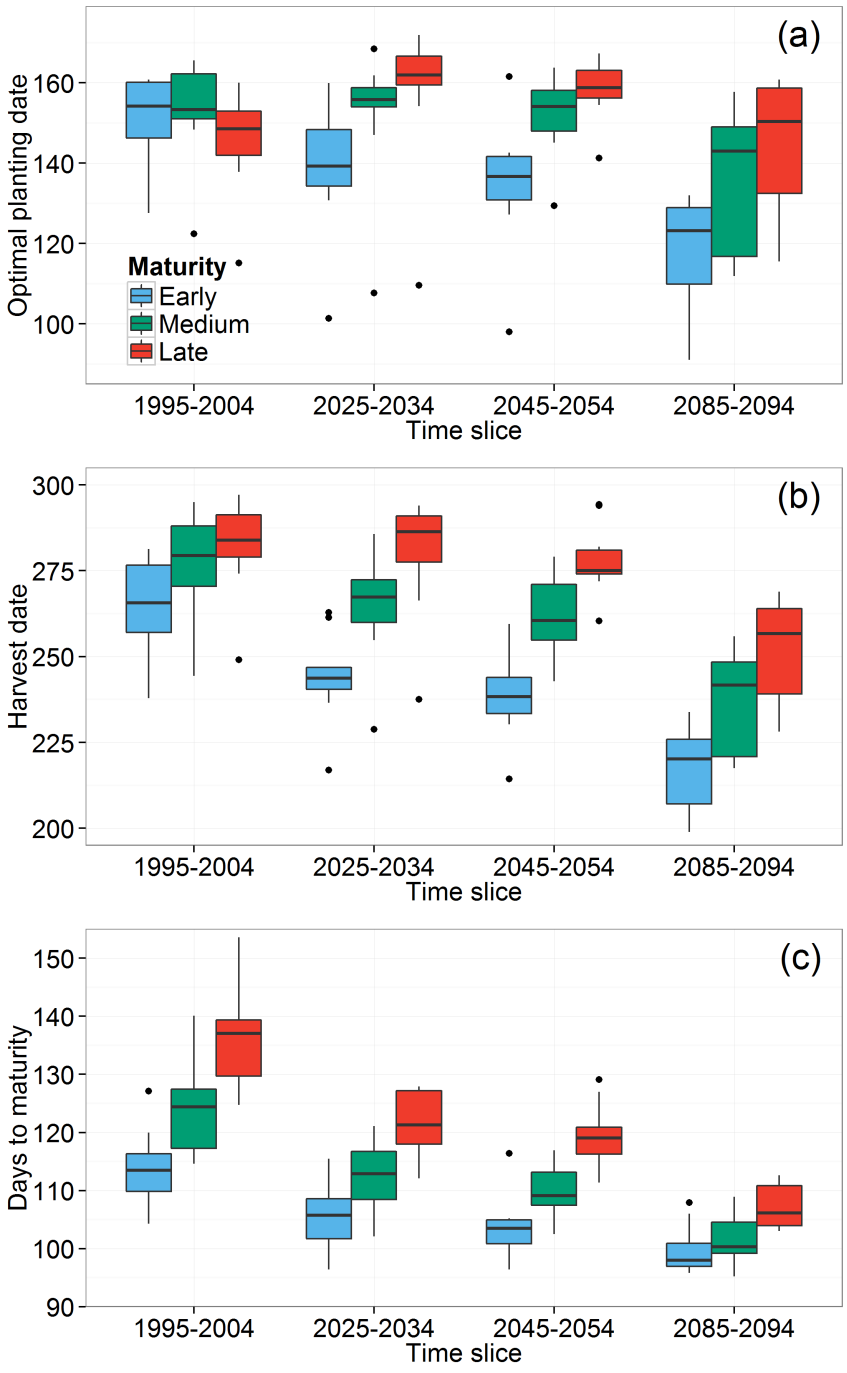

Figure 4.3 Changes of optimal planting date (a), harvest date (b) and days to mature (c) over time grouped by cultivar maturity.

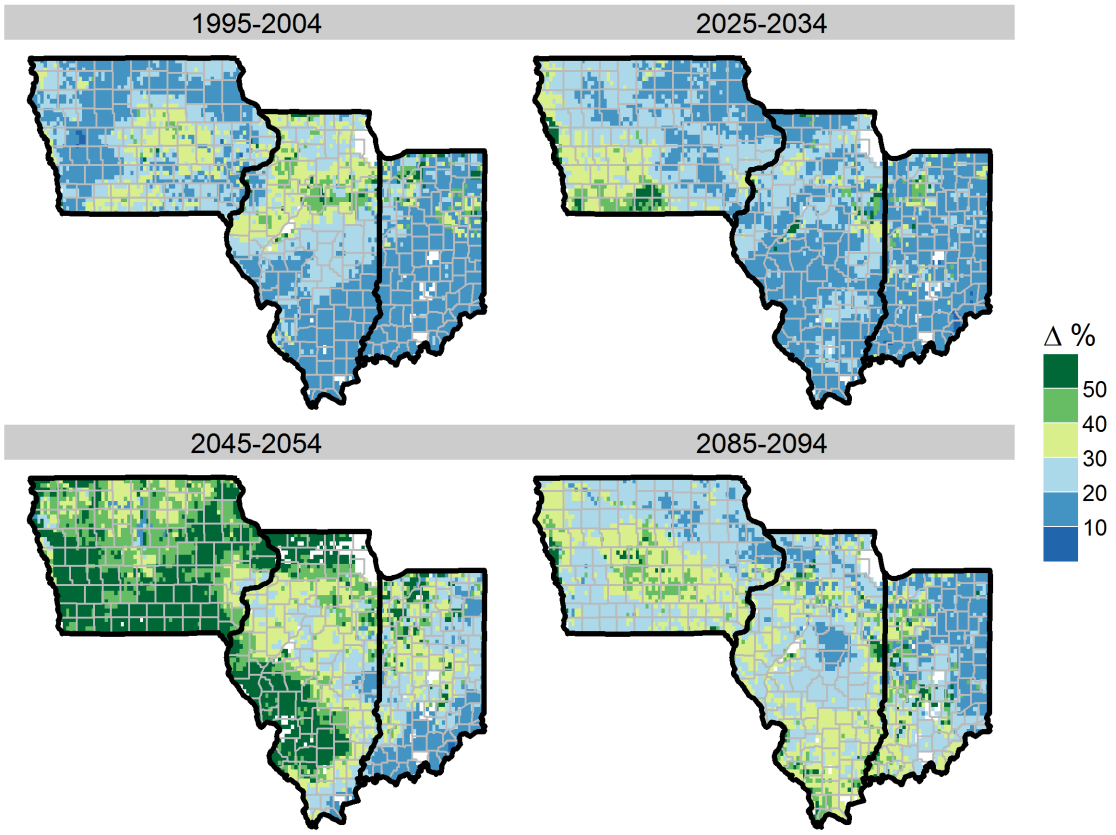

Figure 4.4 Spatial pattern of the grain yield benefit from optimizing the planting date. Yield benefit is measured as the percentage difference of simulated maximum and mean yield by running the APSIM with a series of possible suitable fieldwork days.

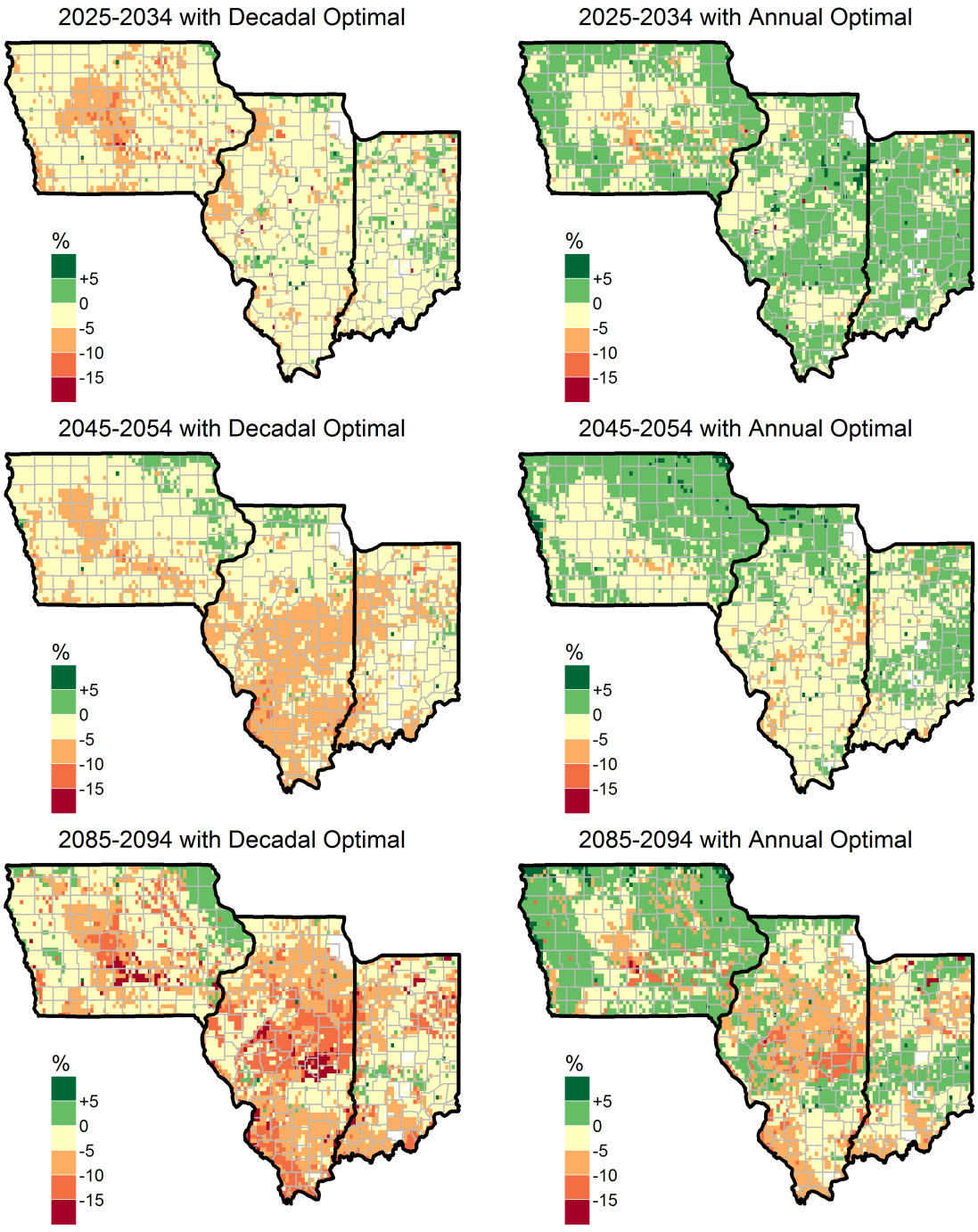

Figure 4.5 Spatial pattern of adaptation potential by applying decadal and annual optimal genotype and management strategy. Adaptation potential is measured as the percentage difference of 90% quantile mean yield of each future time slice and the baseline (i.e. 1995-2004) 90% quantile mean yield.

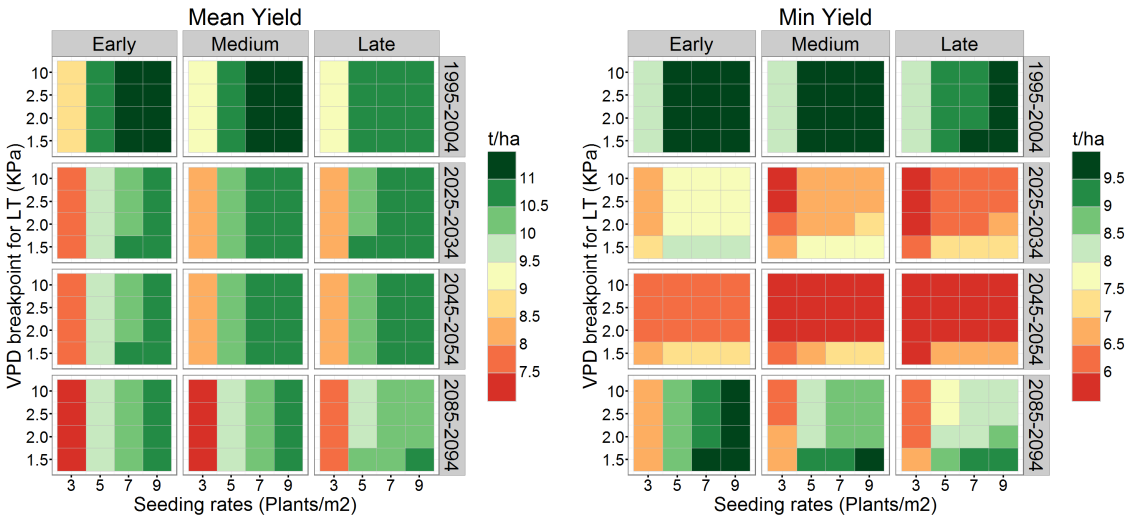

Figure 4.6 Simulated landscapes of decadal mean and minimum maize yield (t/ha) for genotypes varying in maturity and TR_{lim} trait (threshold of 10 kPa means no expression of TR_{lim} trait), and crop management varying in seeding rates. The planting date is in the optimal state.

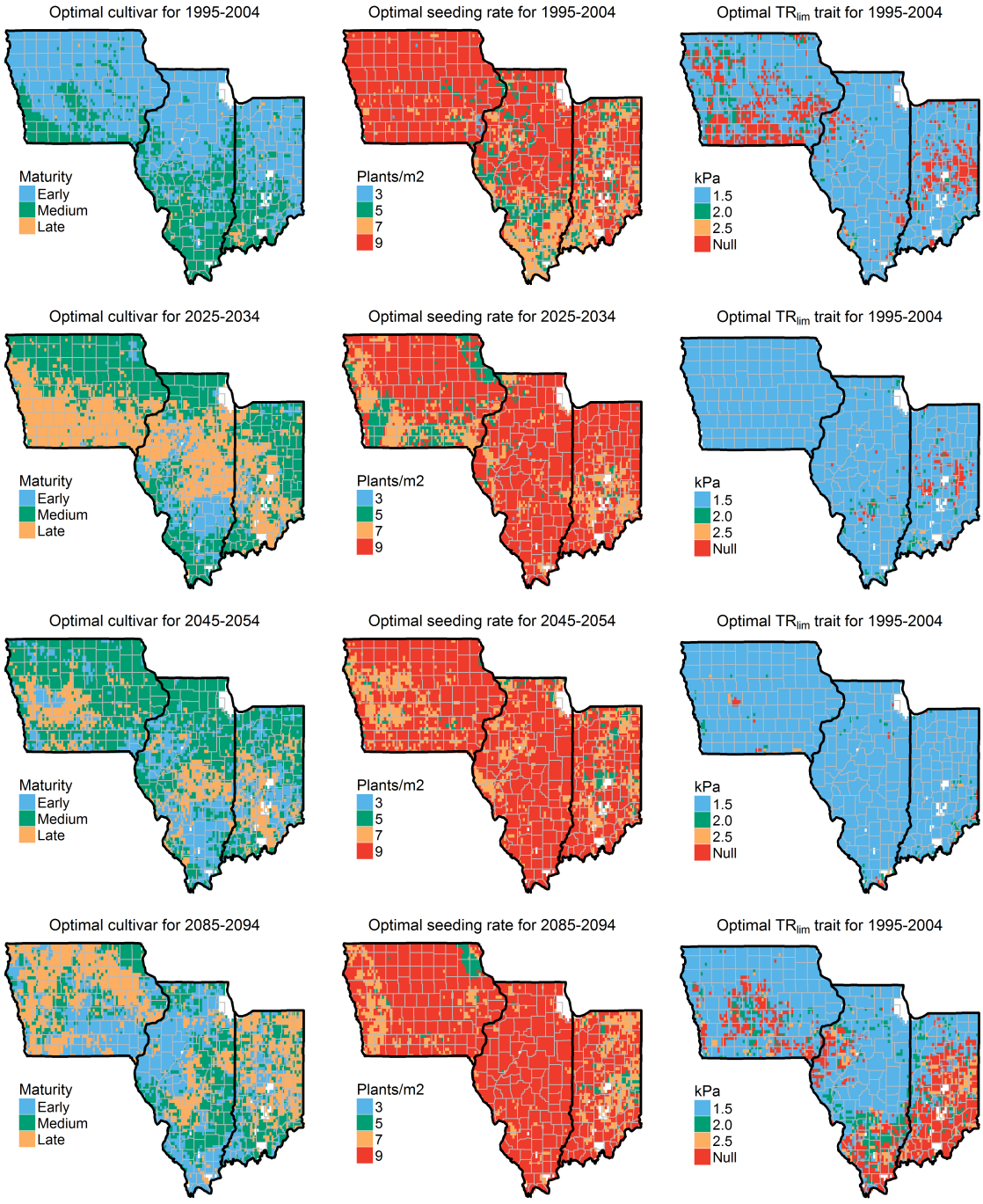

Figure 4.7 Spatial patterns of the optimal cultivar, seeding rate and threshold for TR_{lim} trait over time.

CHAPTER 5. A PROTOTYPE OF CROP MODEL AND SATELLITE IMAGERY BASED PRECISION FERTILIZATION

5.1 Introduction

Nitrogen (N) is one of the most limiting factors that can lower corn (*Zea mays* L.) yield and quality (Miao et al. 2007; Scharf 2015). Corn with deficient N will have dwarfed seedlings and yellowish leaves, leading to partial or complete failure of kernel setting (Ma and Biswas 2015). On the other hand, over-fertilizing causes high risks of water contamination (Keeney, 1986; McIsaac et al. 2002), and nitrous oxide (a potent greenhouse gas) emissions (Park et al. 2012; Scharf et al. 2015). The need to wisely manage N fertilizer is thus compelling for both economic and environmental considerations (Scharf 2015).

In practice, the associated higher cost of under-fertilization relative to over-fertilization drives farmers to apply higher rates, and use additional "insurance" fertilizer applications (Moebius-Clune et al. 2013). It is estimated that 75% of N fertilizer for the US Corn-Belt is applied before planting (Cassman et al. 2002), among which fall application is more widely practiced than spring application. The N fertilizer loss is highly weather dependent, and is greatest in warm and wet winters (Randall et al. 2003; Tremblay et al. 2012; Scarf 2015). Thus to reduce N loss before the growing season, a good strategy is to applying a portion of N in-season (Thompson et al. 2015). Furthermore, applying N based on soil heterogeneity can reduce the overall amount of N

being applied and increase the operational profitability compared with a uniform N application (Mamo et al. 2003).

The optimal management of N requires a farmer to make a series of decisions on the form (what), timing (when), placement (where) and rate (how much) of N fertilizer to be applied. While the N form and timing is often limited by accessibility and logistical constraints, determining where and how much N fertilizer should be applied is more science-oriented (Scharf 2015), and has progressed considerably in recent years (Setiyono et al. 2011; Shahandeh et al. 2011; Solie et al. 2012; Moebius-Clune et al. 2013; Thompson et al. 2015). The optimal N rate for a given field depends on crop demands, indigenous N supply as a net result of mineralization and immobilization, and losses of N fertilizer or soil-derived N via leaching, denitrification and volatilization (see Figure 5.1 for the schematic diagram of N cycling in a corn field). Each of these aforementioned processes interacts among themselves, and is influenced by many factors such as: seasonal temperature, precipitation, soil physical and biogeochemical properties, and management history. Although researchers have spent considerable efforts to understand the complexity associated with nitrogen management, the uncertainty is still substantial (Scharf 2015). The problem is further complicated by spatial variations in soil N contribution, fertilizer losses and crop N uptake from field to field and even place to place within a field. Nitrogen mineralization of SOM may vary because of differences in organic nitrogen release rate as a function of soil temperature and moisture, or differences in past crop removal (Scharf 2015). N leaching loss can vary mainly because of different topography and soil hydrological properties (Prasad et al. 2015). The N fertilizer need by the crop can vary as a result of varying yield potential (Mamo et al. 2003), or differences

in seeding rates. Because of these complexities, fast and accurate diagnostic tool of the optimal N rate for a given field remains a challenge (Ma and Biswas 2015; Scharf 2015).

Crop models that incorporated with all above-mentioned N processes have been identified as a promising tool for synchronizing N fertilizer application with crop N demand (Cassman et al. 2002; Scharf 2015). The recent advent of high-performance computers and communication technologies has made it possible to process massive remotely-sensed or field survey data and weather records in near real-time to inform precision N management. Although many existing crop models are capable of simulating the soil N dynamics and estimate the corn growth in response to N availability with different complexity (Bassu et al. 2014), they are not designed to support pre-plant or in-season decisions on precision N management (Thompson et al. 2015). A few specific tools have been developed to manage N, such as Adapt-N (Melkonian et al. 2008; Moebius-Clune et al, 2013) and Model-N (Setiyono et al. 2011). The Adapt-N model is built on the crop model from Sinclair and Muchow (1995), and N management scheme from Melkonian et al. (2005), but its further development to support full-field variable N rate recommendation is unknown. Maize-N mainly focuses on estimating the economic optimum nitrogen rate, and has been proved to outcompete the university N recommendation approaches (Setiyono et al. 2011). However, its operational use is complicated and cannot be easily mastered by non-expert users.

The objective of this study is to introduce a prototype of fully automated very-high-resolution (5m × 5m) decision support tool for on-farm precision N management. This tool, named N-Prescription, uses remotely-sensed data to delineate within-field management zone, simulates subfield variations in soil and crop status with a crop model

that assimilates in-situ soil database and real-time weather information, and finally delivers either pre-plant or in-season variable rate N recommendations to match fertilizer application with crop demand. The core part of a process-based crop model for estimating indigenous N supply, N losses and crop N demand is built on the APSIM platform (Keating et al. 2003). Although the N-Prescription tool currently only support for rainfed Maize, it will be extended to cover major crops in the near future. In the following sections, we will detail the science and engineering background of N-Prescription, provide model sensitivity analysis and optimization, and present a case study for a typical US Midwest Corn field in Illinois, USA.

5.2 Materials and methods

5.2.1 Overview of workflow

The N-Prescription infrastructure is built on the Amazon Elastic Compute Cloud (EC2), and has been parallelized to support multiple client call at the same time. The scientific workflow is given in Figure 5.2, and major steps include:

1) Determine pre-plant N application rate. We first calculate the total N target rate (N_{target}; kg ha^{-1}) for a given growing season based on the expected yield goal, N credits and management zone variations:

$$N_{target} = c_0 + c_1 \cdot EY - 1.12 * N_{credit} + \varepsilon \quad (5.1)$$

where c_0 and c_1 is the offset and slope for calculating state-specific N fertilizer requirement per unit yield (derived from University extension bulletins), respectively; EY is the expected yield (t ha^{-1}), N_{credit} is the credits for soil organic N from previous legume crops or manure application (Table 5.1) and 1.12 is the unit conversion

coefficient from lb/ac to kg/ha, ε is the adjustment term that further accounts for spatial variability of long-term average soil fertility among management zones and is described in detail below along with management zone delineation. We assume 50% of the N_{target} amount is applied before planting as either fall or spring application.

2) Data query. This step essentially collects all data required and creates a special-format simulation file that will be fed into the APSIM. It starts with importing a 5m × 5m raster shapefile for a customized field. According to the shapefile, soil parameters such as layered soil hydraulic properties, soil pH, and soil organic matter (SOM) are queried from the Soil Survey Geographic (SSURGO) database (Soil Survey Staff, 2015) and resampled to finer vertical layers of at depth 0-10, 10-20, 20-50, 50-100 and 100-200 cm. When there are multiple soil components within a grid, the one takes the largest fraction will be selected. Detailed descriptions for soil parameters required for the model are presented in Archontoulis et al. (2014). Real time weather data including daily maximum and minimum temperature, precipitation and solar radiation are downloaded from the National Climate Data Center (NCDC). Field management information including planting date, density and cultivar relative maturity is input by users if available; otherwise, we assign estimated values according to satellite imagery and USDA National Agricultural Statistics Service report.

3) Crop model simulation. The APSIM is run at a daily time step to provide soil and crop N status, such as N leaching and denitrification, N leftover in soil, and plant N uptake. Instead of running the model for the whole field, we first run the model for virtual grids, and then re-project outputs to the 5m-resolution raster shapefile according to a geographic reference table. A virtual grid is a unique combination of soil type, seeding

rates and management zone. For example, if there are 5 different soil types, 4 levels of seeding rates and 5 management zones for a given field, the number of virtual grids is 100. Using virtual grids substantially reduces the computational cost. To reduce simulation uncertainty, the crop model will be iterated for calibration until it can reasonably match the user reported growth stage (e.g. leaf numbers) or satellite derived leaf area index (LAI) data.

4) Calculating sidedress N application rate. The sidedress fertilizer rate ($N_{sidedress}$) is calculated using the equation:

$$N_{sidedress} = N_{target} + N_{loss} - N_{uptake} - N_{leftover} \quad (5.2)$$

where N_{loss} is the total N losses via denitrification (N_{denit}) and leaching (N_{leach}) up-to-date, N_{uptake} is the cumulative plant N uptake when sidedress N recommendation is requested, and $N_{leftover}$ is the remaining inorganic N up-to-date. We assume that sidedress N application is requested mostly when corn reaches the V6 stage. We also assume that the N losses after sidedress application will be compensated by net mineralization of soil organic matter. Nitrogen losses after R2 stage are not critical since most N uptake by corn plant is completed by R2 stage.

5.2.2 Management zone delineation

For a given field, we first identify the sub-field relative productivity zones based on the wide dynamic range vegetation index (WDRVI) derived from the RapidEye images. The RapidEye system is a constellation of five satellites that produces multispectral images at a spatial resolution of 5m × 5m (RapidEye AG 2012), with detailed description of radiometric and geometric properties of the RapidEye sensor is given in Chander et al.

(2013). The red (630–685 nm) and near infrared red (NIR) (760–850 nm) bands were used to calculate the WDRVI following Gitelson (2004):

$$WDRVI = \frac{\alpha\rho_{NIR} - \rho_{red}}{\alpha\rho_{NIR} + \rho_{red}} \tag{5.3}$$

where ρ is the reflectance and α is weighting coefficient set to be 0.2. To reduce the inconsistency of atmospheric conditions, we applied an atmospheric correction following standard procedures. A cloud filter that can detect the cloudiness based on likelihood (developed by Farmlogs) was used to exclude images with 25% cloud cover or more. The WDRVI was first calculated for each individual RapidEye image collected between July 15th and Septembet 1st for years 2009-2014, and then averaged on time scale at the pixel level. We selected the time window from middle July to early September because previous studies showed that remotely sensed vegetation index during this period are most indicative for the final corn yield (Sibley et al. 2014; Lobell et al. 2015). Using multi-year average is essential to reducing the impact of climate induced yield variability, and otherwise the delineation is prone to inconsistency across years (Derby et al. 2007). The averaged WDRVI image was then fed into an unsupervised k-means algorithm implemented in the "scikit-learn" package for Python. The k-means algorithm divided total pixels (x) into k clusters, by optimizing the choice of cluster specific centroids (c) that can minimize the total within-cluster distance between individual pixel and the corresponding centroid:

$$D_{total} = \sum_{j=1}^{k} \sum_{i=1}^{n_j} \left\| x_i^{(j)} - c_j \right\| \tag{5.4}$$

where $x_i^{(j)}$ is the i-th pixel in j-th cluster, and n_j is the number of pixel classified into j-th cluster. The algorithm includes the following steps:

(a) Choose k pixels as the initial centroids. The k-means++ initialization scheme is used to guarantee distant initial centroids, which provably improves the clustering performance (Arthur and Vassilvitskii 2007).

(b) Assign each pixel to its nearest centroid.

(c) Create new centroids by taking the mean value of all of the samples assigned to each previous centroid.

The last two steps will be repeated until the difference between the old and the new centroids is less than a prescribed threshold (usually very small). We set k equal to 5, and the resulting clusters were labeled as high, high-media, media, media-low and low productivity zones. These productivity zones were then overlapped with the SSURGO map units, and each unique combination of productivity zone and soil map unit was treated as a separate management zone.

5.2.3 Nitrogen simulation in APSIM

The SoilN module simulates the dynamics of soil carbon (C) and N on a daily basis, with N mineralization, immobilization, nitrification, denitrification and urea hydrolysis explicitly described in each soil layer. The layer-specific SOM is divided into a fast decomposing pool (BIOM) and a less active pool (HUM). To account for the age of different organic residuals, part of the HUM pool is further specified as a recalcitrant pool (INERT), with the fraction to be higher in deeper soil layers. Organic N sequestrated by SOM will be gradually released through mineralization according to the decomposing of each soil C pools, with the rate mediated by soil temperature, moisture, and C/N ratio.

More fresh organic matter is stored in a separate pool (FOM), and is initialized by root weight and root C/N ratio. The FOM pool contains three sub-pools, namely the carbohydrate-like, cellulose-like and lignin-like pools, with default fractions set as 0.2, 0.7, 0.1, respectively. APSIM also support manure application through the SurfaceOM module, which describes the organic N fractions in the same way as the FOM pool. When N fertilizer is applied, the N will enter the inorganic N pools of Urea-N, NH_4-N and NO_3-N, with the fraction determined by the fertilizer type.

These soil N processes are primarily controlled by soil temperature, moisture, pH and water flow through the soil profile. Daily soil temperature for each soil layer is simulated by the SoilTemp module. Soil hydrology is simulated by a tipping-bucket water balance model, the SoilWat module. This daily time-step hydrology model includes: surface runoff (estimated via the USDA curve number method), soil evaporation (estimated via the two-stage evaporation method), plant transpiration (estimated via the transpiration efficiency approach), and vertical water flows and fluxes that can transport N in soil solute through the soil profile. Parameters for these soil modules are mainly derived from the SSURGO database, and a few are obtained through calibration.

5.2.4 Sensitivity analysis

In APSIM, the simulation of soil N, hydrology and thermal processes are controlled by more than a hundred parameters and physical constants. To understand the response of model output to variations in parameter setting, and to reduce the dimension of parameter space for calibration, a global sensitivity analysis (GSA) following Pappas et al. (2013) was conducted:

1) Select output of interest. Here we primarily focus on model outputs of N_{dnit}, N_{leach} and N_{uptake} on a prescribed date of June 20th (i.e. roughly 30-40 days after corn planting in the US Corn-Belt), since these variables are directly used to calculate our in-season N recommendation. In addition, we included net N mineralization ($netNmin$), which is the largest uncertain contributor to $N_{leftover}$.

2) Select parameters and assign prior distribution. The majority of parameters for the soil N module is derived from field experiment, thus should not be arbitrarily calibrated without further experiments. Instead, we selected 19 candidate parameters (Table 5.2) that will be assigned in the APSIM simulation file, on the basis of extensive model structure investigation. Parameter ranges were mostly derived from literature if available; otherwise a conservative wide range was assigned so as to cover the full range of plausible values. Each parameter was assumed as an independent variable, following an uniform distribution.

3) Qualitative GSA. This step was to obtain the subset of very influential parameters using the Morris Elementary Effect (EE) approach (Morris 1991). This method based on the randomized experiment design of many one-at-a-time simulations, allows to rank parameters according to the statistic measure:

$$\epsilon = \sqrt{\mu_{EE}^2 + \sigma_{EE}^2} \tag{5.5}$$

where μ_{EE} indicates the overall influence of a parameter to model output, and σ_{EE} is an estimator of high order parameter interactions. To further account for soil variability, the qualitative GSA was applied for 5 generic soil types from the HC27 (Harvest Choice 2010) namely sandy, sandy-silt, silt, silt-clay, and clay soils.

4) Quantitative GSA. The Sobol2007 method (Sobol et al. 2007), a variance-based GSA, was used on the parameter subset suggested in the previous step. For a given generalized crop model:

$$Y(t) = f(X, t|\Theta) + \varepsilon \tag{5.6}$$

where $Y(t)$ is the model output at time t, X is a vector of input data, $\Theta = (\theta_1, \theta_2, \cdots \theta_k)$ is the parameter vector, and ε is the error term, its first-order sensitivity index (i.e. the main effect) of parameter θ_i is calculated as:

$$S_i = \frac{V_i}{V_Y} = \frac{V\left[E[Y|\theta_i]\right]}{V[Y]} = \frac{V\left[E[Y|\theta_i]\right]}{\sum_{i=1}^{k} V_i + \sum_{i=1}^{k}\sum_{j>i}^{k} V_{ij} + \cdots + V_{12\cdots k}} \tag{5.7}$$

where $V_i = V\left[E[Y|\theta_i]\right]$, $V_{ij} = V\left[E\left[Y|\theta_i, \theta_j\right]\right] - V_i - V_j$, and so on. The total-order sensitivity index (i.e. total effect) of parameter θ_i is calculated as:

$$S_{Ti} = \frac{E\left[V[Y|\Theta_{-i}]\right]}{V[Y]} = 1 - \frac{V\left[E[Y|\Theta_{-i}]\right]}{V[Y]} \tag{5.8}$$

where Θ_{-i} is a vector of all parameters but the ith.

5.2.5 Model calibration

Model calibration for a specific location requires a range of field measurement and is very labor costing (Archontoulis et al. 2014). Considering our goal is to develop a N recommendation tool that should be computationally efficient and spatially extensible, our calibration mainly focuses on the simulation of soil moisture and LAI. Soil moisture directly moderating soil N dynamics and the amount of leaching, thus is critical for the calculation of sidedress N rate. However, existing dataset does not support parameterization of soil hydrological model on field scale for most of the US Corn-Belt, therefore we derived parameter values from the SSURGO database. In APSIM, LAI

directly controls the canopy intercepted solar radiation, which further limits the biomass production, and the accumulated biomass will in turn be allocated to build LAI. Because of this feedback cycle, any under- or over-estimation in LAI (especially in early seasons between emergence and V5/V6 stages) will lead to unreasonable simulation of corn growth and N uptake. When the WDRVI data has good quality from last year to present, we calibrate the model-simulated LAI against WDRVI-derived values by adjusting four key parameters, namely, *breadth* (determines the width of LAI seasonal curve), *skewness* (determines the LAI change rate), *area_max* (determines the max potential LAI), *largest_leaf* (determines when the max potential LAI occurs); otherwise, we calibrate the model against a generic curve provided by the Iowa State University Extension (Abendroth et al. 2011). The WDRVI to LAI conversion was based on the empirical relationship built by Vina et al. (2011) in the form of:

$$LAI = \frac{1}{b}[ln(a) - ln(a + y_0 - WDRVI)] \tag{5.9}$$

where $a = 1.4392$, $b = 0.3418$ and $y_0 = -0.6684$. For all processes, the shuffled complex evolution Metropolis algorithm (SCEM-UA), an adaptive MCMC sampler, was implemented to globally optimize these parameters (Jin et al. 2015).

5.2.6 Case study

To test the robustness of this prototype, we applied the workflow to a representative US Midwestern rainfed corn field in Illinois (Holmes' farm; Figure 5.3). For the 2015 growing season, the farmer applied 112 kg/ha spring fertilizer in forms of Urea N on Mar 24th; seeds were sown in variable seeding rates with 30 inch rows on May 25th (Figure 5.4a); a mixture of three corn varieties with same relative maturity ratings

were planted. The cultivar specific parameters were adopted from a similar cultivar for the US Corn-Belt, the Pioneer_P04612XR_106 (see Table 4 in Archontoulis et al. 2014). The prescription for sidedress N was requested on June 24th, and applied by the variable rate fertilizer applicator during the following week. The corn was harvested on October 18th, with final yield logged by Farmlogs' Flow (a device with cellular connectivity plugged into a combine's existing ISOBUS port, and send data to the FarmLogs platform while harvesting).

5.3 Results and discussion

5.3.1 Management zone delineation

The delineation of relative productivity zones derived from the 5-year averaged summer time WDRVI is shown in Figure 5.4c. High productivity zones accounted for 24.3% of the whole field, and were found mainly at the top-left and bottom-right part of the field. Low productivity zones accounted for 9.6%, and distributed as a stripped channel stretching from the bottom-right corner to the middle of the field. Such a channel was also identified from the Google Earth base soil imagery (Figure 5.3). High-medium, medium and medium-low productivity zones accounted for 26.7%, 23.1% and 16.3%, respectively. The spatial variability of productivity zones was comparable to bare soil colors, with high productivity zones generally occurred at light colored soils and low productivity zones corresponding to dark soils. Such a relationship seemed opposite to common observations that darker soils with more SOM in general had higher fertility (Scharf 2015). A possible explanation is that dark-colored soils were prone to flooding as they had on average lower elevation than surrounding areas (Figure D1), and

counteracted the benefit from higher humus accumulation. It is also likely that the spectral properties of surface soils may not reflect the fertility of deeper soils. As is shown in Fleming et al. (2004), management zones retrieved from soil colors differed substantially to the results derived from the soil apparent electrical conductivity (EC_a), and the latter approach was more effective in identifying the expected spatial variability in a case study. Interestingly, the satellite imagery derived productivity zone configurations are not consistent with the SSURGO soil map (Figure 5.4b), suggesting more efforts were required to transfer soil surveys data into directly usable information for subfield precision management. Figure 5.4b and 5.4c were overlaid to generate the final management zones, but results were not shown here due to visualization constraint.

Management zone delineation was so far a critical uncertain step within our workflow. To date, efficient and accurate procedure for creating management zones is still lacking, and no single method fits all situations (Derby et al. 2007). This study utilized the satellite imagery of crop growth to delineate the management zone, mainly because this approach meets our demand of efficiency and spatial extendibility. Canopy sensor or grid soil sampling based approach for in-season N recommendation can be more reliable as they are based on the field measurement, but the considerable labor cost negates the accuracy (Scharf 2015). In cases of low yield due to unfavorable weather conditions, the economic benefit from precision N management may not outcompete the costs for field sampling (Derby et al. 2007). EC_a is more cost-effective than traditional fieldwork based approach, whereas its interpretation often requires the use of additional georeferenced data and expert experience. Topography (e.g. elevation) has long been identified as a yield-limiting factor (Kravchenko and Bullock 2000). With the advent of

high-quality topographic data, soil survey database in conjunction with terrain attributes such as elevation, topographic wetness index, slope percentage and modified catchment area can be used to generate digital maps that better represents the soil functions (Ashtekar and Owens 2013). Our future research efforts will focus on integrating the geospatial information of soil color and topography into the management zone delineation.

5.3.2 Model sensitivity analysis and calibration

The qualitative GSA in general identifies "cn2_bare", "density", "fbiom", "finert", "NO3", "SummerCona", "SummerU", "sw" and "swcon" (alphabetic order) as the ten most sensitive parameters, although slight variations exists among different model outputs of interest and soil type (results not shown). For quantitative GSA, the total parameter sensitivity based on 20,000 model simulations for each combination of model output and soil type is given in Figure 5.5. The most influential parameter for N_{uptake} is "oc", which accounts for nearly 50% of the total variability and is followed by "finert", "fbiom" and "swcon" that each explains more than 10% of the variability. Over 75% of the variability in simulated N_{dnit} can be attributed to the uncertainty of "swcon", much more than the 25% share taken by "oc" (Figure 5.5b). "cn2_bare", "NO3", "oc", "sw" and "swcon" are important parameters to explain the variability in N_{leach}, indicating water drainage and N forms are critical processes controlling leaching loss. The uncertainty in $netNmin$ can be mainly explained by "fbiom", "finer" and "oc" (Figure 5.5d). Differences between soil types are small for all variables investigated except for N_{leach}, which is highly dependent on soil hydraulic properties.

Our sensitivity analysis indicates soil water conductivity and the amount and composition of SOC are the most sensitive parameters to explain the variability in each of interested model output. Although not directly tested here, the importance of parameters like saturated water content (SAT in APSIM), water holding capacity (DUL in APSIM) and wilting point (LL15 in APSIM) to all above-mentioned processes are well established. The accuracy of these parameters are therefore vital to the uncertainty of the in-season N recommendation However, due to a lack of reliable subfield soil sampling that covers a large geographic span, we are not able to do spatially explicit calibration for these parameters at this stage. Water conductivity in theory can be calibrated against soil moisture measurements. Although continuous observations for different soil depth exist at stations affiliated with various networks (e.g. AmeriFlux, llinois Climate Network and ISU Soil Moisture Network), their very limited spatial distribution along with considerable soil heterogeneity making it unsuitable to directly compare the simulated soil moisture to any measurements from a neighboring station (not to mention the nearest station is usually miles away). A possible way to use these measurements is to do calibration at individual sites, and then extrapolate the optimized parameters based on their relationships with more readily available information such as soil texture. However, the numerical uncertainty introduced in the procedures of calibration may jeopardize this method, making it no better than those literature methods. For example, Saxton et al. (1986) introduced a method (Saxton method hereafter) to estimate generalized soil hydraulic characteristics from soil texture, and released an updated version with additional field measurements (Saxton and Rawls, 2006). We compared soil hydraulic parameters calculated by the Saxton method to values obtained from SSURGO, and

found the two sets were close to each. Therefore in this study, we primarily use parameter values in SSURGO database, while filling missing values with the Saxton method. Determining SOC is even more challenging, because the traditional soil sampling is labor and cost intensive and suffers from a high spatial uncertainty (Scharf 2015). Simple, reliable and scalable methods to estimate the spatial heterogeneity in SOC are still lacking. Soil reflectance (color) has the potential to fill this gap, but results obtained using this method so far can be only treated as preliminary (Gomez et al. 2008; Ladoni et al. 2010; Nocita et al. 2012). In our study, the mismatch between subfield variation of soil fertility and bare soil colors partly revealed the challenges ahead, and will be investigated further in the future studies.

Calibration with the SCEM-UA method improved the 2014 LAI simulation, especially for the V5/V6 stage when rapid canopy growth starts in response to a high rate of N uptake (6. 5). The root mean square error (RMSE) decreased from 0.53 for the simulation with default parameters to 0.26 for the optimized set. For the 2015, using the optimized parameters increases the simulated average LAI on June 22nd from 0.053 to 0.269, and hence three times more plant N uptake than simulations with default parameters. Our calibration showed that assimilating WDRVI data to the APSIM model can reduce the uncertainty in LAI simulation, which further improves the prediction of crop growth and N uptake. One caveat to be mentioned is that the number of WDRVI images used for calibration is only a little more than the number of parameters to be calibrated, thus lowers the credibility and efficiency of our calibration. In the future, we will increase the collection frequency of RapidEye imagery up to weekly so that the growing season (especially early stages) will be covered by more samples.

5.3.3 Sub-field sidedress recommendation

By the time when N sidedress was requested, N_{loss} via denitrification and leaching for Holmes' farm was considerable (Figure 5.7a), accounting for an average of 20% of the spring N application. Subfield variations were mostly delineated by soil types (Figure 5.4b), reconfirming the leading role of soil property for determining N loss in this region. However, the highest loss mainly came from the Ashkum silty clay loam soil (map unit 232A) with greater SOM, suggesting higher spring mineralization might have led to greater N loss under specific conditions. The Variations in N_{uptake} were small, with the majority grids showing N uptake between 20-25 kg/ha N (Figure 5.7b), indicating substantial N uptake had not yet happened at this stage. The spatial patterns of N_{uptake} do not follow either soil types or management zones, rather were close to the spatially explicit seeding rates (results not show). Grids with dense corn population in general showed higher N uptakes. Another interesting phenomenon was higher N_{uptake} patches occasionally came along with lower N_{loss} compared to its surroundings with the same soil properties (e.g. N_{uptake} patches with the darkest green in the top-right and middle-left part of the field), indicating appropriate rooting density can improve fertilizer use efficiency (Garnett et al. 2009). The subfield variability of $N_{leftover}$ was primarily characterized by indigenous soil supply potential, with N_{loss} and N_{uptake} played secondary roles (Figure 5.7c). Highest $N_{leftover}$ (> 88% of the spring application amount) occurred in Elliot silty clay loam soil (map unit 146B2), while lowest values occurred in Ashkum silty clay loam soil. The recommended $N_{sidedress}$ rates followed the management zone distribution, with secondary variability further identified by other

factors (Figure 5.7d). Very high rates (> 140 kg/ha) accounted for 24.2% of the total field, because these parts had the high yield potential. The field average sidedress rate was 113.2 kg/ha, and is close to the difference between the N_{target} and flat rate of pre-plant application. Thus the strategy of variable fertilizing did not necessary increase the total fertilizer demand, but rather allocated resources from zones with high loss potentials to the ones with high use efficiency. A RapidEye image was acquired on July-14th, 2015, approximately two weeks after the sidedress, and converted to the WDRVI (Figure 5.7e). Patches with high WDRVI values (i.e. denser corn canopy) closely followed the $N_{sidedress}$, showing the field crop responded quickly to the sidedress fertilizer. The low WDRVI strips on the imagery border were likely due to delay in N discharge resulting from tractor operations.

It should be noted that without assigning a spatial adjustment term (ε) in Eqn-1, the recommended N sidedress had much smaller variations (range from 95.6 to 105.6 kg/ha). The lack of spatial variability was somewhat surprising given the heterogeneity that existed due to combination of soil type, elevation and plant population, but the same was also reported in other studies (e.g. Derby et al. 2007). This was mainly because the N_{loss} was small as it was not been long since the spring N application, and N_{uptake} was similar within the field before rapid growth occurred on V5/V6 stage. Adding adjustment term thus helped to account for the spatial variation in N denitrification, leaching and differential crop yield potential. After the sidedress, our model can run progressively by assimilating new weather data and monitor the soil and crop N state throughout the remaining growing season to alert when N stress occurred.

The harvested yield for 2015 differed substantially within the field, with low yield patches amounted less than 6 tons/ha and highest yield up to 12.8 tons/ha (Figure 5.7f). The spatial variability in yield is comparable with variable sidedress rates (Figure 5.7d), with higher yield generally occurred in places where greater sidedress N was applied. The low yield strip stretching from the southeast to the west is also easily identified, matching closely to the low fertilizing zone in Figure 6d. We also analyzed the zonal mean yield with four different ways of delineating the field (Figure 5.8). Average yield were close for seeding rates between 30,000 and 36,000 per acre, and was approximately 2.6 tons/ha higher than the average yield from zones with 28,000 populations per acre (Figure 5.8a). However, further increasing the seeding rate to 38,000 or 39,000 per acre decreased the average yield, possibly because higher plant population competed for resources. As was expected, average yield increases gradually along the multi-year WDRVI derived productivity zones (Figure 5.8b), showing our method to delineate the productivity zone is robust. Yield differences are insignificant among major soil map units, while within map unit standard deviations are large. This further confirms the fact that the heterogeneity of some key soil properties is overlooked by the SSURGO database. Average yield in general increased with the level of sidedress rate, with the marginal benefit more obvious for lower levels (Figure 5.8d). Interestingly, zones with “>140” kg/ha sidedress N on average yielded slightly less than those with “120-140” kg/ha sidedress N, indicating the saturated fertilizer amount for this field is roughly achieved at this level if no other management strategy is applied.

5.4 Conclusions

In this study, we presented a crop model and satellite imagery based within field scale recommendation tool of variable rate N fertilization at subfield scales for the US Corn system. We used the crop model simulations to track the soil N dynamics, while the satellite images were used to delineate management zones, to train the model, and to assess the crop growth status. The tool successfully captured the subfield variability of crop systems. The recommended sidedress N rates enhanced zones with high yield potential, while prevented over-fertilization at zones with low yield potentials. Model sensitivity analysis and calibrations indicate that soil hydraulic properties and soil organic carbon content are critical to the reliability of our sidedress N prescription. Cumulative N uptake upon the time of sidedress can be well constrained by calibrating the LAI. The benefit from sidedress decreases with the increase of fertilizer amount.

Compared with other N recommendation tools, our framework is efficient, accurate and scalable and requires less upfront information from users. Although the framework presented here can be easily adapted to other crops or regions outside the US, two caveats should be noted. First, information on soil properties is the major source of uncertainty, but high quality data for calibration that covers a large are is unavailable at this time. More creative ways of using multiple sources of data need to be further explored. Microwave and hyperspectral remote sensing for mapping soil structure and organic matter has good potentials to replace the direct soil sampling, and will be investigated in our future research. Second, RapidEye imagery can well capture the crop status on clear days, but may not on cloudy days. Thus higher frequency of image collection and complementary data sources need to be considered to use this tool.

Table 5.1 N credits from legume crops and manures.

Type	Application	N credit (lb/ac)
	Legume	
Alfalfa dense		100*
Alfalfa dense		40
Bean		25
Clover dense		50
Clover thin		0
Fallow		10
Soya		40
Sugarbeet		50
Vetch		50
	Manure	
Beef_solid	Broadcast	3.5
	Incorporated	5.9
Beef_liquid	Broadcast	6.7
	Incorporated	11.8
Dairy_solid	Broadcast	2.3
	Incorporated	4.6
Dairy_liquid	Broadcast	6.2
	Incorporated	12.4
Poultry_solid	Broadcast	18.8
	Incorporated	24.4
Poultry_liquid	Broadcast	23.5
	Incorporated	31.0
Turkey_solid	Broadcast	21.6
	Incorporated	30.2
Turkey_liquid	Broadcast	28.8
	Incorporated	37.2
Swine_solid	Broadcast	4.9
	Incorporated	8.5
Swine_liquid	Broadcast	14.2
	Incorporated	20.8

Table 5.2 Parameter definitions and initial ranges for sensitivity analysis

Variable	Definition	LB	UB	Units
sw	Initial soil water content; same for all layers	0.2	1	mm/mm
SummerCona	Stage II evaporation coefficient for summer	2	6	$Mm/day^{0.5}$
SummerU	Stage I soil evaporation coefficient for summer	3	9	mm
WinterCona	Stage II evaporation coefficient for winter	2	6	mm^0.5
WinterU	Stage I soil evaporation coefficient for winter	3	9	mm
diffus_const	Coefficient for calculating soil water diffusivity	30	100	$mm/day^{0.5}$
diffus_slope	Coefficient for calculating soil water diffusivity	10	40	
cn2_bare	Runoff curve number for bare soils	40	90	
cn_red	Maximum reduction in curve number when residual cover = cn_cov	10	30	
cn_cov	Threshold for residual cover	5	100	%
swcon	Soil water conductivity	0.05	1	
root_cn	C/N ratio for root residuals	30	50	
soil_cn	C/N ratio for soil organic matters (SOM)	10	15	
oc	Soil organic content	0.5	3.5	%
fbiom	Fraction of BIOM pool in SOM for top layer; assume decrease exponentially for deeper layers	0.02	0.08	
finert	Fraction of INERT in SOM for top layer; assume increase exponentially for deeper layers	0.4	0.85	
ph	Soil pH values; assume constant for all layers	6	7.5	
no3ppm	Residual inorganic N in forms of NO3-N; assume constant for all layers	0	3	mu g /g
density	Crop population density	6	9	plant/m2

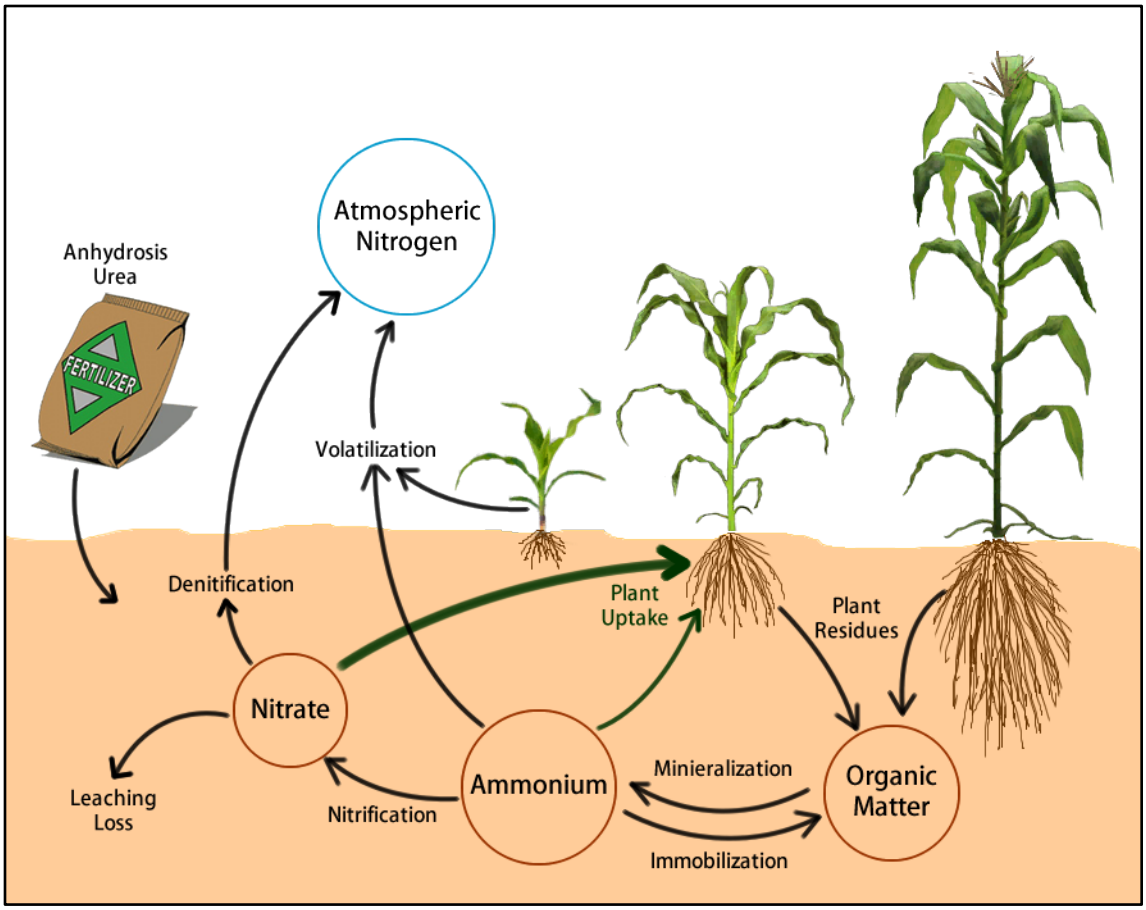

Figure 5.1 Schematic diagram of nitrogen (N) cycling in a field. Corn growth relies on the uptake inorganic N, in forms of nitrate (NO_3^-) and ammonium (NH_4^+), throughout the growing season. In organic N mainly comes from fertilizer input and indigenous N supply released by soil organic matter, but is susceptible to losses through several processes, including denitrification and volatilization to the atmosphere and leaching to the groundwater. Plant residues (e.g. dead roots and leaves) brings a portion of N back to the soil organic carbon pool. Organic and inorganic N interconvert with each other through mineralization and immobilization.

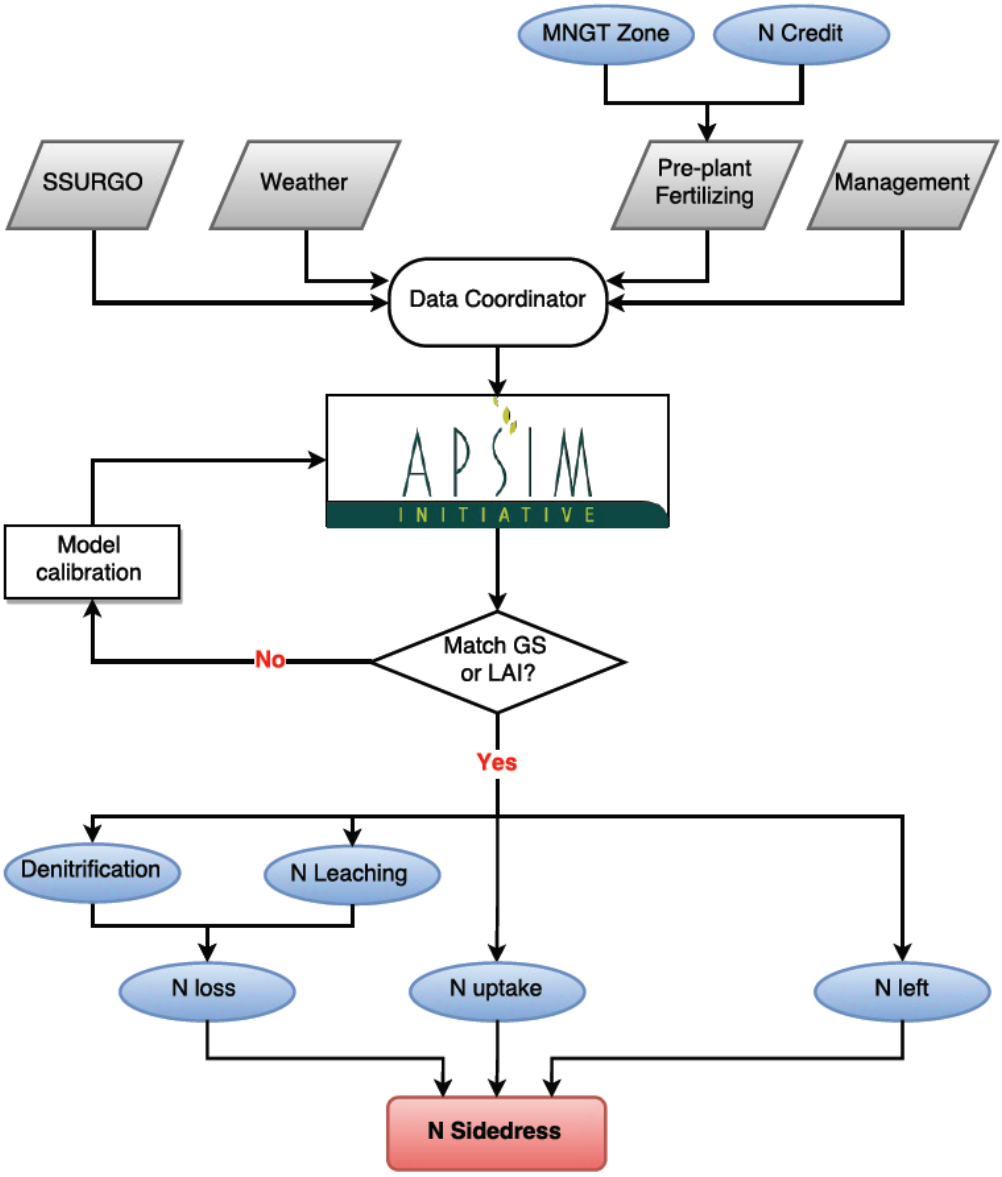

Figure 5.2 A schematic diagram for the workflow used in this study to generate the in-season N sidedress.

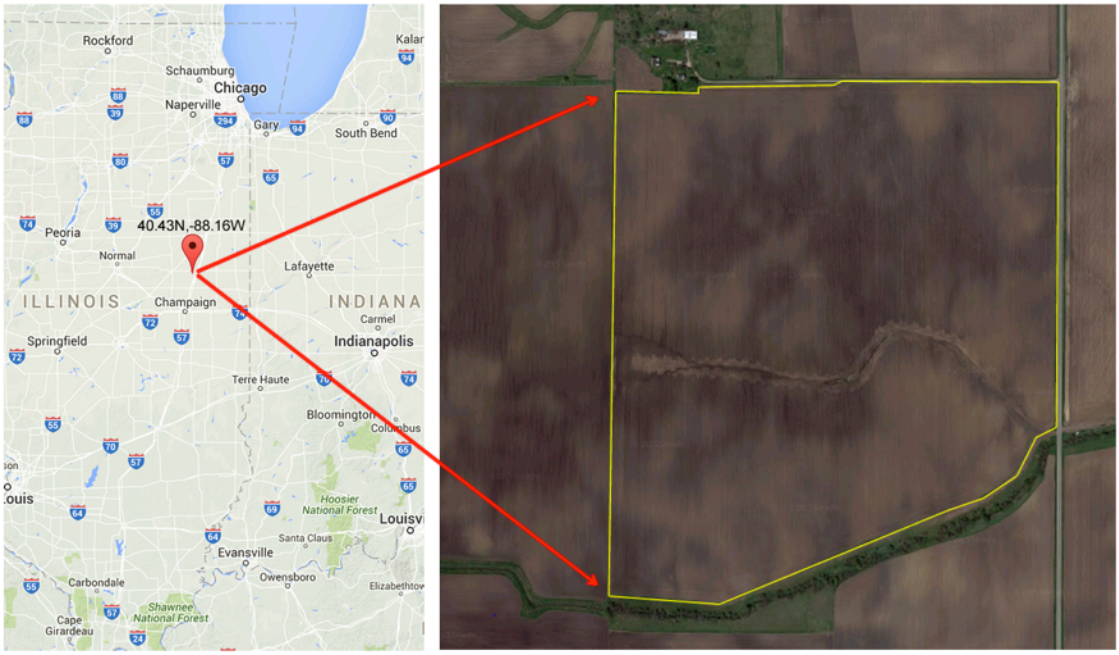

Figure 5.3 Study area of Holmes' farm (the focus field is highlighted by the yellow polygon).

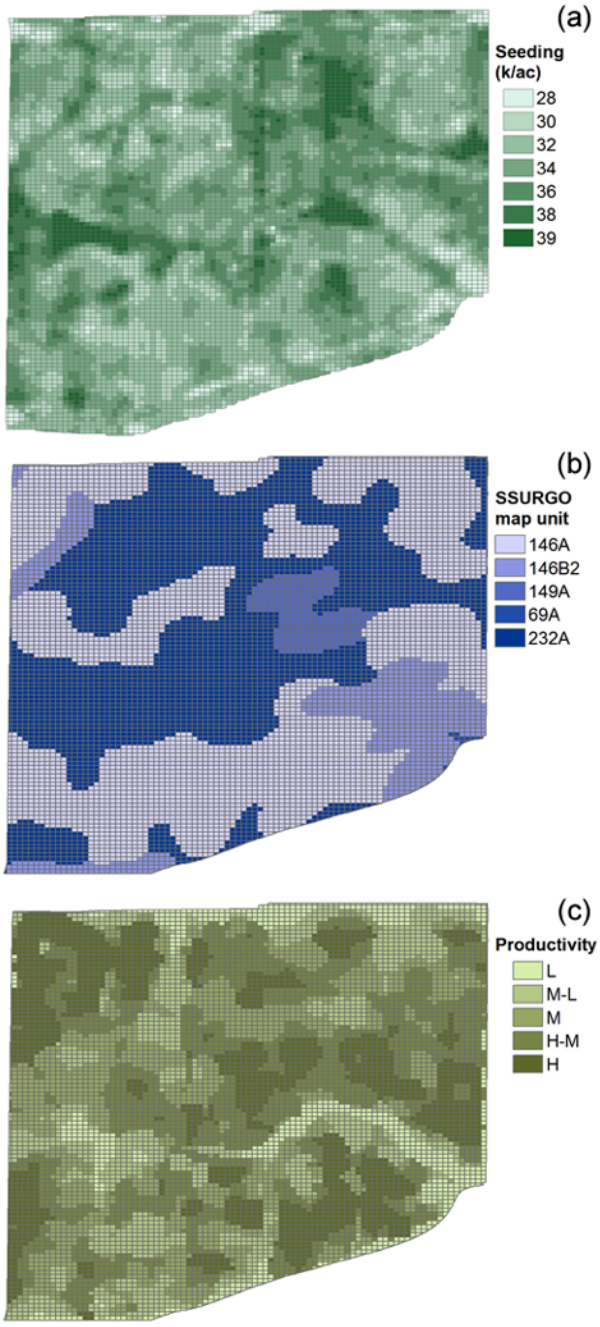

Figure 5.4 Spatial delineation of Holmes' farm according to (a) seeding rates in thousands population per acre (k/ac; 1 plants/m2 ≈ 4 k/ac), (b) soil map units from SSURGO database ("146A" denotes Elliot silt loam soil, "146B2" denotes Elliot silty clay loam soil, "149A" denotes Brenton silt loam soil, "69A" denotes Milford silty clay loam soil and "232A" denotes Ashkum silty clay loam soil), and (c) relative productivity derived from multi-year averaged WDRVI data.

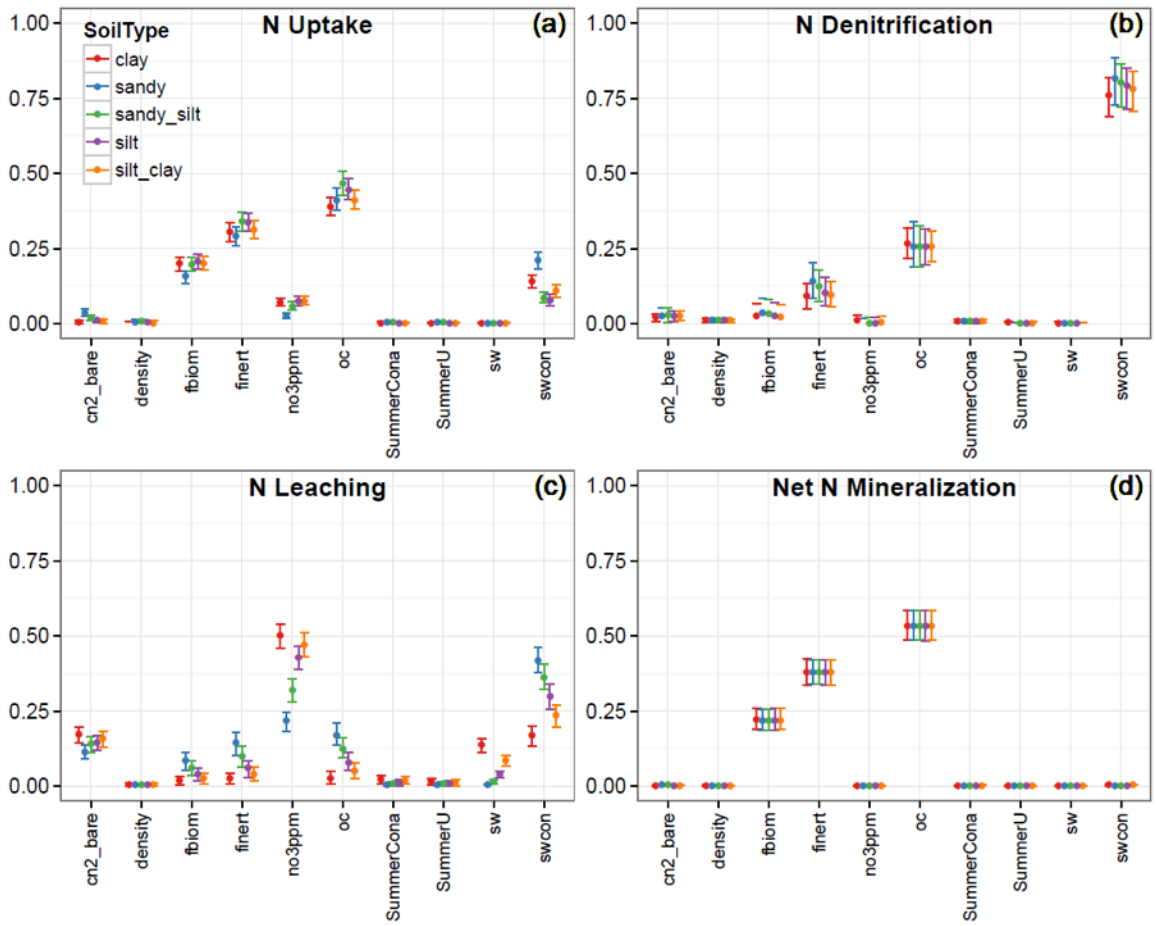

Figure 5.5 Total effects of parameter sensitivity for cumulative (a) plant N uptake, (b) denitrification, (c) N loss through leaching, and (d) net N mineralization under five generic soil conditions.

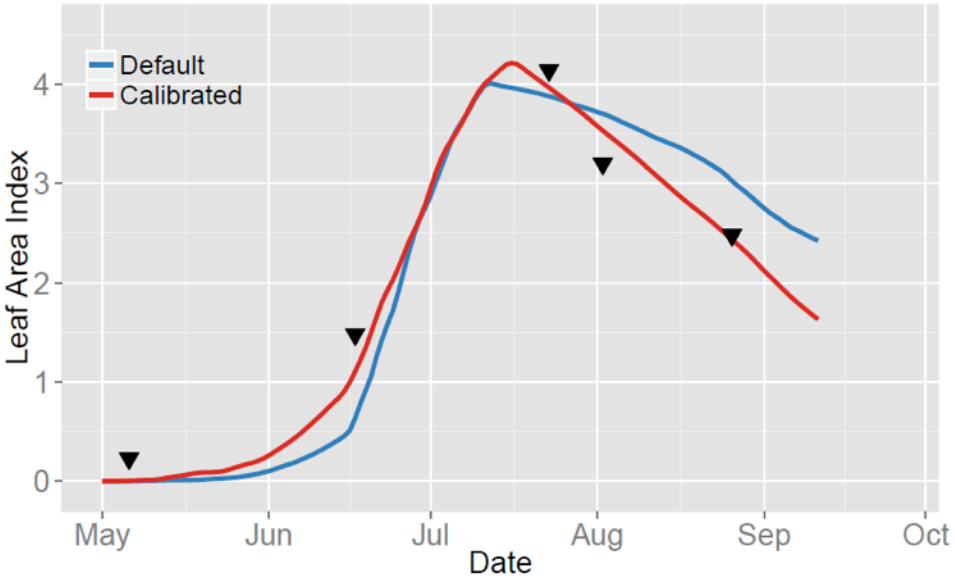

Figure 5.6 Model simulated leaf area index (LAI) with default (blue) and calibrated (red) parameters. Black triangle represents the 90% quantile of field average LAI converted from the WDRVI.

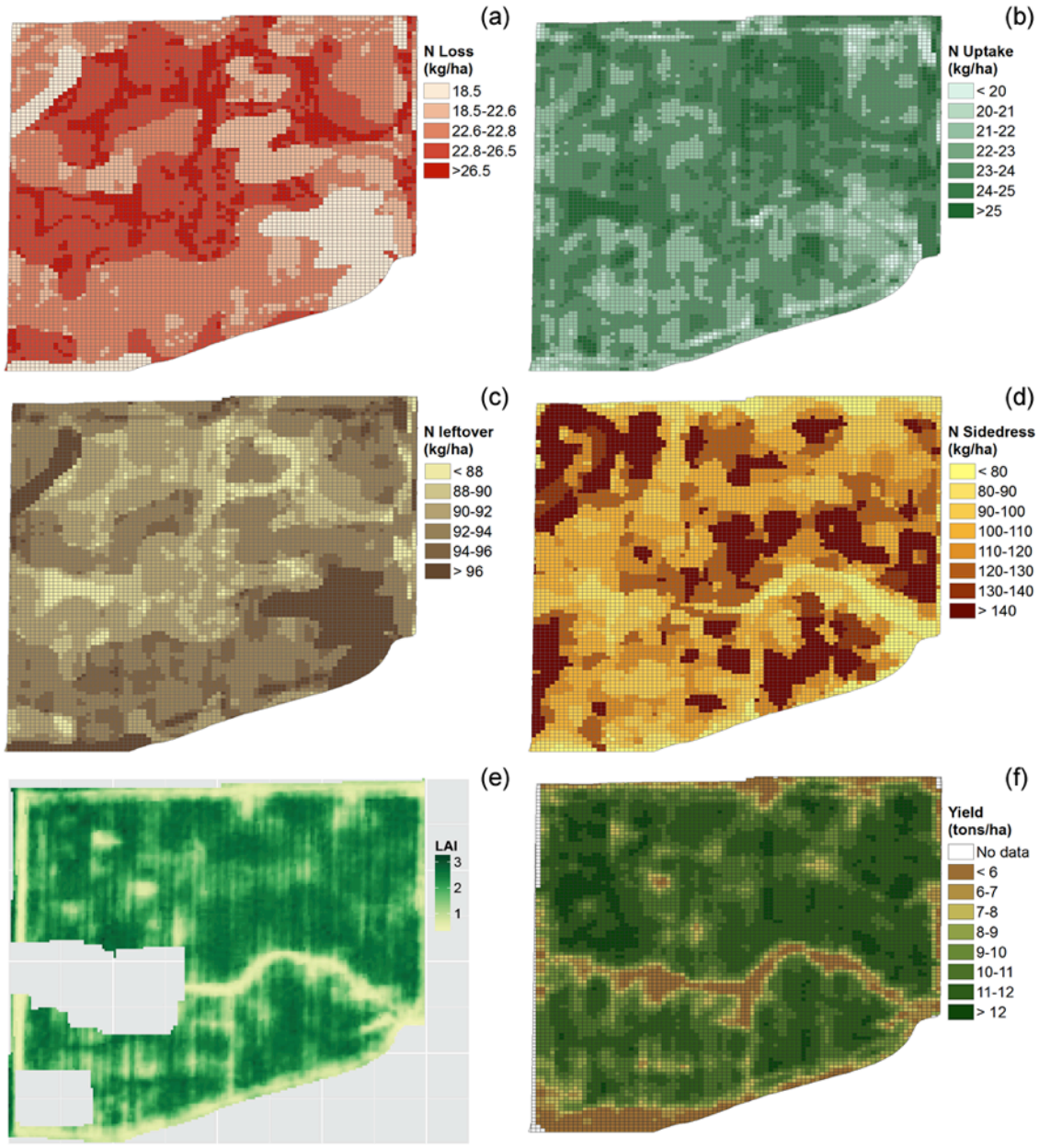

Figure 5.7 The spatial variation of model simulated (a) N loss, (b) plant N uptake, (c) N leftover in soil, and (d) N sidedress rate. (e) LAI from RapidEye imagery acquired on July-14, 2015. (f) harvested yield for 2015.

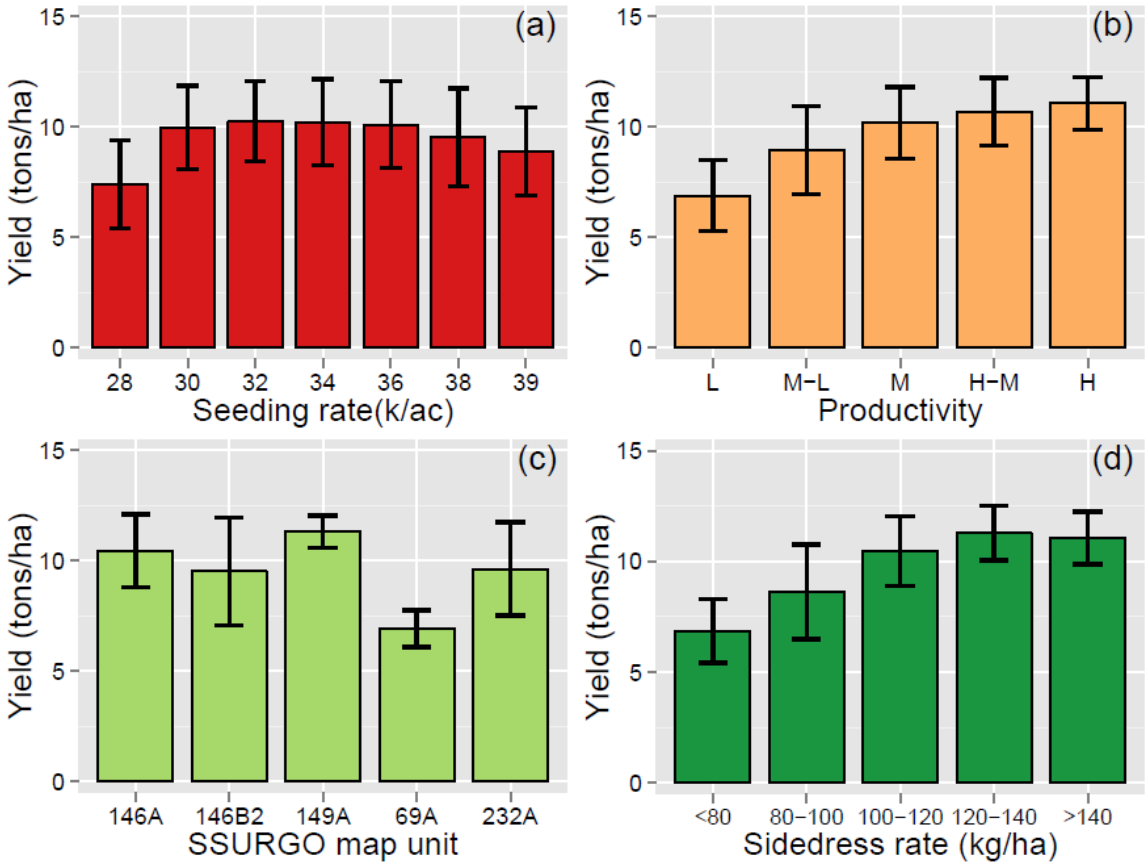

Figure 5.8 Zonal statistics for average yield. Zones are delineated according to (a) seeding rate, (b) relative productivity, (c) SSURGO map unit, and (d) N sidedress rate. Error bars represent one standard deviation.

CHAPTER 6. CONCLUDING REMARKS AND FUTURE WORK

6.1 Summary and conclusions

The increasingly severe and frequent extreme climatic events, such as heat waves and droughts, are impairing crops growth and threatening the food security. Although elevated atmospheric CO_2 may partially compensate yield losses caused by adverse climate, and adaptation of crop breeding and management practice can increase the resilience of agriculture system to climate change, the high uncertainty in the climate projections makes planned adaptation very difficult. Understanding climatic risks to food security in face of the complex interactions of biophysical, social-economical and political factors at various scales is one part of the challenges (Ewert et al., 2015). On the other hand, any knowledge advances, eventually, will need to be translated to tangible recommendations or tools to farmers, who are required to make a series of decisions throughout a growing season. Such complexities call for more integrated cropping system models and novel approaches to use these models, while this dissertation is exactly an early step in this direction.

Chapter 2 evaluates the algorithms that determine impacts of heat and drought stress on maize in 16 major crop models by incorporating these algorithms into the APSIM, and running an ensemble of simulations at typical farms from the US Midwest. Results show that both daily mean temperature and daylight temperature can be used to

simulate heat stress as long as the corresponding algorithm is parameterized correctly; however, current parameterizations in most models favor the use of daylight temperature even though the algorithm was designed for using daily mean temperature. Different drought algorithms (i.e. a function of soil water content, of soil water supply to demand ratio and of actual to potential transpiration ratio) simulate considerably different patterns of water shortage over the growing season, but nonetheless predicted similar decreases in annual yield. The review of algorithms in 16 crop models suggests that the impacts of heat and drought stress on crop yield can be best described by models that: (i) incorporate event-based descriptions of heat and drought stress, (ii) consider the effects of nighttime warming, and (iii) coordinate the interactions among multiple stresses.

Chapter 3 quantifies the current and future yield responses of US rainfed maize and soybean to climate extremes, and for the first time characterizes spatial shifts in the relative importance of temperature, heat and drought stress. By simulating maize and soybean yields with APSIM driven by the 12 km WRF Model downscaled future climate scenarios at two time slices (1995-2005 and 2085-2094), this study concludes that: (i) yield losses and inter-annual variability are greater in the core production area than in the remaining US by the late 21st century, with the magnitude of impacts highly depending on the current climate sensitivity and vulnerability; (ii) elevated CO_2 partially offsets the climatic yield gaps and reduces interannual yield variability, and effect is more prominent in soybean than in maize; (iii) drought will continue to be the largest threat to US rainfed maize and soybean production, but shifts in the geographic distributions of dominant stressors are characterized by increases in the concurrent stress.

Chapter 5 presents a prototype of crop model and satellite imagery based within-field scale N sidedress prescription tool for the US rainfed maize system. As an early attempt to integrate advances in multiple areas for precision agriculture, this tool successfully captures the subfield variability of N dynamics and gives reasonable spatially explicit sidedress N recommendations. The prescription enhances zones with high yield potential, while prevents over-fertilization at zones with low yield potentials. Compared with existing N recommendation tools, the framework shown here is efficient, scalable and requires less upfront information from users. Model sensitivity analysis and calibrations indicate that soil hydraulic properties and soil organic carbon content are critical to the reliability of the sidedress N prescription. Future improvements could be achieved by focusing on: (i) digital soil mapping that retrieves more heterogeneity in soil fertility and hydraulic properties, and (ii) satellite data assimilation with the utilization of additional missions and advanced algorithms so as to better constrain the simulation of crop phenology and development.

6.2 Reflections and future work

Although results presented in this dissertation are promising and encouraging, some generic limitations that span across modeling studies are inevitable, such as inadequate model structure, the propagation of uncertainties in model parameterization and input data. More efforts are thus needed in the future in order to overcome these problems. However, what I really want to reflect in this section, as the end of my dissertation, is the challenge of crop model scalability. My past few years of research and job interview experience has repeatedly confirmed me a truth that both the academia and

industry face a bottleneck of model scalability and geospatial extrapolation. At site level, with sufficient local monitoring and measurements as training sample, it is no longer an unattainable task for crop modelers to come up with a localized model with ~90% accuracy by tuning model parameters using modern optimization techniques (e.g. Archontoulis et al., 2014). But scaling up this measurement-calibration-application framework to a large region with spatial and temporal heterogeneity remains a significant challenge since there is often no ground measurement can be utilized to train a model beyond research stations, thus lowers the credibility and universality of crop and cropping system models.

By their nature of spatial coverage and frequent revisit, satellite imagery has long been incorporated into crop models as a simulation steering (Bouman et al., 1992), and becomes the most popular substitutions of ground measurements with the recent development in public and commercial satellite missions (Lobell, 2013). Sequential data assimilation (e.g. remotely-sensed vegetation indices) to integrate models and observations for minimizing the simulation uncertainty is now robust in terms of the methodology, and the Monte Carlo-based Ensemble Kalman Filter (EnKF) is one such technique with many successful applications in agriculture for the research purpose (Inez et al., 2013). Recently, scientists have started to incorporate radiative transfer models into cropping system models in order to utilize additional spectral information beyond the commonly used vegetation indices derived merely from red and near-infrared bands (Machwitz et al., 2014; Hank et al., 2015). Yet the progresses so far are still not enough for real farming purpose. For example, current data assimilation algorithms are computationally heavy, thus cannot afford applications on massive scales yet need to be

delivered within a few days. In addition, one underlying assumption of using satellite data is that errors in the data are acceptable to propagate throughout the models (Inez et al., 2013), whereas most existing remote sensing measurements are uncertain due to a lack of missions that acquires data with both sufficient spatial resolutions to identify individual fields and within field variability, and adequate frequency of temporal coverage to ensure several cloud-free images during a growing season (Lobell, 2013). Some commercial companies, such as the Planet Lab INC., have shed light on this dilemma because they are sending over 100 satellites into the orbit to watch the entire global, every single day, with 3-5m resolutions.

While remote sensing is able to provide images of aboveground crops and shallow topsoil, it is so far weak in retrieving variables of soil properties. Although soil hydraulic parameters can be inversely estimated by matching model simulations with aboveground satellite data such as LAI and ET (Charoenhirunyinyos et al., 2011), and soil organic content or soil fertility can be linked to soil reflectance (Ladoni et al., 2010), these techniques are still premature and far away from being capable to generate estimation with ~90% accuracy. In this sense, digital soil mapping (DSM) that combines expert knowledge in soil formation and the wealth of existing soil survey database could be one direction with full potential. Ashtekar & Owens (2013) presented a DSM method that predict soil functions by selective sampling and fuzzy logic approach that utilizes multiple terrain attributes, with the assumption that water movement and redistribution across the landscape is the driving force of functional difference and topography controls water movement. Crop modeling and satellite data can further facilitate DSM by providing estimates of some variables that co-vary with specific soil property.

The incorporation of new mechanisms into crop models will also help to reduce the spatial uncertainty in model predictions. James W. Kirchner, an eminent expert in earth surface processes, wrote in his recent paper (Kirchner, 2016) that, “It is often tacitly assumed/hoped that spatial heterogeneity problem will be solved or masked by model calibration”. He questioned why the underlying mechanisms (or relationship between variables), which are supposed to be universally true, for system models failed to fit across scales without re-calibrating. His argument was that many of those seemingly right relationships only validate under certain circumstances, thus suffer from aggregation biases. Alternatively one might expect to use some predictors that are spatially stable in its relationship with the dependent variable, and Dr. Kirchner successfully found one for his research purpose. Unfortunately, the crop modeling community has too little choices of variables that are free of spatial aggregation errors when developing yield predictions; vegetation indices such as LAI might count one. The recent advances in the retrieval of solar-induced fluorescence (SIF) signal have opened up a new approach (or a new generation of crop models) to estimate the crop yield and to directly monitor the impact of environmental stresses (Guanter et al., 2014; Guan et al., 2015), because the relationship between SIF and crop photosynthesis activity (i.e. electron transport rate) is less susceptible to aggregation errors. But the research of SIF is still in the very early stage.

While the way forward is deemed to have challenges and uncertainty, I am very happy that my past few years of study and research have eventually helped me figure out an area that is full of potential and possibility, and most importantly, is full of my passion. I am fully prepared for a bigger stage to continue my agriculture modeling research.

REFERENCES

REFERENCES

Ainsworth EA, Leakey ADB, Ort DR, Long SP (2008) FACE-ing the facts: inconsistencies and interdependence among field, chamber and modeling studies of elevated [CO 2] impacts on crop yield and food supply. *New Phytologist*, **179**, 5–9.

Ainsworth EA, Yendrek CR, Sitch S, Collins WJ, Emberson LD (2012) The effects of tropospheric ozone on net primary productivity and implications for climate change. *Annual review of plant biology*, **63**, 637–61.

Alderman P, Quilligan E, Asseng S, Ewert F, Reynolds M (2013) *Modeling wheat response to high teperature*. 142 pp.

Allen RG, Pereira LS, Raes D, Smith M, W a B (1998) Crop evapotranspiration - Guidelines for computing crop water requirements - FAO Irrigation and drainage paper 56. *Irrigation and Drainage*, 1–15.

Anapalli SS, Ma L, Nielsen DC, Vigil MF, Ahuja LR (2005) Simulating planting date effects on corn production using RZWQM and CERES-maize models. *Agronomy Journal*, **97**, 58–71.

Anderson WK (2010) Closing the gap between actual and potential yield of rainfed wheat. The impacts of environment, management and cultivar. *Field Crops Research*, **116**, 14–22.

Angulo C, Rötter R, Lock R, Enders A, Fronzek S, Ewert F (2013) Implication of crop model calibration strategies for assessing regional impacts of climate change in Europe. *Agricultural and Forest Meteorology*, **170**, 32–46.

Archontoulis S V., Miguez FE, Moore KJ (2014a) A methodology and an optimization tool to calibrate phenology of short-day species included in the APSIM PLANT model: Application to soybean. *Environmental Modelling & Software*, **62**, 465–477.

Archontoulis S V., Miguez FE, Moore KJ (2014b) Evaluating APSIM Maize, Soil Water, Soil Nitrogen, Manure, and Soil Temperature Modules in the Midwestern United States. *Agronomy Journal*, **106**, 1025.

Ashtekar JM, Owens PR (2013) Remembering Knowledge: An Expert Knowledge Based Approach to Digital Soil Mapping. *Soil Horizons*, **54**.

Asseng S., Ewert F., Rosenzweig C. et al. (2013) Uncertainty in simulating wheat yields under climate change. *Nature Climate Change*, **3**, 827–832.

Barlow KM, Christy BP, O'Leary GJ, Riffkin PA, Nuttall JG (2015) Simulating the impact of extreme heat and frost events on wheat crop production: A review. *Field Crops Research*, **171**, 109–119.

Basso B, Ritchie J (2014) Temperature and drought effects on maize yield. *Nature Climate Change*, **4**, 48823.

Bassu S, Brisson N, Durand J-LL et al. (2014) How do various maize crop models vary in their responses to climate change factors? *Global Change Biology*, **20**, 2301–20.

Bernacchi CJ, Morgan PB, Ort DR, Long SP (2005) The growth of soybean under free air [CO(2)] enrichment (FACE) stimulates photosynthesis while decreasing in vivo Rubisco capacity. *Planta*, **220**, 434–46.

Bernacchi CJ, Kimball BA, Quarles DR, Long SP, Ort DR (2007) Decreases in stomatal conductance of soybean under open-air elevation of [CO2] are closely coupled with decreases in ecosystem evapotranspiration. *Plant physiology*, **143**, 134–44.

Bezlepkina I, Reidsma P, Sieber S, Helming K (2011) Integrated assessment of sustainability of agricultural systems and land use: Methods, tools and applications. *Agricultural Systems*, **104**, 105–109.

Bishop KA, Betzelberger AM, Long SP, Ainsworth EA (2015) Is there potential to adapt soybean (Glycine max Merr.) to future [CO_2]? An analysis of the yield response of 18 genotypes in free-air CO_2 enrichment. *Plant, cell & environment*, **38**, 1765–74.

Boote KJ, Jones JW, White JW, Asseng S, Lizaso JI (2013) Putting mechanisms into crop production models. *Plant, Cell and Environment*, **36**, 1658–1672.

Borrás L, Curá JA, Otegui ME (2002) Maize kernel composition and post-flowering source-sink ratio. *Crop Science*, **42**, 781–790.

Borrás L, Maddonni G., Otegui M. (2003) Leaf senescence in maize hybrids: plant population, row spacing and kernel set effects. *Field Crops Research*, **82**, 13–26.

BOUMAN BAM (1992) Linking physical remote sensing models with crop growth simulation models, applied for sugar beet. *International Journal of Remote Sensing*, **13**, 2565–2581.

Bouman BAM, van Kasteren HWJ, Uenk D (1992) Standard relations to estimate ground cover and LAI of agricultural crops from reflectance measurements. *European Journal of Agronomy*, **1**, 249–262.

Boyer JS, Byrne P, Cassman KG et al. (2013) The U.S. drought of 2012 in perspective: A call to action. *Global Food Security*, **2**, 139–143.

Bunce JA (2014) Limitations to soybean photosynthesis at elevated carbon dioxide in free-air enrichment and open top chamber systems. *Plant science : an international journal of experimental plant biology*, **226**, 131–5.

Butler EE, Huybers P (2013) Adaptation of US maize to temperature variations. *Nature Climate Change*, **3**, 68–72.

Carberry PSS, Muchow RCC, McCown RLL (1989) Testing the CERES-Maize simulation model in a semi-arid tropical environment. *Field Crops Research*, **20**, 297–315.

Challinor AJ, Wheeler TR, Craufurd PQ, Slingo JM (2005) Simulation of the impact of high temperature stress on annual crop yields. *Agricultural and Forest Meteorology*, **135**, 180–189.

Challinor AJ, Wheeler T, Hemming D, Upadhyaya HD (2009) Ensemble yield simulations: Crop and climate uncertainties, sensitivity to temperature and genotypic adaptation to climate change. *Climate Research*, **38**, 117–127.

Chapin III, FS, Matson PA and Vitousek P (2011) Principles of terrestrial ecosystem ecology. Springer Science & Business Media.

Chapman SC (2008) Use of crop models to understand genotype by environment interactions for drought in real-world and simulated plant breeding trials. *Euphytica*, **161**, 195–208.

Charoenhirunyingyos S, Honda K, Kamthonkiat D, Ines AVM (2011) Soil moisture estimation from inverse modeling using multiple criteria functions. *Computers and Electronics in Agriculture*, **75**, 278–287.

Collatz GJ, Ribas-Carbo M, Berry J a. (1992) Coupled photosynthesis-stomatal conductance model for leaves of C4 plants. *Australian Journal of Plant Physiology*, **19**, 519–539.

Cooper M, Gho C, Leafgren R, Tang T, Messina C (2014) Breeding drought-tolerant maize hybrids for the US corn-belt: Discovery to product. *Journal of Experimental Botany*, **65**, 6191–6194.

Coumou D, Rahmstorf S (2012) A decade of weather extremes. *Nature Climate Change*, **2**, 1–6.

Degener JF, Kappas M (2015) Differences in biomass yield development of early, medium, and late maize varieties during the 21st century in Northern Germany. *Environmental Sciences Europe*, **27**, 10.

DERMODY O, LONG SP, McCONNAUGHAY K, DeLUCIA EH (2008) How do elevated CO 2 and O 3 affect the interception and utilization of radiation by a soybean canopy? *Global Change Biology*, **14**, 556–564.

Deryng D, Sacks WJJ, Barford CCC, Ramankutty N (2011) Simulating the effects of climate and agricultural management practices on global crop yield. *Global Biogeochemical Cycles*, **25**, 1–18.

Deryng D, Conway D, Ramankutty N, Price J, Warren R (2014) Global crop yield response to extreme heat stress under multiple climate change futures. *Environmental Research Letters*, **9**, 34011–13.

Dietzel R, Liebman M, Ewing R, Helmers M, Horton R, Jarchow M, Archontoulis S (2016) How efficiently do corn- and soybean-based cropping systems use water? A systems modeling analysis. *Global change biology*, **22**, 666–81.

Diffenbaugh NS, Ashfaq M (2010) Intensification of hot extremes in the United States. *Geophysical Research Letters*, **37**, n/a–n/a.

Djanaguiraman M, Prasad PV V., Boyle DL, Schapaugh WT (2011) High-Temperature Stress and Soybean Leaves: Leaf Anatomy and Photosynthesis. *Crop Science*, **51**, 2125.

Donatelli M, Bregaglio S, Confalonieri R, De Mascellis R, Acutis M (2014) A generic framework for evaluating hybrid models by reuse and composition – A case study on soil temperature simulation. *Environmental Modelling & Software*, **62**, 478–486.

Drewry DT, Kumar P, Long SP (2014) Simultaneous improvement in productivity, water use, and albedo through crop structural modification. *Global change biology*, **20**, 1955–67.

Dumont B, Leemans V, Mansouri M, Bodson B, Destain J-P, Destain M-F (2014) Parameter identification of the STICS crop model, using an accelerated formal MCMC approach. *Environmental Modelling & Software*, **52**, 121–135.

Eitzinger J, THALER S, SCHMID E et al. (2013) Sensitivities of crop models to extreme weather conditions during flowering period demonstrated for maize and winter wheat in Austria. *The Journal of Agricultural Science*, **151**, 813–835.

Elnesr MN, Alazba AA (2016) A spreadsheet model to select vegetables planting dates for maximum yield and water use efficiency. *Computers and Electronics in Agriculture*, **124**, 55–64.

Ewert F, Rötter RP, Bindi M et al. (2015) Crop modelling for integrated assessment of risk to food production from climate change. *Environmental Modelling & Software*, **72**, 287–303.

Eyshi Rezaei E, Webber H, Gaiser T, Naab J, Ewert F (2015) Heat stress in cereals: Mechanisms and modelling. *European Journal of Agronomy*, **64**, 98–113.

Geng G, Wu J, Wang Q et al. (2016) Agricultural drought hazard analysis during 1980-2008: a global perspective. *International Journal of Climatology*, **36**, 389–399.

Gerde JA, Tamagno S, Di Paola JC, Borrás L (2016) Genotype and Nitrogen Effects over Maize Kernel Hardness and Endosperm Zein Profiles. *Crop Science*.

González-Dugo MP, Moran MS, Mateos L, Bryant R (2006) Canopy temperature variability as an indicator of crop water stress severity. *Irrigation Science*, **24**, 233–240.

Grant RF (1989) Simulation of carbon assimilation and partitioning in maize. *Agronomy Journal*, **81**, 563–571.

Grassini P, Yang H, Cassman KG (2009) Limits to maize productivity in Western Corn-Belt: A simulation analysis for fully irrigated and rainfed conditions. *Agricultural and Forest Meteorology*, **149**, 1254–1265.

Guan K, Pan M, Li H et al. (2015) Photosynthetic seasonality of global tropical forests constrained by hydroclimate. *Nature Geoscience*, **8**, 284–289.

Guan K, Berry JA, Zhang Y, Joiner J, Guanter L, Badgley G, Lobell DB (2016) Improving the monitoring of crop productivity using spaceborne solar-induced fluorescence. *Global change biology*, **22**, 716–26.

Guanter L, Zhang Y, Jung M et al. (2014) Global and time-resolved monitoring of crop photosynthesis with chlorophyll fluorescence. *Proceedings of the National Academy of Sciences of the United States of America*, **111**, E1327–33.

Hammer GL, Dong Z, McLean G et al. (2009) Can Changes in Canopy and/or Root System Architecture Explain Historical Maize Yield Trends in the U.S. Corn Belt? *Crop Science*, **49**, 299.

Hammer GL, Van Oosterom E, McLean G, Chapman SC, Broad I, Harland P, Muchow RC (2010) Adapting APSIM to model the physiology and genetics of complex adaptive traits in field crops. *Journal of Experimental Botany*, **61**, 2185–2202.

Hank T, Bach H, Mauser W (2015) Using a Remote Sensing-Supported Hydro-Agroecological Model for Field-Scale Simulation of Heterogeneous Crop Growth and Yield: Application for Wheat in Central Europe. *Remote Sensing*, **7**, 3934–3965.

Harrison MT, Tardieu F, Dong Z, Messina CD, Hammer GL (2014) Characterizing drought stress and trait influence on maize yield under current and future conditions. *Global Change Biology*, **20**, 867–878.

Hartman GL, West ED, Herman TK (2011) Crops that feed the World 2. Soybean—worldwide production, use, and constraints caused by pathogens and pests. *Food Security*, **3**, 5–17.

Hatfield JL, Boote KJ, Kimball BA et al. (2011) Climate impacts on agriculture: Implications for crop production. *Agronomy Journal*, **103**, 351–370.

Hochholdinger F, Tuberosa R (2009) Genetic and genomic dissection of maize root development and architecture. *Current Opinion in Plant Biology*, **12**, 172–177.

Holzworth DP, Huth NI, deVoil PG et al. (2014) APSIM – Evolution towards a new generation of agricultural systems simulation. *Environmental Modelling & Software*, **62**, 327–350.

Holzworth DP, Snow V, Janssen S et al. (2015) Agricultural production systems modelling and software: Current status and future prospects. *Environmental Modelling & Software*, **72**, 276–286.

Honda K, Ines AVM, Yui A, Witayangkurn A, Chinnachodteeranun R, Teeravech K (2014) Agriculture Information Service Built on Geospatial Data Infrastructure and Crop Modeling. In: *Proceedings of the 2014 International Workshop on Web Intelligence and Smart Sensing - IWWISS '14*, pp. 1–9. ACM Press, New York, New York, USA.

Hussain MZ, Vanloocke A, Siebers MH et al. (2013) Future carbon dioxide concentration decreases canopy evapotranspiration and soil water depletion by field-grown maize. *Global change biology*, **19**, 1572–84.

Ines AVM, Das NN, Hansen JW, Njoku EG (2013) Assimilation of remotely sensed soil moisture and vegetation with a crop simulation model for maize yield prediction. *Remote Sensing of Environment*, **138**, 149–164.

IPCC (2012) *Managing the Risks of Extreme Events and Disasters to Advance Climate Change Adaptation: Special Report of the Intergovernmental Panel on Climate Change*, Vol. 1. 582 pp.

Karp A, Richter GM (2011) Meeting the challenge of food and energy security. *Journal of experimental botany*, **62**, 3263–71.

Keating B. A, Carberry P. S, Hammer G. L et al. (2003) An overview of APSIM, a model designed for farming systems simulation. In: *European Journal of Agronomy*, Vol. 18, pp. 267–288.

Kirchner JW (2016) Aggregation in environmental systems – Part 1: Seasonal tracer cycles quantify young water fractions, but not mean transit times, in spatially heterogeneous catchments. *Hydrology and Earth System Sciences*, **20**, 279–297.

Koenker RW, Bassett GW (1978) Regression Quantiles. *Econometrica*, **46**, 33–50.

Kotsuki S, Tanaka K (2015) SACRA-a method for the estimation of global high-resolution crop calendars from a satellite-sensed NDVI. *Hydrology and Earth System Sciences*, **19**, 4441–4461.

Kucharik CJ (2006) A multidecadal trend of earlier corn planting in the central USA. *Agronomy Journal*, **98**, 1544–1550.

Kucharik CJ (2008) Contribution of planting date trends to increased maize yields in the central United States. *Agronomy Journal*, **100**, 328–336.

Kucharik CJ, Brye KR (2003) Integrated BIosphere Simulator (IBIS) yield and nitrate loss predictions for Wisconsin maize receiving varied amounts of nitrogen fertilizer. *Journal of Environment Quality*, **32**, 247–268.

Kumudini S, Andrade FH, Boote KJ et al. (2014) Predicting maize phenology: Intercomparison of functions for developmental response to temperature. *Agronomy Journal*, **106**, 2087–2097.

Kurtz B, Gardner CAC, Millard MJ, Nickson T, Smith JSC (2016) Global Access to Maize Germplasm Provided by the US National Plant Germplasm System and by US Plant Breeders. *Crop Science*.

Ladoni M, Bahrami H, Alavipanah S, Norouzi A (2010) Estimating soil organic carbon from soil reflectance: a review. *Precision Agriculture*, **11**, 82–99.

Leakey ADB, Uribelarrea M, Ainsworth EA, Naidu SL, Rogers A, Ort DR, Long SP (2006) Photosynthesis, productivity, and yield of maize are not affected by open-air elevation of CO2 concentration in the absence of drought. *Plant physiology*, **140**, 779–90.

Leakey ADB, Ainsworth EA, Bernacchi CJ, Rogers A, Long SP, Ort DR (2009) Elevated CO2 effects on plant carbon, nitrogen, and water relations: Six important lessons from FACE. In: *Journal of Experimental Botany*, Vol. 60, pp. 2859–2876.

Lehmann N, Finger R, Klein T, Calanca P, Walter A (2013) Adapting crop management practices to climate change: Modeling optimal solutions at the field scale. *Agricultural Systems*, **117**, 55–65.

Leitner D, Felderer B, Vontobel P, Schnepf A (2014) Recovering root system traits using image analysis exemplified by two-dimensional neutron radiography images of lupine. *Plant physiology*, **164**, 24–35.

Lesk C, Rowhani P, Ramankutty N (2016) Influence of extreme weather disasters on global crop production. *Nature*, **529**, 84–87.

Liu Z, Hubbard KG, Lin X, Yang X (2013) Negative effects of climate warming on maize yield are reversed by the changing of sowing date and cultivar selection in Northeast China. *Global Change Biology*, **19**, 3481–3492.

Lizaso JI, Batchelor WD, Boote KJ, Westgate ME (2005) Development of a leaf-level canopy assimilation model for CERES-Maize. *Agronomy Journal*, **97**, 722–733.

Lobell DB (2013) The use of satellite data for crop yield gap analysis. *Field Crops Research*, **143**, 56–64.

Lobell DB, Gourdji SM (2012) The Influence of Climate Change on Global Crop Productivity 1. *Plant Physiology*, **160**, 1686–1697.

Lobell DB, Schlenker W, Costa-Roberts J (2011) Climate trends and global crop production since 1980. *Science (New*, **333**, 616–20.

Lobell DB, Hammer GL, McLean G, Messina C, Roberts MJ, Schlenker W (2013a) The critical role of extreme heat for maize production in the United States. *Nature Climate Change*, **3**, 497–501.

Lobell DB, Ortiz-Monasterio JI, Sibley AM, Sohu VS (2013b) Satellite detection of earlier wheat sowing in India and implications for yield trends. *Agricultural Systems*, **115**, 137–143.

Lobell DB, Roberts MJ, Schlenker W, Braun N, Little BB, Rejesus RM, Hammer GL (2014) Greater sensitivity to drought accompanies maize yield increase in the U.S. Midwest. *Science (New York, N.Y.)*, **344**, 516–9.

Lobell DB, Hammer GL, Chenu K, Zheng B, McLean G, Chapman SC (2015a) The shifting influence of drought and heat stress for crops in northeast Australia. *Global change biology*, **21**, 4115–27.

Lobell DB, Thau D, Seifert C, Engle E, Little B (2015b) A scalable satellite-based crop yield mapper. *Remote Sensing of Environment*, **164**, 324–333.

Lombardozzi D, Levis S, Bonan G, Sparks JP (2012) Predicting photosynthesis and transpiration responses to ozone: decoupling modeled photosynthesis and stomatal conductance. *Biogeosciences*, **9**, 3113–3130.

Lombardozzi D, Levis S, Bonan G, Hess PG, Sparks JP (2015) The Influence of Chronic Ozone Exposure on Global Carbon and Water Cycles. *Journal of Climate*, **28**, 292–305.

Long SP, Ainsworth EA, Leakey ADB, Morgan PB (2005) Global food insecurity. treatment of major food crops with elevated carbon dioxide or ozone under large-scale fully open-air conditions suggests recent models may have overestimated future yields. *Philosophical transactions of the Royal Society of London. Series B, Biological sciences*, **360**, 2011–20.

Long SP, Anisworth EA, Leakey ADB, N�sberger J, Ort DR (2006) Food for Thought: Lower-than-exepted crop yield stimulation with rising CO2 concentrations. *Science*, **312**, 918–921.

Lynch JP (2013) Steep, cheap and deep: An ideotype to optimize water and N acquisition by maize root systems. *Annals of Botany*, **112**, 347–357.

Machwitz M, Giustarini L, Bossung C et al. (2014) Enhanced biomass prediction by assimilating satellite data into a crop growth model. *Environmental Modelling & Software*, **62**, 437–453.

Madhu M, Hatfield JL (2014) Interaction of Carbon Dioxide Enrichment and Soil Moisture on Photosynthesis, Transpiration, and Water Use Efficiency of Soybean. *Agricultural Sciences*, **05**, 410–429.

Manschadi AM, Christopher J, Devoil P, Hammer GL (2006) The role of root architectural traits in adaptation of wheat to water-limited environments. *Functional Plant Biology*, **33**, 823–837.

Martin MMS, Olesen JE, Porter JR (2014) A genotype, environment and management (GxExM) analysis of adaptation in winter wheat to climate change in Denmark. *Agricultural and Forest Meteorology*, **187**, 1–13.

Martre P, Wallach D, Asseng S et al. (2015) Multimodel ensembles of wheat growth: Many models are better than one. *Global Change Biology*, **21**, 911–925.

Matthews RB, Rivington M, Muhammed S, Newton AC, Hallett PD (2013) Adapting crops and cropping systems to future climates to ensure food security: The role of crop modelling. *Global Food Security*, **2**, 24–28.

Mazdiyasni O, AghaKouchak A (2015) Substantial increase in concurrent droughts and heatwaves in the United States. *Proceedings of the National Academy of Sciences of the United States of America*, **112**, 11484–9.

McGrath JM, Lobell DB (2013) Regional disparities in the CO2 fertilization effect and implications for crop yields. *Environmental Research Letters*, **8**, 014054.

McGrath JM, Betzelberger AM, Wang S, Shook E, Zhu X-G, Long SP, Ainsworth EA (2015) An analysis of ozone damage to historical maize and soybean yields in the United States. *Proceedings of the National Academy of Sciences of the United States of America*, **112**, 14390–5.

McKee IF, Mulholland BJ, Craigon J, Black CR, Long SP (2000) Elevated concentrations of atmospheric CO2 protect against and compensate for O3 damage to photosynthetic tissues of field-grown wheat. *New Phytologist*, **146**, 427–435.

Melillo JM, Richmond TC and Yohe GW (2014) Climate change impacts in the United States: the third national climate assessment. US Global change research program, 841. doi:10.7930/J0Z31WJ2.

Mendoza PA, Clark MP, Barlage M, Rajagopalan B, Samaniego L, Abramowitz G, Gupta H (2015) Are we unnecessarily constraining the agility of complex process-based models? *Water Resources Research*, **51**, 716–728.

Messina CD, Podlich D, Dong Z, Samples M, Cooper M (2011) Yield-trait performance landscapes: from theory to application in breeding maize for drought tolerance. *Journal of experimental botany*, **62**, 855–68.

Messina CD, Sinclair TR, Hammer GL et al. (2015) Limited-transpiration trait may increase maize drought tolerance in the US corn belt. *Agronomy Journal*, **107**, 1978–1986.

Mills G, Buse A, Gimeno B, Bermejo V, Holland M, Emberson L, Pleijel H (2007) A synthesis of AOT40-based response functions and critical levels of ozone for agricultural and horticultural crops. *Atmospheric Environment*, **41**, 2630–2643.

Mishra V, Cherkauer KA, Shukla S (2010) Assessment of Drought due to Historic Climate Variability and Projected Future Climate Change in the Midwestern United States. *Journal of Hydrometeorology*, **11**, 46–68.

Moriondo M., Giannakopoulos C., Bindi M. (2011) Climate change impact assessment: The role of climate extremes in crop yield simulation. *Climatic Change*, **104**, 679–701.

Neitsch S., Arnold J., Kiniry J., Williams J. (2011) Soil & Water Assessment Tool Theoretical Documentation Version 2009. *Texas Water Resources Institute, TR-406*, 1–647.

Neukam D, Böttcher U, Kage H (2015) Modelling Wheat Stomatal Resistance in Hourly Time Steps from Micrometeorological Variables and Soil Water Status. *Journal of Agronomy and Crop Science*, n/a–n/a.

O'Leary GJ, Christy B, Nuttall J et al. (2014) Response of wheat growth, grain yield and water use to elevated CO2 under a Free-Air CO2 Enrichment (FACE) experiment and modelling in a semi-arid environment. *Global change biology*.

Ort DR, Long SP (2014) Limits on yields in the Corn Belt. *Science*, **344**, 484–5.

Parent B, Tardieu F (2012) Temperature responses of developmental processes have not been affected by breeding in different ecological areas for 17 crop species. *New Phytologist*, **194**, 760–774.

Parent B, Tardieu FF (2014) Can current crop models be used in the phenotyping era for predicting the genetic variability of yield of plants subjected to drought or high temperature? *Journal of Experimental Botany*, **65**, 6179–6189.

Parton WJ, Hartman M, Ojima D, Schimel D (1998) DAYCENT and its land surface submodel: Description and testing. *Global and Planetary Change*, **19**, 35–48.

Peng S, Piao S, Ciais P et al. (2013) Asymmetric effects of daytime and night-time warming on Northern Hemisphere vegetation. *Nature*, **501**, 88–92.

Prasad PV V., Staggenborg SA, Ristic Z (2008) *Response of Crops to Limited Water: Understanding and Modeling Water Stress Effects on Plant Growth Processes*, Vol. advancesin. American Society of Agronomy, Crop Science Society of America, Soil Science Society of America, 301-355 pp.

Priestley CHB, Taylor RJ (1972) On the Assessment of Surface Heat Flux and Evaporation Using Large-Scale Parameters. *Monthly Weather Review*, **100**, 81–92.

Raes D, Steduto P, Hsiao TC, Fereres E (2009) Aquacrop-The FAO crop model to simulate yield response to water: II. main algorithms and software description. *Agronomy Journal*, **101**, 438–447.

Ramankutty N, Evan AT, Monfreda C, Foley JA (2008) Farming the planet: 1. Geographic distribution of global agricultural lands in the year 2000. *Global Biogeochemical Cycles*, **22**, n/a–n/a.

Reichstein M, Bahn M, Ciais P et al. (2013) Climate extremes and the carbon cycle. *Nature*, **500**, 287–295.

Rezaei EE, Siebert S, Ewert F (2015) Intensity of heat stress in winter wheat—phenology compensates for the adverse effect of global warming. *Environmental Research Letters*, **10**, 024012.

Riahi K, Grübler A, Nakicenovic N (2007) Scenarios of long-term socio-economic and environmental development under climate stabilization. *Technological Forecasting and Social Change*, **74**, 887–935.

Rippke U, Ramirez-Villegas J, Jarvis A et al. (2016) Timescales of transformational climate change adaptation in sub-Saharan African agriculture. *Nature Climate Change*, **advance on**.

Röotter RP, Höhn J, Trnka M, Fronzek S, Carter TR, Kahiluoto H (2013) Modelling shifts in agroclimate and crop cultivar response under climate change. *Ecology and Evolution*, **3**, 4197–4214.

Rosenzweig C, Jones JW, Hatfield JL et al. (2012) The Agricultural Model Intercomparison and Improvement Project (AgMIP): Integrated regional assessment projects. In: *Handbook of Climate Change and Agroecosystems: Global and Regional Aspects and Implications*, pp. 263–280.

Rosenzweig C, Elliott J, Deryng D et al. (2014) Assessing agricultural risks of climate change in the 21st century in a global gridded crop model intercomparison. *Proceedings of the National Academy of Sciences of the United States of America*, **111**, 3268–73.

Ruane AC, Cecil LD, Horton RM et al. (2013) Climate change impact uncertainties for maize in Panama: Farm information, climate projections, and yield sensitivities. *Agricultural and Forest Meteorology*, **170**, 132–145.

Sacks WJ, Deryng D, Foley JA, Ramankutty N (2010) Crop planting dates: an analysis of global patterns. *Global Ecology and Biogeography*, no–no.

Sakamoto T, Wardlow BD, Gitelson AA, Verma SB, Suyker AE, Arkebauer TJ (2010) A Two-Step Filtering approach for detecting maize and soybean phenology with time-series MODIS data. *Remote Sensing of Environment*, **114**, 2146–2159.

Saseendran S a., Ahuja LR, Ma L, Timlin D, Stockle CO, Boote KJ, Hoogenboom G (2008) Current Water Deficit Stress Simulations in Selected Agricultural System Models. *Response of Crops to Limited Water: Understanding and Modeling Water Stress Effects on Plant Growth Processes. Advances in Agricultural Systems Modeling Series 1.*, 1–38.

Sau F, Boote KJ, Bostick WM, Jones JW, Mínguez MI (2004) Testing and improving evapotranspiration and soil water balance of the DSSAT crop models. *Agronomy Journal*, **96**, 1243–1257.

Schlenker W, Roberts MJ (2009) Nonlinear temperature effects indicate severe damages to U.S. crop yields under climate change. *Proceedings of the National Academy of Sciences of the United States of America*, **106**, 15594–15598.

Seifert C a, Lobell DB (2015) Response of double cropping suitability to climate change in the United States. *Environmental Research Letters*, **10**, 024002.

Sharpley A, Williams J (1990) EPIC-erosion/productivity impact calculator: 1. Model documentation. *Technical Bulletin-United States Department of Agriculture*, 235.

Shekoofa A, Sinclair TR, Messina CD, Cooper M (2016) Variation among maize hybrids in response to high vapor pressure deficit at high temperatures. *Crop Science*, **56**, 392–396.

Shiferaw B, Prasanna BM, Hellin J, Bänziger M (2011) Crops that feed the world 6. Past successes and future challenges to the role played by maize in global food security. *Food Security*, **3**, 307–327.

Siebert S, Ewert F, Rezaei EE, Kage H, Graß R (2014) Impact of heat stress on crop yield—on the importance of considering canopy temperature. *Environmental Research Letters*, **9**, 1–8.

Sinclair TR, Messina CD, Beatty A, Samples M (2010) Assessment across the United States of the Benefits of Altered Soybean Drought Traits. *Agronomy Journal*, **102**, 475.

Singer JW, Meek DW, Sauer TJ, Prueger JH, Hatfield JL (2011) Variability of light interception and radiation use efficiency in maize and soybean. *Field Crops Research*, **121**, 147–152.

Smith MD (2011) The ecological role of climate extremes: current understanding and future prospects. *Journal of Ecology*, **99**, 651–655.

Souza EJ, Martin JM, Guttieri MJ et al. (1998) Influence of Genotype, Environment, and Nitrogen Management on Spring Wheat Quality. 425–432.

STREETER JG (2003) Effects of drought on nitrogen fixation in soybean root nodules. *Plant, Cell and Environment*, **26**, 1199–1204.

Tabashnik BE, Brévault T, Carrière Y (2013) Insect resistance to Bt crops: lessons from the first billion acres. *Nature biotechnology*, **31**, 510–21.

Tai APK, Martin MV, Heald CL (2014) Threat to future global food security from climate change and ozone air pollution. *Nature Climate Change*, **4**, 817–821.

Taub DR, Seemann JR, Coleman JS (2000) Growth in elevated CO2 protects photosynthesis against high-temperature damage. *Plant, Cell and Environment*, **23**, 649–656.

Testa G, Reyneri A, Blandino M (2016) Maize grain yield enhancement through high plant density cultivation with different inter-row and intra-row spacings. *European Journal of Agronomy*, **72**, 28–37.

Tester M, Langridge P (2010) Breeding Technologies to Increase Crop Production in a Changing World. *Science*, **327**, 818–822.

Tilman D, Balzer C, Hill J, Befort BL (2011) Global food demand and the sustainable intensification of agriculture. *Proceedings of the National Academy of Sciences of the United States of America*, **108**, 20260–4.

Tollenaar M, Aguilera A (1992) Radiation Use Efficiency of an Old and a New Maize Hybrid. *Agronomy Journal*, **84**, 536.

Trachsel S, Kaeppler SM, Brown KM, Lynch JP (2013) Maize root growth angles become steeper under low N conditions. *Field Crops Research*, **140**, 18–31.

Tsimba R, Edmeades GO, Millner JP, Kemp PD (2013) The effect of planting date on maize grain yields and yield components. *Field Crops Research*, **150**, 135–144.

Twine TE, Bryant JJ, T Richter K, Bernacchi CJ, McConnaughay KD, Morris SJ, Leakey ADB (2013) Impacts of elevated CO2 concentration on the productivity and surface energy budget of the soybean and maize agroecosystem in the Midwest USA. *Global change biology*, **19**, 2838–52.

Urban DW, Sheffield J, Lobell DB (2015) The impacts of future climate and carbon dioxide changes on the average and variability of US maize yields under two emission scenarios. *Environmental Research Letters*, **10**, 045003.

USDA 2013. Crop Production 2012 Summary. United States Department of Agriculture.

Wang J, Kotamarthi VR (2015) High-resolution dynamically downscaled projections of precipitation in the mid and late 21st century over North America. *Earth's Future*, **3**, 268–288.

Wang E, Robertson MJ, Hammer GL et al. (2002) Development of a generic crop model template in the cropping system model APSIM. In: *European Journal of Agronomy*, Vol. 18, pp. 121–140.

Wang J, Swati FNU, Stein ML, Kotamarthi VR (2015) Model performance in spatiotemporal patterns of precipitation: New methods for identifying value added by a regional climate model. *Journal of Geophysical Research: Atmospheres*, **120**, 1239–1259.

Webber H, Martre P, Asseng S et al. (2015) Canopy temperature for simulation of heat stress in irrigated wheat in a semi-arid environment: A multi-model comparison. *Field Crops Research*.

Webber H, Ewert F, Kimball BAA et al. (2016) Simulating canopy temperature for modelling heat stress in cereals. *Environmental Modelling and Software*, **77**, 143–155.

Wise M, Calvin K, Thomson A et al. (2009) Implications of limiting CO2 concentrations for land use and energy. *Science (New York, N.Y.)*, **324**, 1183–6.

Xu Z, Hennessy DA, Sardana K, Moschini GC (2013) The realized yield effect of genetically engineered crops: U.S. maize and soybean. *Crop Science*, **53**, 735–745.

Yang Z, Sinclair TR, Zhu M, Messina CD, Cooper M, Hammer GL (2012) Temperature effect on transpiration response of maize plants to vapour pressure deficit. *Environmental and Experimental Botany*, **78**, 157–162.

Zheng B, Chenu K, Chapman SC (2016) Velocity of temperature and flowering time in wheat - assisting breeders to keep pace with climate change. *Global change biology*, **22**, 921–33.

APPENDICES

Appendix A

Text A1. Documentation of algorithms

In this section, we reviewed and re-documented algorithms of heat and drought stress on biomass production and yield formation with detailed equations for each crop model we have reviewed. The models we reviewed have different levels of documentation support. A few models (e.g. AquaCrop, HYBRID-maize, STICS and SWAT) provide well-organized documentation on theoretical background and detailed algorithms, whereas most of them only have partial documentations on specific modules or narrative descriptions rather than explicit mathematical equations for the algorithms. Therefore we also reviewed model source codes (if publically accessible) as a complementary. It should also be mentioned that inconsistence between documentations and the implementation happened occasionally. In this case, we prioritized the actual source code over literatures and documentations. The algorithms documented here can serve as a quick reference for or a gateway to the heat and drought stress algorithms implemented in major crop models.

The detailed documentation can be accessed in GitHub with the following link: https://github.com/Zhenong/APSIM-source/blob/master/Appendix%20A1.PDF.

Text A2. Temperature response of GPP/APAR

We used the observations (available from 06/04/2001 to 05/31/2013) at the AmeriFlux Mead Rainfed station (US-Ne3) , Saunders, Nebraska (41.18°, -96.44°), to investigate the temperature response of radiation use efficiency (RUE). This rainfed station is one of three fields at the University of Nebraska Agricultural Research and Development Center. The site has a maize-soybean rotation, with maize planted in odd years. The growing season typically begins in May and ends in October. Here, we used all data from middle May to August for years when maize is planted (i.e. 2001, 2003, 2005, 2007, 2009, and 2011) to do the analysis

This station archived hourly-observed temperature, absorbed photosynthetically active radiation (APAR) and calculated Gross Primary Production (GPP). The calculation of GPP is based on the observed net ecosystem exchange (NEE; negative for net carbon sink) and ecosystem respiration (RECO; positive for flux outside the ecosystem):

$$GPP = RECO - NEE$$

Detailed descriptions on data processing and the method to calculate RECO are given in Reichstein et al. (2005). The ratio of GPP/APAR is an approximation of RUE. We also aggregated the hourly data to get the response curve of RUE to daytime and daily mean temperature. We applied the "geom_smooth" function in the R *ggplot2* package to fit a smooth line for the paired points of GPP/APAR vs. temperature. The locally weighted scatterplot smoothing (*loess*) method is used by the "geom_smooth" function to fit smoothing the points for dataset with n<1000; the generalized additive model (*gam*) is used for datasets with 1000 or more observations. The results of GPP/APAR were given in Figure A1.

It should be noted that the ratio of GPP/APAR is not exactly (instead should be higher than) the RUE used in most crop models that use RUE to calculate the daily biomass production (i.e. Net Primary Production; NPP). Therefore we have to make an assumption that NPP at a particular location will follow the dynamics of GPP, thus the temperature response curve of NPP/APAR will have similar shape of GPP/APAR except the magnitude. In other words, we should rather focus on those temperature thresholds where optimal is reached. Ideally, the parameterization of a temperature response curve should be based on experimental data that measures RUE at a temperature continuum. Given that these type of experimental measurements are currently unavailable, using the AmeriFlux data is by far the best approximation we can do provide.

Text A3. Description of EDD and KDD

Extreme degree days (EDD) is an indicator of accumulative heat above a prescribed temperature threshold. For each growing season, we calculate EDD following Lobell et al. (2013) who uses 30 °C as the threshold:

$$EDD = \sum_{t=1}^{N} DD_{30+,t}, \qquad and\ DD_{30+,t} = \begin{cases} 0 & if\ T_t < 30℃ \\ (T_t - 30)/24 & if\ T_t \geq 30℃ \end{cases}$$

where T_t is the hourly temperature for hour t, and t spans from June 1st to August 31th (thus the total hour N equals 2,208), $DD_{30+,t}$ is the hourly accumulative heat above 30 °C.

The hourly temperature T_t is interpolated based on daily minimum (T_{min}) and maximum (T_{max}) temperature using a sinusoidal function. Assuming daily minimum temperature occurs at H_{min} and daily maximum temperature occurs at H_{max}, following Hoogenboom & Huck (1986), we calculate T_t for three stages,

$$T_t = \begin{cases} \frac{T_{max} + T_{min}}{2} + \frac{T_{max} - T_{min}}{2} cos\left(\frac{\pi(t+10)}{10 + H_{min}}\right) & if\ 0 \leq t \leq H_{min} \\ \frac{T_{max} + T_{min}}{2} + \frac{T_{max} - T_{min}}{2} cos\left(\frac{\pi(t - H_{min})}{H_{max} - H_{min}}\right) & if\ H_{min} < t \leq H_{max} \\ \frac{T_{max} + T_{min}}{2} + \frac{T_{max} - T_{min}}{2} cos\left(\frac{\pi(t-14)}{10 + H_{min}}\right) & if\ t > H_{max} \end{cases}$$

in which we assume H_{min} is 6:00 am and H_{max} is 14:00pm.

Killing degree days (KDD) is the cumulative heat extremes by summing maximum temperatures in excess of the maximum optimal growth temperature:

$$KDD = \sum_{i=1}^{N} max\left(T_{max} - T_{opt}, \qquad 0\right)$$

where T_{max} is the daily maximum temperature, T_{opt} is the crop-specific maximum optimal growth temperature, N is the number of days to accumulate the excessive heat and is defined as the period from June 1st to August 31th. Following Butler & Huybers (2013), we use 29 °C for T_{opt}.

Text A4. C4 Photosynthesis Model

We incorporated a coupled photosynthesis-stomatal conductance model for C4 plants into the APSIM following Collatz et al. (1992). To quantify the C4 photosynthesis rate, three variables to know are stomatal conductance (g_s), net photosynthesis (A_n), and the intercellular partial pressure of CO_2 (p_i).

The stomatal conductance can be calculated following Ball et al. (1987):

$$g_s = m\frac{h_s A_n P}{p_s} + b \tag{A4.1}$$

where m and b are coefficients derived from linear regression, h_s is the leaf surface relative humidity, P and p_s are atmospheric ($10^5\ Pa$) and leaf surface partial pressure of CO_2.

The leaf level instantaneous photosynthesis rate A ($\mu mol\ m^{-2}\ s^{-1}$) is derived from a quadratic equation:

$$\beta A^2 - A\left(M + \frac{k_T p_i}{P}\right) + \frac{M k_T p_i}{P} = 0 \tag{A4.2}$$

in which M is the flux determined by the rubisco and light limitation, k_T describes the temperature dependency of a constant with respect to p_i, β is a parameter gives a gradual transition from the limitation by M to CO_2 limitation. M is calculated by a similar quadratic equation:

$$\theta M^2 - M\left(V_T + \alpha Q_p\right) + V_T \alpha Q_p = 0 \tag{A4.3}$$

in which V_T is the temperature dependent maximum carboxylation rate, α is the quantum efficiency and Q_p is the incident quantum flux density. The smaller roots for both Eqn-4.2 and Eqn-4.3 are reasonable solutions.

A_n is then calculated as:

$$A_n = A - R_T \tag{A4.4}$$

where R_T is the temperature dependent daytime leaf dark respiration.

The temperature dependency of each above mentioned parameters are given as:

$$V_T = \frac{V_{max} Q_{10}^{\frac{T_l - 25}{10}}}{(1 + e^{0.3\times(13 - T_l)})(1 + e^{0.3\times(T_l - 36)})}$$

$$R_T = \frac{R_d Q_{10}^{\frac{T_l - 25}{10}}}{1 + e^{1.3\times(T_l - 55)}} \tag{A4.5}$$

$$k_T = k Q_{10}^{\frac{T_l - 25}{10}}$$

where the leaf temperature, T_l, is approximated by daily mean temperature in our implementation.

The last equation is for the intercellular CO_2 partial pressure:

$$p_i = p_s - \frac{1.6 A_n P}{g_s} \tag{A4.6}$$

The analytical solution to these coupled equations is provided by Collatz et al. (1992), which combines Eqn-4.1 to Eqn-4.6 to eliminate p_i and g_s.

To reduce the big-leaf assumption errors, we calculated A_n for both sunlit and shaded leaves according to the implementation in Biome-BGC v4.2 (White et al., 2000). The total canopy photosynthesis is the summation of CO_2 assimilation by the sunlit and shaded leaf fractions:

$$\mathrm{A_{canopy}} = \mathrm{A_{sun}} \cdot \mathrm{LAI_{sun}} + \mathrm{A_{shade}} \cdot \mathrm{LAI_{shade}} \tag{A4.7}$$

We simulate the sunlit and shaded LAI following Biome-BGC 4.2, which estimate the albedo and extinction coefficients for the shortwave and PAR spectra from the values given for the entire shortwave range according to Jones (1992).

Finally, to calculate daily biomass accumulation, we need deduct autotrophic respiration, which consists of maintenance respiration (R_m) and growth respiration (R_g).

$$\Delta\text{biomass} = \text{A}_{\text{canopy}} - R_m - R_g \quad \text{(A4.8)}$$

The method for calculating R_m and R_g can be found in Chen et al. (1999), whereas parameters for C4 crop are derived from Biome-BGC 4.2. Specifically, the maintenance respiration is calculated as

$$R_m = Mc_{rm}Q_{10}^{(T-T_b)/10}$$

where M is the current biomass (approximated by total green dry matter calculated by APSIM), c_{rm} is the coefficient for maintenance respiration, and Q_{10} is temperature sensitivity factor, T_b is the base temperature. And the growth respiration is calculated as:

$$R_g = c_{rg}A_{canopy}$$

where c_{rg} is the coefficient for growth respiration.

Parameters used in the C4 photosynthesis model

Parameter	Definition	Value	Unit
k	Initial slope of CO_2 response	0.9	$mol\ m^{-2}\ s^{-1}$
V_{max}	Maximum rubisco capacity	50	$\mu mol\ m^{-2}\ s^{-1}$
α	Initial slope of photosynthetic light response	0.04	$mol\ m^{-2}\ s^{-1}$
R_d	Leaf dark respiration	1.05	$\mu mol\ m^{-2}\ s^{-1}$
m	Stomatal slope	3	-
b	Stomatal intercept	0.08	-
β	Curvature parameter	0.93	-
θ	Curvature parameter	0.83	-
c_{rm}	Coefficient for maintenance respiration	0.002	*g g-1 day-1*
c_{rg}	Coefficient for growth respiration	0.25	-
Q_{10}	Respiration temperature sensitivity factor	2.0	-
T_b	Base temperature for Q10 function	20	°C

Table A1 Annual management information reported by USDA National Agricultural Statistics Service.

	N Amount[1] (kg/ha)			Sowing Date[2]			Sowing Density (plants/m2)		
Year	IL	IN	IA	IL	IN	IA	IL	IN	IA
1980	165	166	150	5-May	7-May	3-May	5.4	5.2	5.1
1981	170	164	159	10-May	1-Jun	7-May	5.5	5.3	5.2
1982	171	170	147	4-May	7-May	10-May	5.6	5.4	5.3
1983	174	167	158	15-May	21-May	12-May	5.5	5.2	5.5
1984	166	174	160	15-May	17-May	16-May	5.5	5.3	5.4
1985	177	181	162	1-May	3-May	4-May	5.6	5.3	5.4
1986	175	176	147	30-Apr	6-May	8-May	5.6	5.4	5.4
1987	180	152	148	1-May	3-May	1-May	5.9	5.5	5.5
1988	183	164	156	30-Apr	3-May	4-May	5.5	5.2	5.5
1989	179	149	143	2-May	16-May	7-May	5.5	5.4	5.4
1990	184	156	142	6-May	7-May	3-May	5.6	5.5	5.6
1991	178	151	134	2-May	8-May	16-May	5.9	5.6	5.7
1992	174	160	132	6-May	9-May	7-May	5.8	5.8	5.8
1993	168	150	128	17-May	15-May	20-May	5.8	5.8	5.9
1994	171	165	136	3-May	9-May	28-Apr	5.8	5.7	6
1995	172	148	134	27-May	22-May	18-May	5.9	6	6.2
1996	186	155	148	8-May	29-May	5-May	6.1	5.9	6.2
1997	171	164	136	29-Apr	1-May	3-May	6.2	6	6.4
1998	174	164	142	13-May	16-May	5-May	6.4	6.1	6.4
1999	174	172	141	7-May	7-May	6-May	6.4	6.3	6.5
2000	180	171	147	28-Apr	4-May	29-Apr	6.5	6.3	6.6
2001	170	157	134	28-Apr	30-Apr	4-May	6.7	6.5	6.6
2002	180	166	137	11-May	27-May	3-May	6.6	6.3	6.7
2003	180	172	149	27-Apr	3-May	2-May	6.8	6.5	6.8
2004	172	168	154	21-Apr	27-Apr	28-Apr	6.9	6.6	7
2005	164	165	158	20-Apr	30-Apr	30-Apr	7	6.3	7
2006	169	172	158	26-Apr	6-May	27-Apr	7	6.6	7.2
2007	174	179	158	1-May	7-May	5-May	7	6.8	7.3
2008	179	186	159	9-May	8-May	12-May	7.2	7.1	7.3
2009	183	193	159	21-May	22-May	27-Apr	7.4	7.1	7.4
2010	187	199	159	20-Apr	23-Apr	22-Apr	7.4	7.1	7.5
2011	186	193	159	11-May	22-May	5-May	7.6	7.3	7.7
2012	185	187	158	19-Apr	24-Apr	29-Apr	7.5	7.3	7.5
2013	184	181	158	16-May	16-May	16-May	7.7	7.6	7.5
2014	183	175	158	5-May	9-May	8-May	7.7	7.7	7.7

Table A2. General circulation models (GCMs) used in this study.

Model	Institution	Resolution
BNU-ESM	Beijing Normal University, China	T42
CanESM2	Canadian Center for Climate Modelling and Analysis	Spectral T63
CCSM4	US National Centre for Atmospheric Research	0.9° × 1.25°
CESM1-BGC	NSF-DOE-NCAR, USA	0.9° × 1.25°
GFDL-ESM2G	NOAA Geophysical Fluid Dynamics Laboratory, USA	2.5° × 2°
IPSL-CM5A-MR	Institut Pierre Simon Laplace, France	1.25° X 2.5°
MPI-ESM-MR	Max Planck Institute for Meteorology, Germany	pprox. 1.8° T63
MRI-CGCM3	Meteorological Research Institute, Japan	320 × 160 TL159

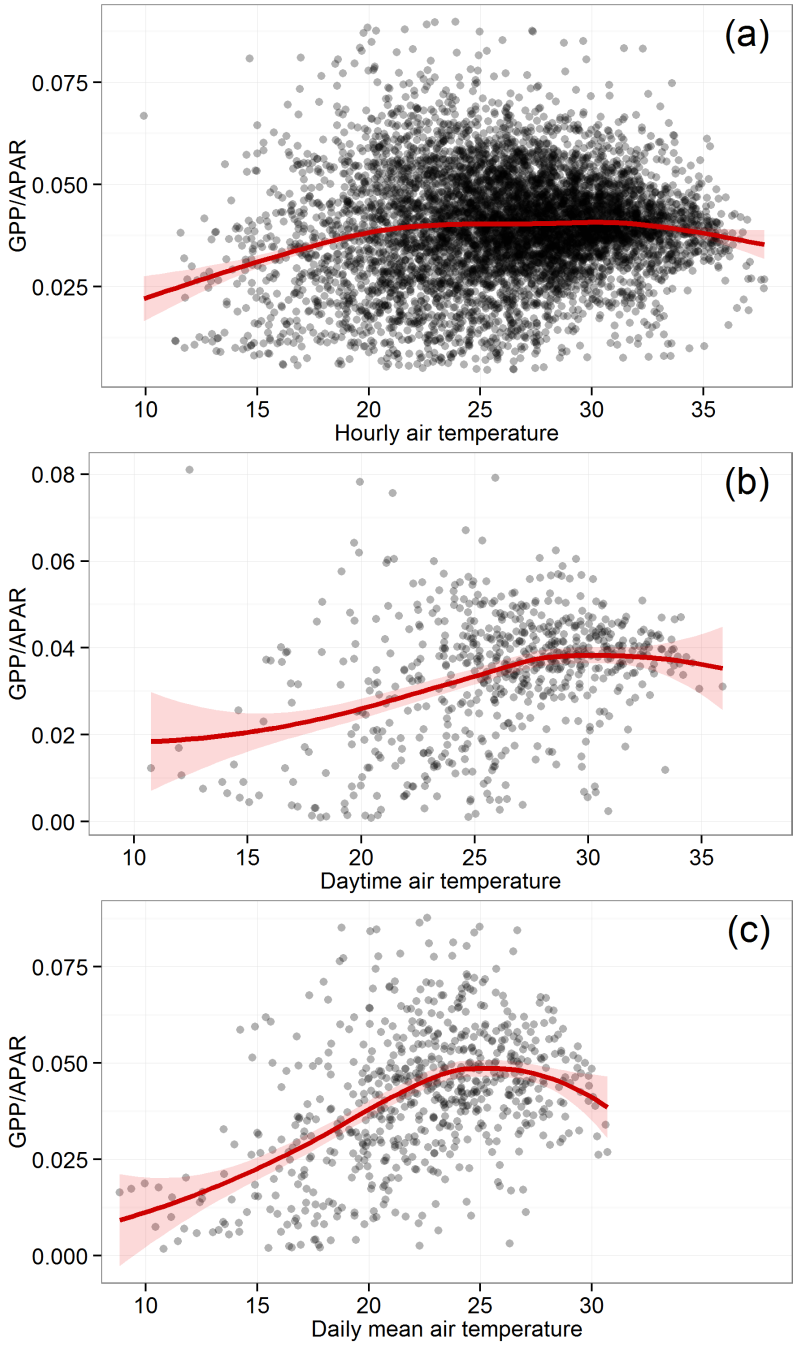

Figure A1Temperature response of radiation use efficiency derived from AmeriFlux hourly observations at Mead rainfed maize, Mead, Nebraska. Here "daytime air temperature" refers to the mean temperature from 8:00 am to 17:00 pm.

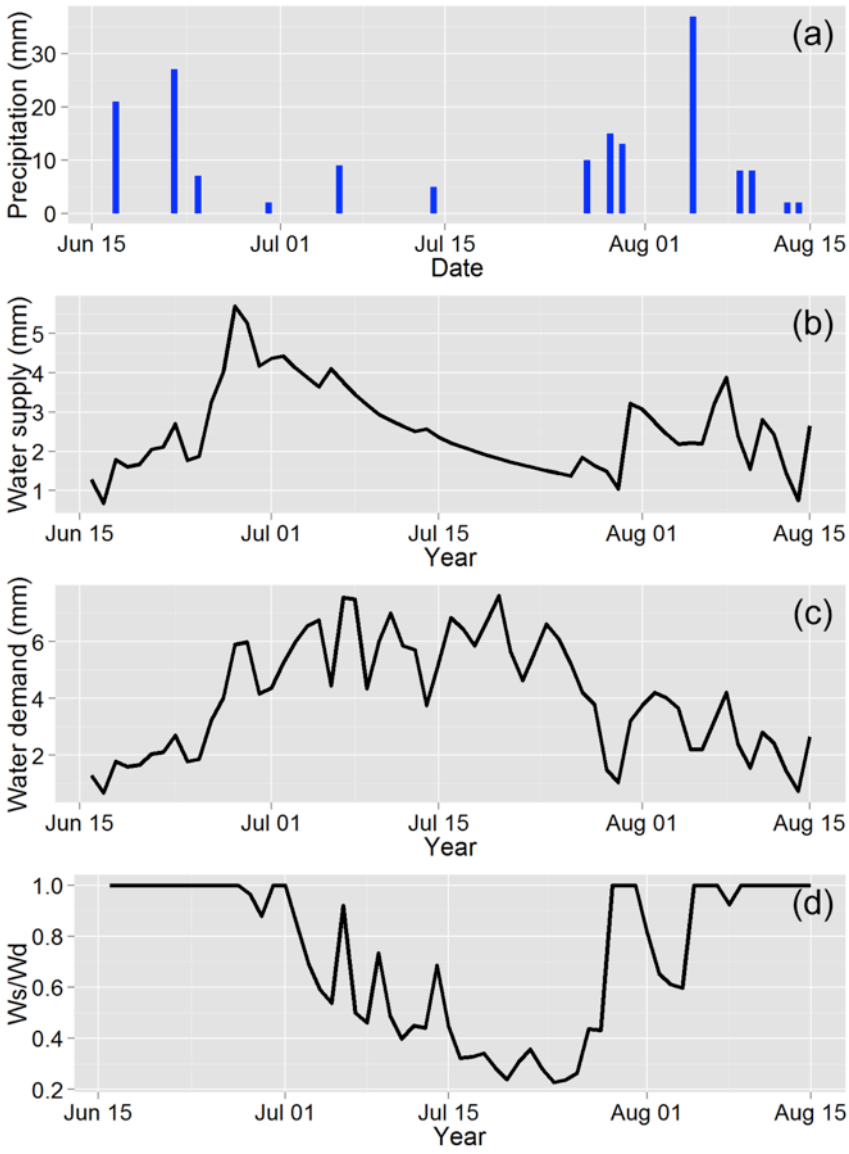

Figure A2 Supplementary information for the 2012 Iowa drought at Agricultural Engineering and Agronomy Research Farms of Iowa State University, Boone, IA (42.02^{o}, -93.78^{o}). Daily precipitation (a), soil water supply (b), crop transpiration water demand (c) and the ratio of water supply to demand (d) are given for days from June 16th to August 31st.

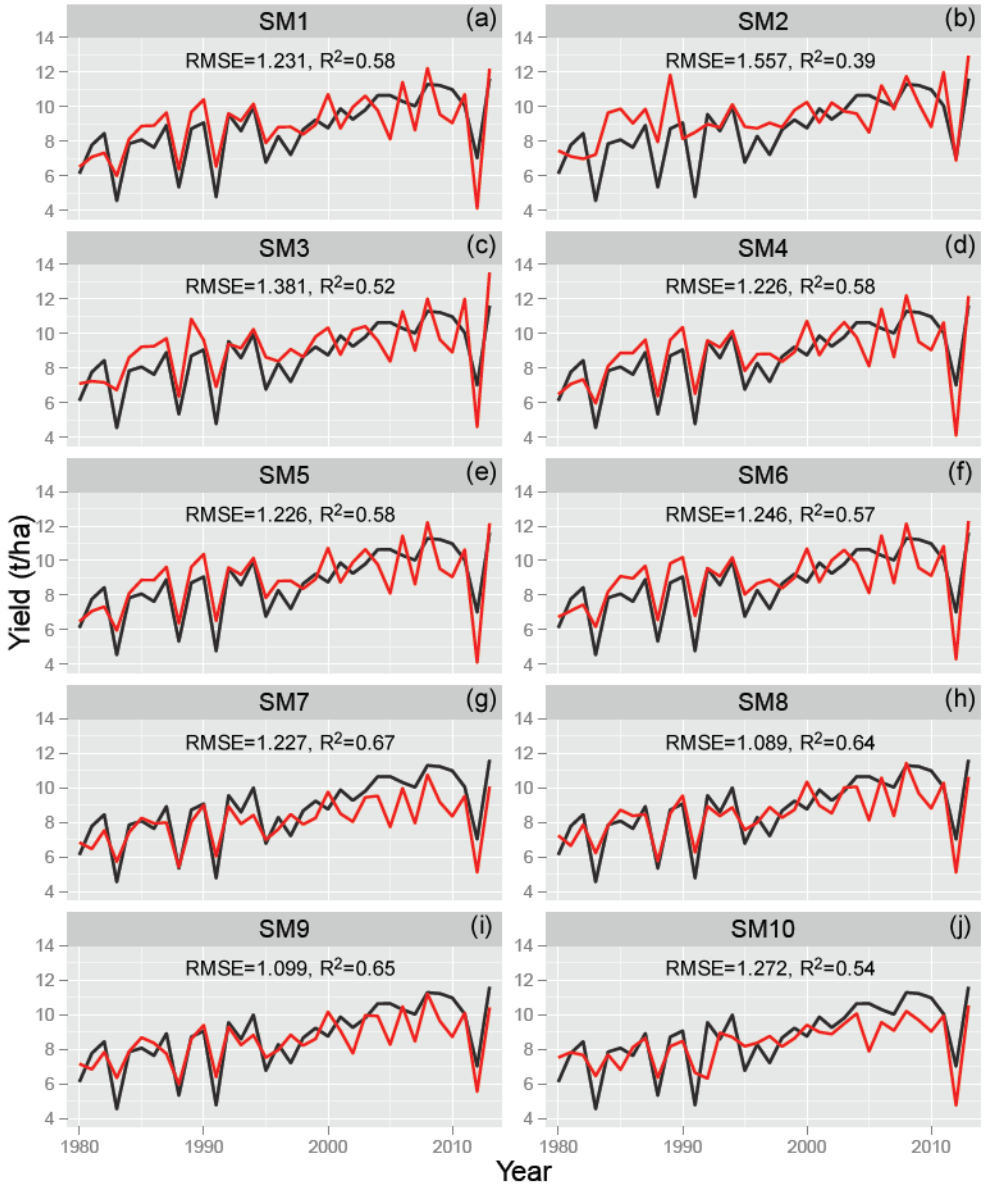

Figure A3 Time series of APSIM simulated (red lines) maize yield and NASS county level yield statistics (black lines) for the Indiana farm from 1980 to 2013. Each panel denotes one simulation as described in Figure 2.1.

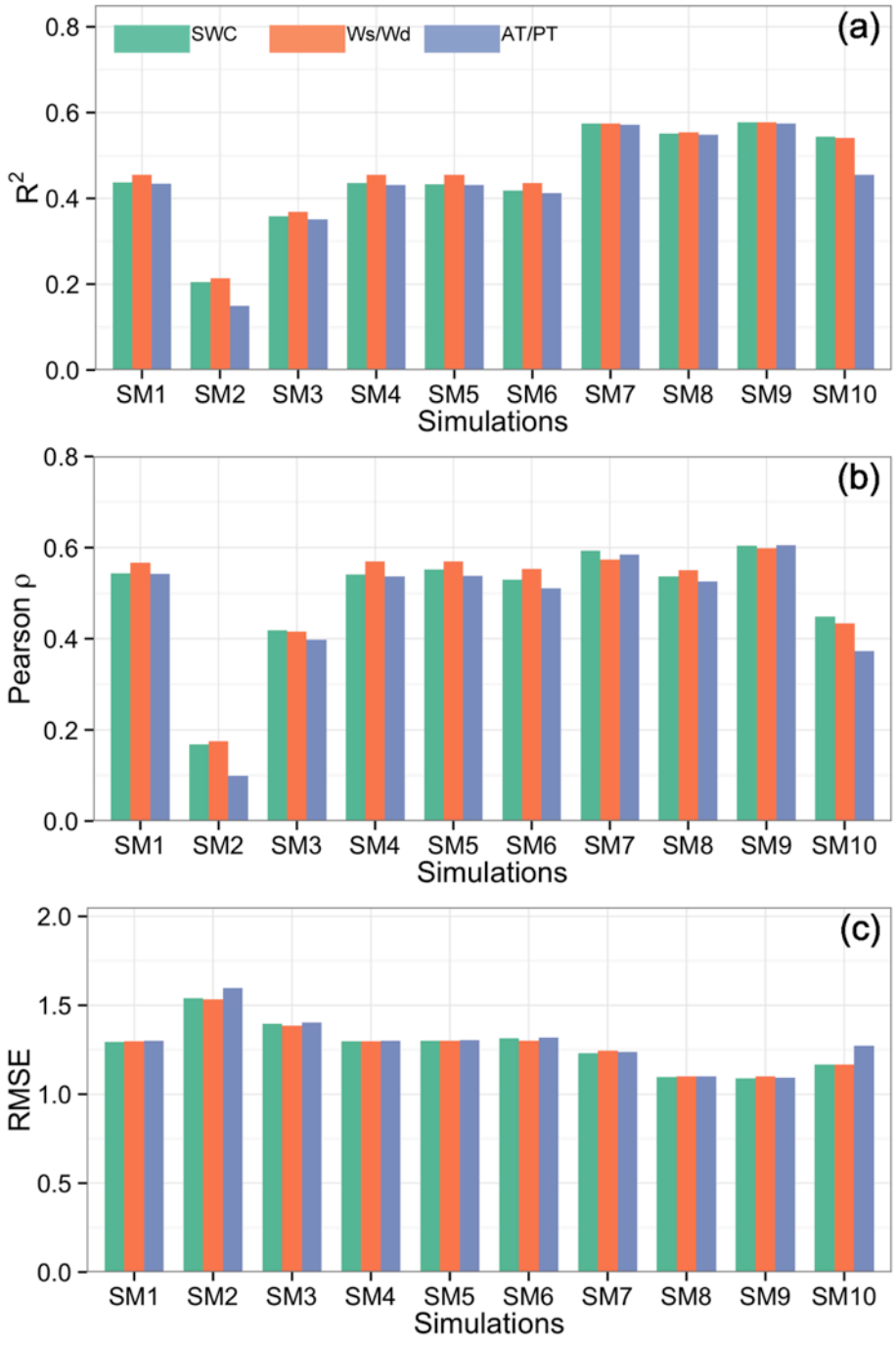

Figure A4 Evaluation of model performance for the Illinois farm under 30 ensemble simulation trials (10 heat × 3 drought stress algorithms) with respect to reproducing the USDA county-level yield statistics from 1980 to 2013. Model predictability is measured collectively by (a) R^2, (b) Pearson correlation coefficient (ρ), and (c) root mean square error (RMSE). See Figure 2.1 for detailed algorithm combinations for each ensemble.

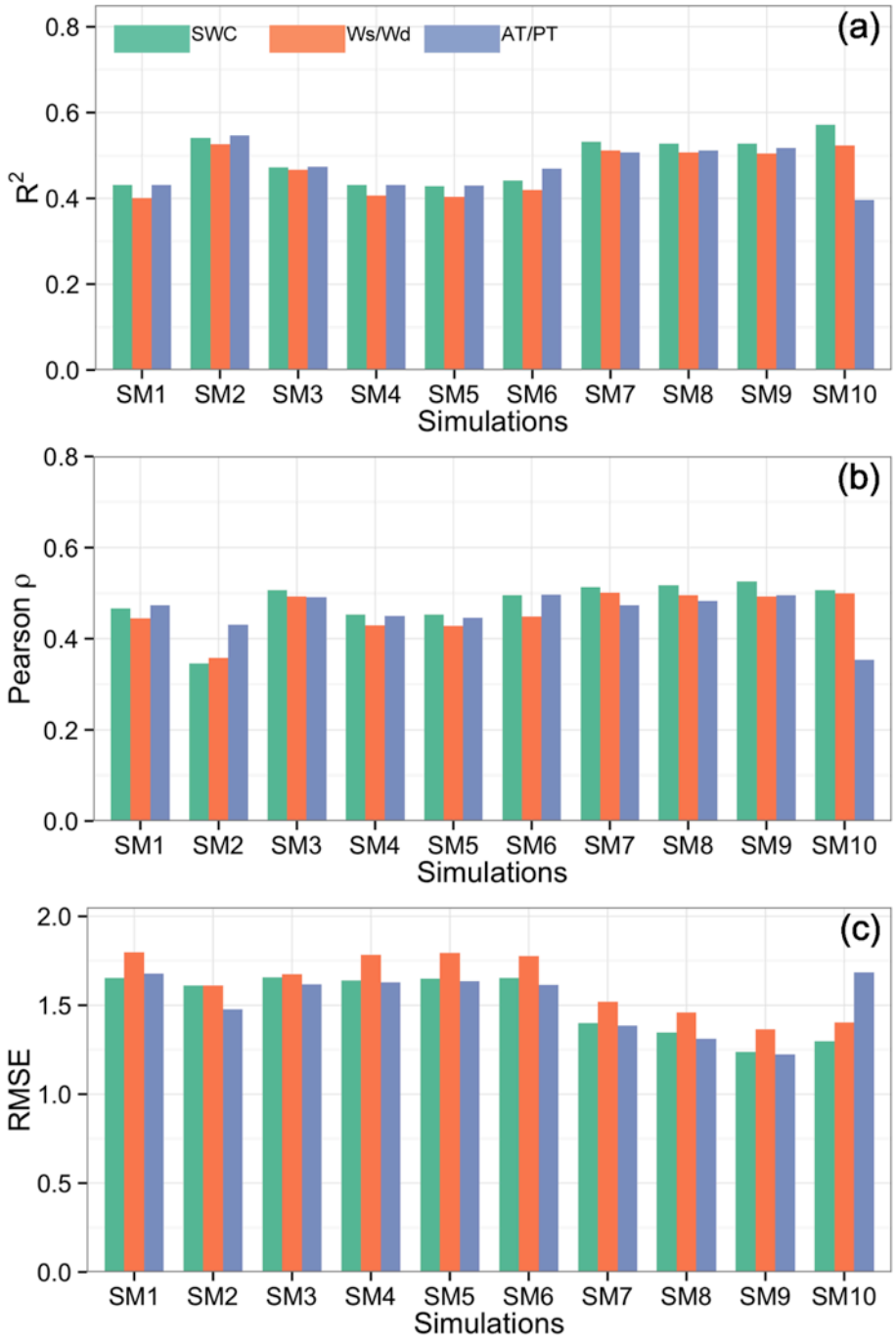

Figure A5 Evaluation of model performance for the Iowa farm under 30 ensemble simulation trials (10 heat × 3 drought stress algorithms) with respect to reproducing the USDA county-level yield statistics from 1980 to 2013. Model predictability is measured collectively by (a) R^2, (b) Pearson correlation coefficient (ρ), and (c) root mean square error (RMSE). See Figure 2.1 for detailed algorithm combinations for each ensemble.

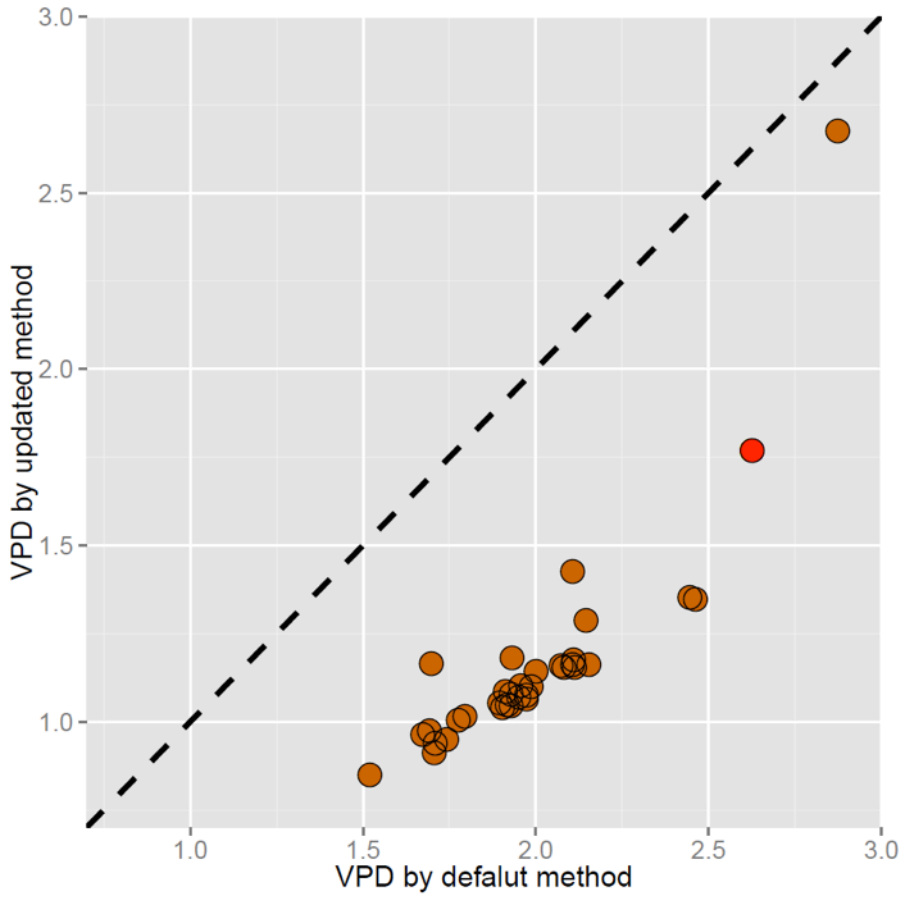

Figure A6 Maximum mean weekly vapor pressure deficit (VPD) for the Indiana farm from 1980-2013 simulated by the default APSIM method and an updated method that uses actual vapor pressure as a meteorological input.

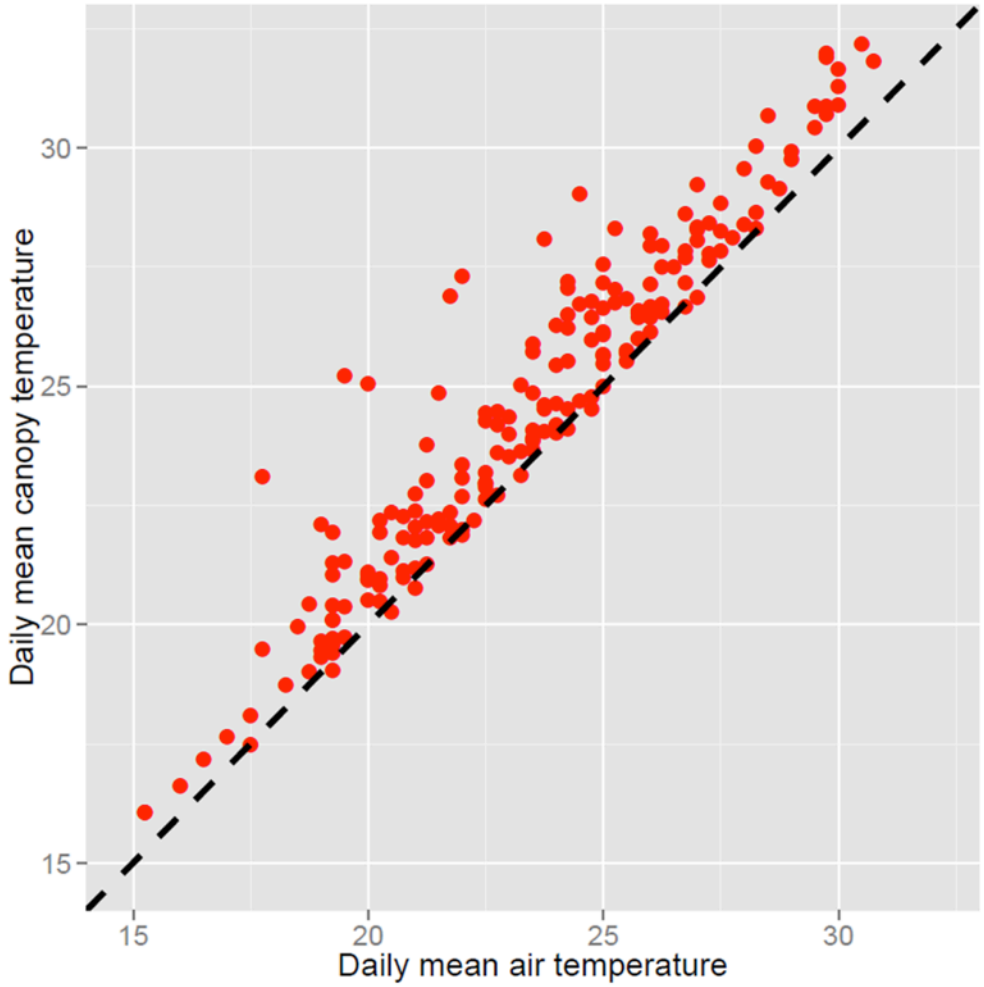

Figure A7 Simulated daily mean canopy temperature by the STICS empirical relation algorithm vs. daily mean air temperature.

Appendix B

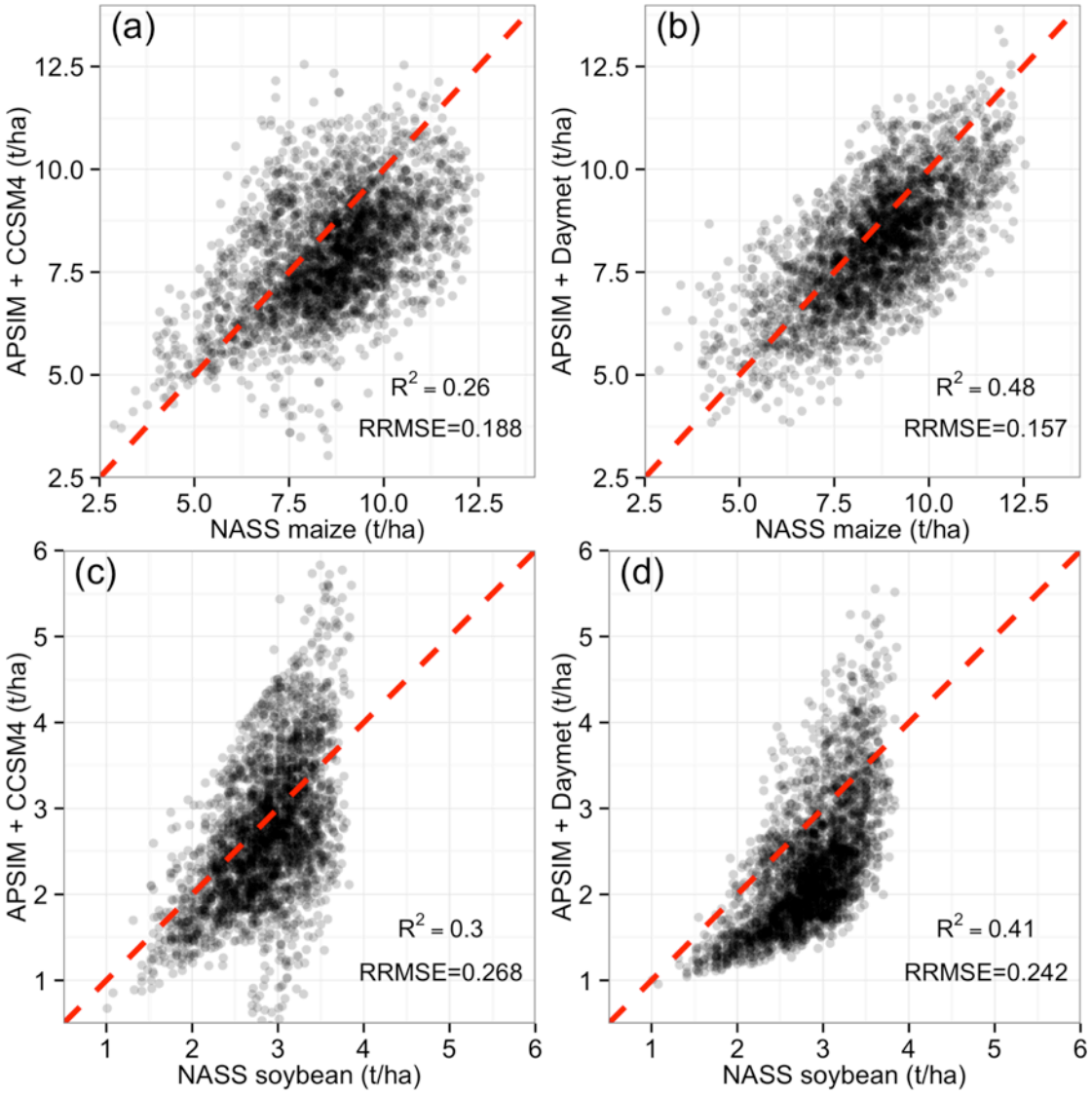

Figure B1 Comparison of simulated maize and soybean yield with USDA National Agricultural Statistics Service (NASS) survey report county-level yield. Simulations are run for Daymet reanalysis weather data and WRF downscaled CCSM4 output, respectively.

Appendix C

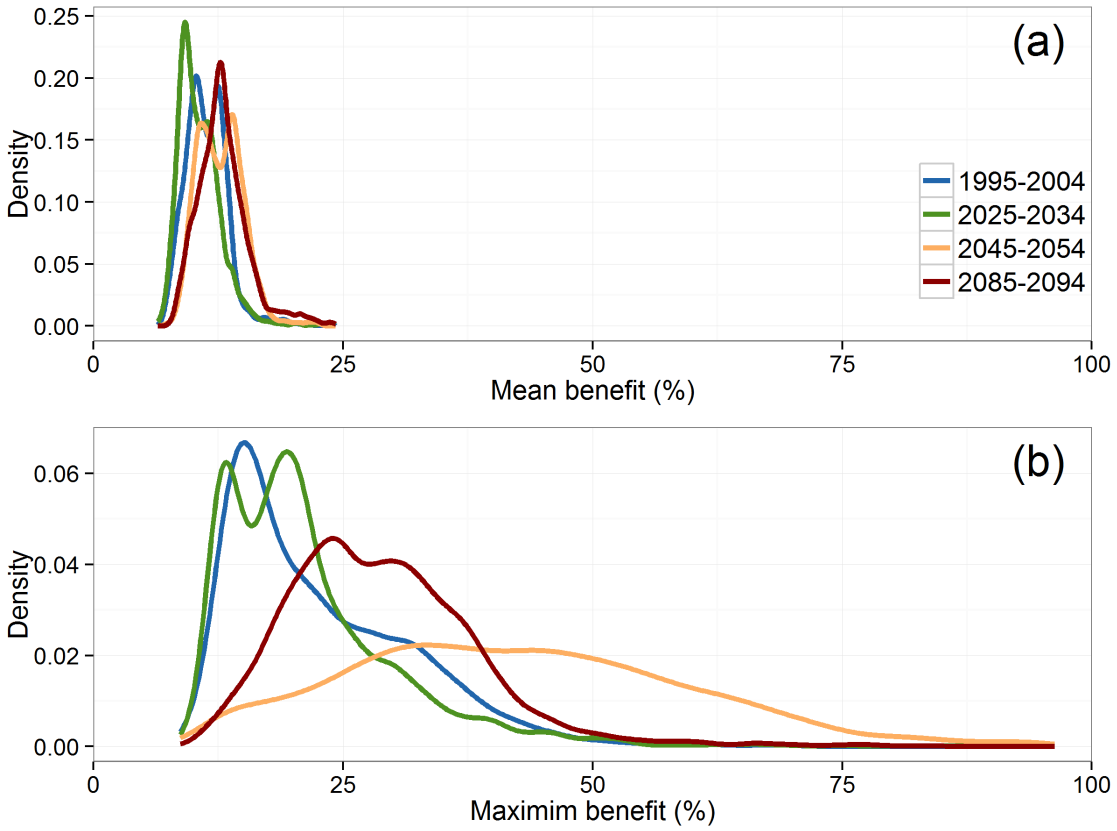

Figure C1 Distribution of mean and maximum yield benefit from optimizing the planting date.

Appendix D

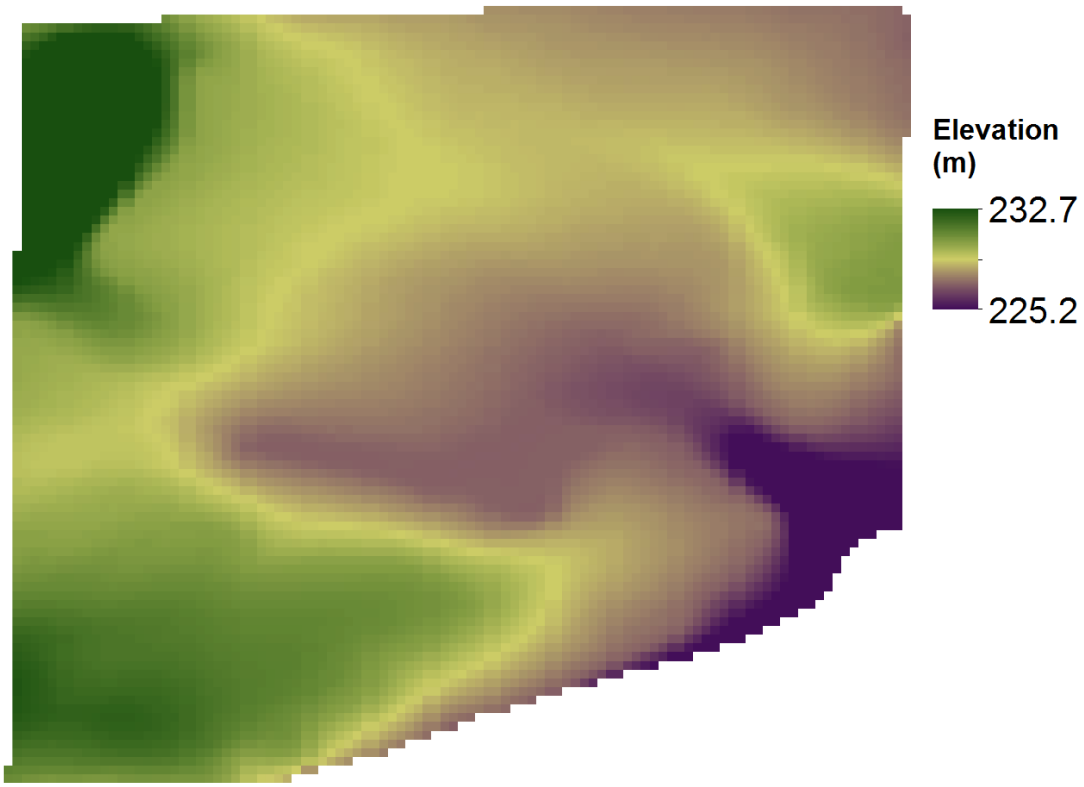

Figure D1 Topography information for the study field.

VITA

VITA

Education

2011 - Present	Purdue University, Dept. of Earth, Atmospheric & Planetary Science, West Lafayette, IN Ph.D. in Ecosystem Modeling
2007 - 2011	Peking University, College of Urban & Environmental Science, China B.S. in Ecology (with highest honor)

Working Experience

Jun. 2015 – Aug.2015	Science Team Intern, Farmlogs First contributor of crop model development for N prescription.
Sep. 2011 – Present	Research Assistant Dept. of Earth, Atmospheric and Planetary Sci., Purdue University
Jun. 2010 – Aug. 2010	Consultant Intern Horizon-China Consultant Inc.

Publications

Peer-reviewed Journal papers:

Hao G, Zhuang Q*, Zhu Q, He Y, **Jin Z-N**, Shen W (2015) Quantifying microbial ecophysiological effects on the carbon fluxes of forest ecosystems over the conterminous United States. ***Climatic Change***, 1-14. doi: 10.1007/s10584-015-1490-3

Jin Z-N, Zhuang Q*, He J-S, Zhu X, Song W (2015). Net exchanges of methane and carbon dioxide on the Qinghai-Tibetan Plateau from 1979 to 2100. ***Environmental Research Letters***, 10(8), 085007.

Song W, Wang H, Wang G, Chen L, **Jin Z-N**, Zhuang Q, He J-S* (2015) Methane emissions from an alpine wetland on the Tibetan Plateau: Neglected but vita contribution of non-growing season. J. Geophys. Res. Biogeosci., 120, 1475-149, doi:10.1002/2015JG003043.

Hao G, Zhuang Q*, Pan J, **Jin Z-N,** Zhu X, Liu S (2014) Soil temperature trends from 1948 to 2008 in contiguous United States: an analysis with a process-based soil physical model and AmeriFlux data. ***Climatic Change***. 126, 135-150.

Jin Z-N*, Zhuang Q, He J-S, Luo T, Shi Y (2013) Phenology shift from 1989 to 2008 on the Tibetan Plateau: An analysis with a process-based soil physical model and remote sensing data. ***Climatic Change,*** 119, 435-449.

Manuscript in progress:

Jin Z-N, Zhuang Q*, Dukes JS, Chen M, Sokolov A, He J-S, Zhang T, Luo T (in revision) Phenological acclimation and its effects on carbon cycling on the Tibetan Plateau during the 21st century: A process-based ecosystem modeling analysis. *Climatic Change.*

Jin Z-N, Zhuang Q*, Tan Z, Dukes JS, Melillo JM (in revision) Do crop models capture the impacts of extreme heat and drought stress on yield? Using algorithm ensembles to identify successful approaches. *Global Change Biology*.

Jin Z-N*, Prasad R, Shriver J, Zhuang Q (in revision) Crop model and satellite imagery based recommendation tool of variable rate N fertilizer application for the US Corn system. *Precision Agriculture.*

Jin Z-N, Zhuang Q*, Wang J, Kotamarthi R (in revision) Assessing the US Maize and Soybean productions in response to future extreme climatic events. *Global Change Biology.*

Jin Z-N, Zhuang Q* (in prep) Mitigating future heat and drought stress by changing the sowing strategy in the US Midwest.

Presentations

Jin Z-N, Zhuang Q, Assessing the impact of future climate extremes on the US corn and soybean production, AGU Annual Conference, December 14-18, 2015, San Francisco, CA.

Jin Z-N, Zhuang Q, Quantifying the US crop yield in response to extreme climatic events from 1981 to 2013, AGU Annual Conference, December 15-19, 2014, San Francisco, CA.

Jin Z-N. TEM documentations. Terrestrial Ecosystem Model (TEM) Workshop in University of Alaska. Fairbanks, AK. Jun. 2013. Oral presentation.

Selected Awards

Nov. 2015	Purdue Climate Change Research Center Travel Grant.
Apr. 2015	Bisland Dissertation Fellowship for 2016
Feb. 2014	Andrews/Blosser Environmental Travel Grant, Purdue University
Sep. 2011	Ross Fellowship, Purdue University